LSU Doctoral Dissertations   Graduate School

2007

Channel modeling and resource allocation in OFDM systems

Xiang Gao
Louisiana State University and Agricultural and Mechanical College, xgao3@lsu.edu

CHANNEL MODELING AND RESOURCE ALLOCATION IN OFDM SYSTEMS

A Dissertation

Submitted to the Graduate Faculty of the
Louisiana State University and
Agricultural and Mechanical College
in partial fulfillment of the
requirements for the degree of
Doctor of Philosophy

in

The Department of Electrical and Computer Engineering

by
Xiang Gao
B.S., Peking University, China, 1998
M.S., Peking University, China, 2001
May 2007

To my wife and my parents.

ACKNOWLEDGMENTS

My first and foremost gratitude must go to my advisor and committee chair, Dr. Morteza Naraghi-Pour, for his indispensable instructs, enlightening discussions, and strong support at all levels. This dissertation would not come out without his insightful advices and judicious corrections.

My special thanks goes to Dr. Guoxiang Gu, whose knowledge and perception in theoretical research have made important contributions to part of this dissertation.

Furthermore, I would like to thank Dr. Shuangqing Wei for his generous advices and sincere encouragement during my dissertation research.

I am deeply indebted to Dr. Peter Wolenski for his spending the precious time to serve as my minor professor and committee member.

I also want to express my thanks to Dr. A. Ravi P. Rau for reading this dissertation and offering constructive comments.

My tribute also extends to my fellow EE students, Jianqiang He, Zhongshan Wu, Xiaozhou Huang, Chi Zhang, Min Luo and Chung-Yu Wei. I treasure the great time we have in LSU.

Last but not least, my heartfelt acknowledgment must go to my wife Xiaomin. Her encouragement, companionship and constant trust in me has turned my journey through graduate school into a pleasure.

Xiang Gao
May, 2007

TABLE OF CONTENTS

LIST OF TABLES

LIST OF FIGURES

ABSTRACT

The increasing demand for high data rate in wireless communication systems gives rise to broadband communication systems. The radio channel is plagued by multipath propagation, which causes frequency-selective fading in broadband signals. Orthogonal Frequency-Division Multiplexing (OFDM) is a modulation scheme specifically designed to facilitate high-speed data transmission over frequency-selective fading channels.

The problem of channel modeling in the frequency domain is first investigated for the wideband and ultra wideband wireless channels. The channel is converted into an equivalent discrete channel by uniformly sampling the continuous channel frequency response (CFR), which results in a discrete CFR. A necessary and sufficient condition is established for the existence of parametric models for the discrete CFR. Based on this condition, we provide a justification for the effectiveness of previously reported autoregressive (AR) models in the frequency domain of wideband and ultra wideband channels.

Resource allocation based on channel state information (CSI) is known to be a very powerful method for improving the spectral efficiency of OFDM systems. Bit and power allocation algorithms have been discussed for both static channels, where perfect knowledge of CSI is assumed, and time-varying channels, where the knowledge of CSI is imperfect. In case of static channels, the optimal resource allocation for multiuser OFDM systems has been investigated. Novel algorithms are proposed for subcarrier allocation and bit-power allocation with considerably lower complexity than other schemes in the literature. For time-varying channel, the error in CSI due to channel variation is recognized as the main obstacle for achieving the full potential of resource allocation. Channel prediction is proposed to suppress errors in the CSI and new bit and power allocation schemes incorporating imperfect CSI are presented and their performance is evaluated through simulations.

Finally, a maximum likelihood (ML) receiver for Multiband Keying (MBK) signals is discussed, where MBK is a modulation scheme proposed for ultra wideband systems (UWB). The receiver structure and the associated ML decision rule is derived through analysis. A suboptimal algorithm based on a depth-first tree search is introduced to significantly reduce the computational complexity of the receiver.

CHAPTER 1. INTRODUCTION

This dissertation uses the technical paper style approved by the Graduate School. It contains chapters based on papers that have been published, or are under review, or are to be submitted to peer-reviewed journals. Therefore, the consistency of notations are not maintained for all chapters and some essential information may be repeated for the sake of completeness and independence of each chapter.

1.1   Overview

Since its emergence in late nineteenth century, wireless communication has been evolving constantly. In the past decade, the wireless communications industry has been expanding dramatically in part due to great progress in the areas of digital signal processing, analog and digital circuit manufacturing, and very large-scale integrated circuits (VLSI), which make the implementation of complex communication systems more and more affordable. Many new technologies and services based on wireless communication have been launched, such as the mobile telephone system, global positioning system (GPS), wireless local area network (WLAN), wireless metropolitan area network (WMAN), and so on. In recent years, in order to satisfy the increasing demand for higher data rates, much attention has been devoted to broadband wireless communication systems. Unlike the conventional narrowband systems, where the channel-induced distortion of data symbols can be eliminated using a channel equalizer with sensible complexity [58], broadband systems generally have a symbol duration that is much shorter than the channel delay spread resulting in severe intersymbol interferences (ISI). At the receiver, a very sophisticated equalizer is needed to remove the ISI effect of the channel. This has been recognized as a major obstacle for reliable communication in a broadband system. Several data transmission schemes have been proposed to cope with this problem.

Orthogonal Frequency-Division Multiplexing (OFDM) is a widely used data transmission technique particularly suitable for broadband systems. It has been successfully applied in the physical layers of many wireless communication protocols such as IEEE802.11a/g (WiFi), IEEE802.16 (WiMax), Digital Audio Broadcasting (DAB), Digital Video Broadcasting (DVB), and HIPERLAN/2. The OFDM system breaks up a high-rate data stream into a large number of low-rate data streams. These are then transmitted in parallel over low bandwidth subchannels or subcarriers and combined into the high-rate stream at the receiver. In OFDM systems, the frequencies and phases of these "subcarriers" are deliberately selected such that they are orthogonal to each other and can share a common radio frequency (RF) circuit without interference. Since each subcarrier is modulated by a low-rate data stream and therefore can be viewed as a narrowband system, then the OFDM system has a property

of transforming a broadband channel into multiple narrowband subchannels. It can be shown in the remainder of this chapter that only a very simple channel equalizer is needed for a properly designed OFDM system. Additional advantages of the OFDM system include high spectral efficiency, simple transceiver design, flexibility in terms of link adaptation, and so on.

In the OFDM system, the effect of channel on each OFDM symbol is characterized by a complex vector known as the channel frequency response (CFR) [52]. The received complex symbols in all subchannels experience attenuation and phase shift determined by the CFR. Hence, for the purpose of coherent demodulation, CFR need to estimated at the receiver. For this reason, channel estimation has received a great deal of attention in OFDM systems.

In order to facilitate the simulation and/or estimation of channels in OFDM systems, it is of great interests to investigate statistical models for the CFRs. In this dissertation, the problem of parametric modeling in the frequency domain for wideband and ultra wideband channels will be discussed.

A major drawback of the OFDM system over frequency-selective fading channels is the high probability of bit error rate (BER) due to the possible existence of "weak" subcarriers. The signal-to-noise ratio (SNR) of these subcarriers is low resulting in high error probability, which tends to dominate the performance of the entire system. For the sake of reliable communication, an approach using forward error-control code and frequency and/or time interleaving may be employed, which results in the so-called "Coded-OFDM (C-OFDM)" system [1]. However, in this case, spectral efficiency is sacrificed, and a complicated decoding algorithm is always needed in the receiver. Another effective method is the adaptive modulation, which proposes to select for each subcarrier a proper size of modulation signal set and transmit power, according to the instantaneous frequency response of the channel, such that the desired quality of service (QoS) can be achieved with maximum spectral efficiency. This method is also referred to as "bit and power allocation" or simply "resource allocation". In this dissertation, the problem of bit and power allocation has been investigated for OFDM systems having perfect or imperfect channel state information. Simulation studies have also been conducted to show the efficiency and effectiveness of these methods.

In addition to the OFDM system, there exits other signal transmission techniques proposed for broadband wireless communications. Among them is the emerging Ultra-Wideband (UWB) technique, which is based on a principle totally different from that of the OFDM system. It suggests using extremely narrow pulse signals that have a period of up to several nanoseconds to modulate data symbols. The terminology of UWB comes from the fact that an extremely narrow pulse in the time domain corresponds to an ultra wide bandwidth in the frequency domain. In the United States, according to the Federal Communications Commission (FCC), a signal is qualified to be a UWB signal only when its -10dB bandwidth exceeds 500MHz or 20% of its center frequency [43]. In UWB systems, multiple versions of the pulse signals are
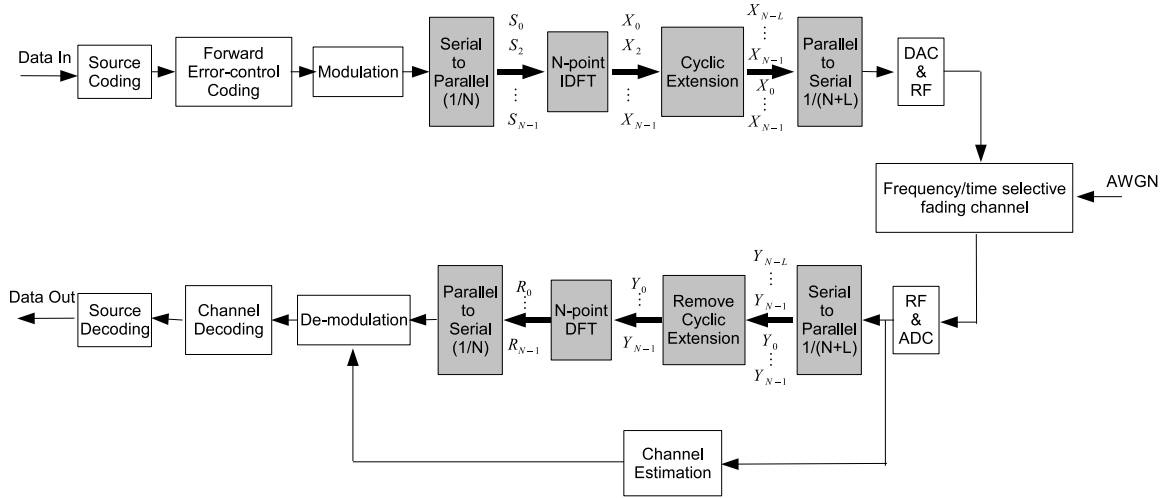
Figure 1.1: The architecture of a typical OFDM system

received from various propagation paths, which have differences in delay time greater than the pulse intervals. Generally speaking, the resulting ISI is negligible in UWB systems. Meanwhile, the transmit power has been dispersed into multiple (independent) components, and a RAKE receiver is needed to collect these components for better decision [53]. In this dissertation, a UWB system known as "Multiband Keying" is addressed, whose maximum likelihood (ML) receiver over AWGN channel is investigated.

1.2 OFDM System over Frequency-Selective Fading Channels

As mentioned in [52], OFDM systems can be realized with low complexity using the discrete Fourier transform (DFT). The structure of a typical OFDM system is illustrated in Figure 1.1, where the shadowed blocks correspond to the processing of OFDM. In this system, the number of subcarriers is denoted by N and the sampling rate is fixed to be $1/T_S$, where $T_S = 1/(N\Delta f)$ and where Δf is the frequency offset between neighboring subcarriers. In general, a complete OFDM symbol consists of N data samples and a cyclic prefix (CP) of size L. Thus, $T_B = (N + L)T_S$ is the duration of each OFDM symbol.

Let $\{S_{0,k}, \cdots, S_{N-1,k}\}$ denote the complex symbols that are transmitted within the kth OFDM block. Then the output of the IDFT module in Figure 1.1 can be represented by

$$X_{m,k} = \sum_{n=0}^{N-1} S_{n,k} \cdot e^{j2\pi \frac{mn}{N}}, \ m = 0, 1, \cdots, N-1 \tag{1.1}$$

After cyclic extension, parallel-to-serial operation, and digital-to-analog conversion,

3

the transmitted signal can be represented in baseband by the following:

$$x(t) = \sum_{k=-\infty}^{\infty} \left[\sum_{u=0}^{N-1} X_{u,k} \cdot w(t - kT_B - uT_S) + \sum_{v=N-L}^{N-1} X_{v,k} \cdot w(t - kT_B + (N - v)T_S) \right]$$

$$(1.2)$$

where $w(\cdot)$ is the pulse shaping function determined by the entire analog system except the physical channel.

Let $c(\tau; t)$ denote the equivalent lowpass impulse response of a time-varying, frequency-selective multipath fading channel. According to [59], $c(\tau; t)$ can be written as follows

$$c(\tau; t) = \sum_{i=0}^{I-1} \alpha_i e^{-j2\pi\{(f_c + f_{d,i})\tau_i - f_{d,i}t\}} \delta(\tau - \tau_i)$$

$$(1.3)$$

where I denotes the number of propagation paths, and τ_i, α_i, and $f_{d,i}$ are, respectively, the propagation delay, the attenuation factor and the Doppler frequency offset for the ith path. Moreover, $\delta(\cdot)$ is the Dirac delta function, and f_c is the center carrier frequency. Suppose $x(t)$ passes through the channel defined by (1.3), the received baseband signal is given by

$$
\begin{aligned}
y(t) &= \int_0^\infty c(\tau; t)x(t - \tau)d\tau + \zeta(t) \\
&= \sum_{i=0}^{I-1} r_i(t)x(t - \tau_i) + \zeta(t)
\end{aligned}
$$

$$(1.4)$$

where $r_i(t) = \alpha_i e^{-j2\pi\{(f_c + f_{d,i})\tau_i - f_{d,i}t\}t}$ and $\zeta(t)$ is the noise process. At the receiver, $y(t)$ is sampled with a sampling rate of $1/T_S$ to yield $N + L$ samples for each block, where the first L samples corresponding to CP are dropped. Assuming perfect time synchronization, the N samples input to the DFT module during block k are denoted by $\{Y_{0,k}, \cdots, Y_{N-1,k}\}$, where $Y_{n,k}$ is obtained by sampling $y(t)$ at the time $t = kT_B + nT_S$. Equations (1.2) and (1.4) result in

$$
\begin{aligned}
Y_{n,k} &= \sum_{m=-\infty}^{\infty} \sum_{i=0}^{I-1} \sum_{u=0}^{N-1} r_i(kT_B + nT_S)X_{u,l} \cdot w\left((n - u)T_S + (k - m)T_B - \tau_i\right) \\
&+ \sum_{m=-\infty}^{\infty} \sum_{i=0}^{I-1} \sum_{v=N-L}^{N-1} r_i(kT_B + nT_S)X_{v,l} \cdot w\left((N + n - v)T_S + (k - m)T_B - \tau_i\right) \\
&+ \zeta(kT_B + nT_S)
\end{aligned}
$$

$$(1.5)$$

It is noted that, $w(\cdot)$ is generally a function with a limited duration T_P, i.e., $w(\tau) = 0$ for any τ outside the interval $[0, \ T_P]$.

Assumptions:

1: *Quasi-Stationary Channel*: $r_i(kT_B + t) = r_i(kT_B)$ for all $0 \le t \le T_B$ and arbitrary integer k

2: *ISI-Free Condition*: $L \geq \lceil \frac{T_P + \max_i \{\tau_i\}}{T_S} \rceil$

If $k \neq m$, the following can be verified using the above assumptions:

$$w((n-u)T_S + (k-m)T_B - \tau_i) = 0$$
$$w((N+n-v)T_S + (k-m)T_B - \tau_i) = 0$$
$$\forall n, u = 0, \cdots, N-1; \ \forall v = N-L, \cdots, N-1; \ \forall i = 0, \cdots, I-1$$

In this case, Equation (1.5) can be simplified as the following:

$$
\begin{aligned}
Y_{n,k} &= \sum_{u=0}^{N-1} X_{u,k} \left\{ \sum_{i=0}^{I-1} r_i(kT_B) w\left((n-u)T_S - \tau_i\right) \right\} \\
&+ \sum_{v=N-L}^{N-1} X_{v,k} \left\{ \sum_{i=0}^{I-1} r_i(kT_B) w\left((N+n-v)T_S - \tau_i\right) \right\} \\
&+ \zeta(kT_B + nT_S)
\end{aligned}
\tag{1.6}
$$

Let

$$g_{l,k} := \sum_{i=0}^{I-1} r_i(kT_B) w(lT_S - \tau_i). \tag{1.7}$$

The ISI-Free Condition stated previously imply that $g_{l,k}$ achieves nonzero values only when $l = 0, 1, \cdots, L-1$. Therefore, (1.6) can be rewritten in a matrix form as follows:

$$
\begin{bmatrix}
Y_{0,k} \\
Y_{1,k} \\
\vdots \\
Y_{N-1,k}
\end{bmatrix}
=
\begin{bmatrix}
X_{0,k} & X_{N-1,k} & \cdots & X_{N-L-1,k} \\
X_{1,k} & X_{0,k} & \cdots & X_{N-L-2,k} \\
\vdots & \vdots & \vdots & \vdots \\
X_{N-1,k} & X_{N-2,k} & \cdots & X_{N-L,k}
\end{bmatrix}
\begin{bmatrix}
g_{0,k} \\
g_{1,k} \\
\vdots \\
g_{L-1,k}
\end{bmatrix}
+
\begin{bmatrix}
\zeta_{0,k} \\
\zeta_{1,k} \\
\vdots \\
\zeta_{N-1,k}
\end{bmatrix}
\tag{1.8}
$$

where $\zeta_{n,k} = \zeta(kT_B + nT_S)$ for all n and k.

Define $\mathbf{g}_k := [g_{0,k}, \cdots, g_{L-1,k}]^T$, $\mathbf{y}_k := [Y_{0,k}, \cdots, Y_{N-1,k}]^T$, $\mathbf{v}_k := [\zeta_{0,k}, \cdots, \zeta_{N-1,k}]^T$, and $\mathbf{x}_k = [X_{0,k}, \cdots, X_{N-1,k}]^T$, where $(\cdot)^T$ denotes the matrix transpose operation. Furthermore, let $\mathbf{C}_k$ be an N-by-N *Circulant Matrix*, whose first column is $\mathbf{x}_k$ [56]. It is well known that $\mathbf{C}_k = \mathbf{F}^{-1}\text{diag}(\mathbf{Fx}_k)\mathbf{F}$, where $\text{diag}(\cdot)$ and $(\cdot)^{-1}$ denote, respectively, the diagonal matrix and the matrix inversion operation, and where $\mathbf{F}$ is the linear transform matrix for the N-point DFT. Equation (1.1) suggests that $\mathbf{x}_k = \mathbf{F}^{-1}\mathbf{s}_k$, where $\mathbf{s}_k = [S_{0,k}, \cdots, S_{N-1,k}]^T$. So $\mathbf{C_k} = \mathbf{F}^{-1}\text{diag}(\mathbf{s_k})\mathbf{F}$.

Equation (1.8) can be rewritten as the following

$$\mathbf{y}_k = \mathbf{C}_k \begin{pmatrix} \mathbf{g}_k \\ \mathbf{0}_{N-L} \end{pmatrix} + \mathbf{v}_k \tag{1.9}$$
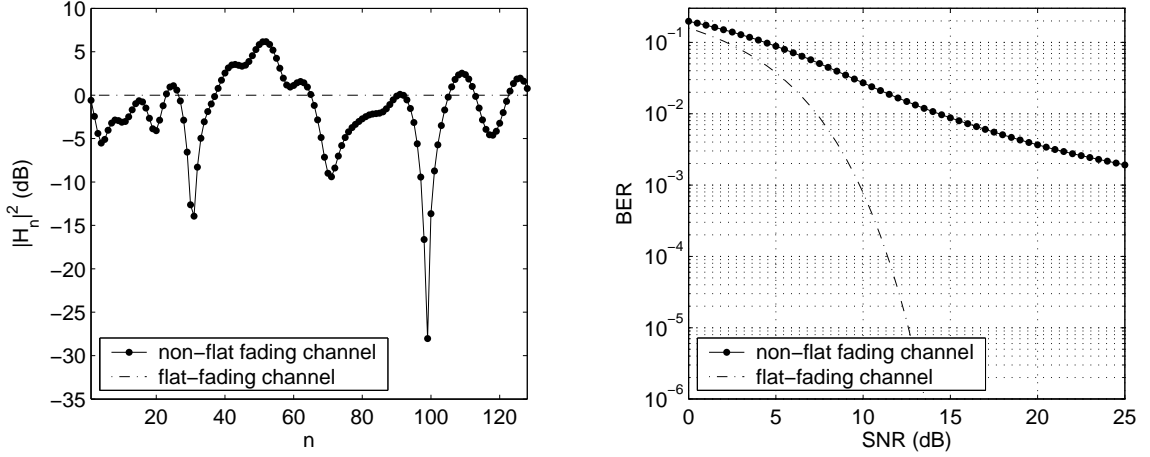
Figure 1.2: Performance of OFDM systems with uniform bit and power allocation

where $\mathbf{0}_{N-L}$ is a column vector of size $(N-L)$, whose elements are all zero. Using (1.9), the output of the DFT module in Figure 1.1 can be written as follows:

$$
\begin{aligned}
\mathbf{r}_k &= \mathbf{F} \left\{ \mathbf{F}^{-1}\mathrm{diag}(\mathbf{s}_k)\mathbf{F} \begin{pmatrix} \mathbf{g}_k \\ \mathbf{0}_{N-L} \end{pmatrix} + \mathbf{v}_k \right\} \\
&= \mathrm{diag}(\mathbf{s}_k)\mathbf{F}_L\mathbf{g}_k + \mathbf{F}\mathbf{v}_k \\
&= \mathrm{diag}(\mathbf{F}_L\mathbf{g}_k)\mathbf{s}_k + \mathbf{F}\mathbf{v}_k
\end{aligned}
\tag{1.10}
$$

where $\mathbf{F}_L$ is an N-by-L matrix containing the first L columns of the matrix $\mathbf{F}$. Let $\mathbf{h}_k = [H_{0,k}, \cdots, H_{N-1,k}]^T = \mathbf{F}_L\mathbf{g}_k$. Equation (1.10) suggests that, using OFDM, the received complex symbols are given by $R_{n,k} = H_{n,k}S_{n,k} + W_{n,k}$, $\forall k$, $\forall n = 0, \cdots, N-1$, where the noise part $W_{n,k}$ is the nth element of $\mathbf{F}\mathbf{v}_k$. It is clear that, the sequence $\mathbf{h}_k$ defined previously represents the discrete CFR of the OFDM system, and it is obtained by applying N-point DFT to the discrete channel impulse response (CIR) $\mathbf{g}_k$, which is defined in (1.7).

1.3 Motivation of Resource Allocation in OFDM Systems

In conventional OFDM systems, the size of modulation signal sets and the associated transmit power are the same for all subcarriers. The main drawback of this approach is its poor performance in terms of bit error probability under frequency-selective ("non-flat") fading channels. Figure 1.2 highlights this problem by comparing the system's bit error rate (BER) over a given non-flat fading channel with that of a flat fading channel. In this figure, QPSK modulation has been used for all subcarriers. The plot on the left hand side provides a snap shot of the channel power gain $\{|H_{n,k}|^2\}_{n=0}^{N-1}$ during block k, and the plot on the right hand side illustrates for both channels the

system BERs under different SNR. It is observed that the efficiency of this OFDM system is very low if channel is non-flat fading. This is attributed to the fact that, under the non-flat fading channel, there exist weak subcarriers, whose power gain is much less than the average level and result in high error rate. These weak subcarriers tend to dominate the overall performance of the whole OFDM system such that, in order to have a low BER, the power of all subcarriers need to be increased resulting in a very low efficiency.

A technique known as *Adaptive Modulation* can be used in OFDM systems to solve the problem mentioned previously. The idea of adaptive modulation can be traced back to the early studies for the theoretical limit of achievable data rate, i.e., the capacity, of a general fading channel. Gallager (1968) had shown in [64] that, a non-uniform power distribution determined by the attenuation profile of the fading channel is necessary to achieve channel capacity. For an OFDM system with frequency-selective fading channels, the capacity-achieving power adaptation should be performed along the subcarriers. Moreover, the data rate of each subcarrier also need to be adjusted to match the capacity of individual subchannel. This gives rise to the scheme of bit and power allocation for OFDM systems, which proposes to select for each subcarrier a proper size of modulation signal set and transmit power according to the instantaneous channel response such that the desired quality of service can be achieved with the maximum spectral efficiency. Figure 1.3 illustrates an example of bit and power allocation scheme [1] designed for the non-flat fading channel profile shown in Figure 1.2. In this case, the number of bits sent by each OFDM block is the same as that of Figure 1.2. The performance of this bit and power allocation scheme is compared with the that of the flat fading channel with uniform bit and power allocation, and the results are plotted in Figure 1.3. It can be seen by comparing performance curves in Figure 1.2 and Figure 1.3 that the OFDM system using resource allocation has a much higher spectral efficiency than the system without it.

In order to create bit and power allocation schemes for a specific OFDM system, it is necessary for the transmitter to have some knowledge of the channel state information (CSI), such as the CFR. According to Figure 1.1, the OFDM receiver performs channel estimation and thus has the knowledge of CSI. In practice, the transmitter is also able to obtain the knowledge of CSI. One option is to transmit CSI from the receiver to the transmitter through a dedicated reverse channel known as "control channel". Another method is to use the Time Division Duplex (TDD) structure, where each OFDM terminal has both a transmitter and a receiver operating in the same radio frequency. In order to avoid confliction between transmission and receiving, the operation mode of the transceiver switches with a time-division fashion. In this case, both directions have similar radio environment and should result in CSIs akin to each other. Thus, in this case, the CSI from the receiver is also valid to the transmitter for bit and power allocation.

---

[1]The method of generating this bit and power allocation is discussed in Chapter 3
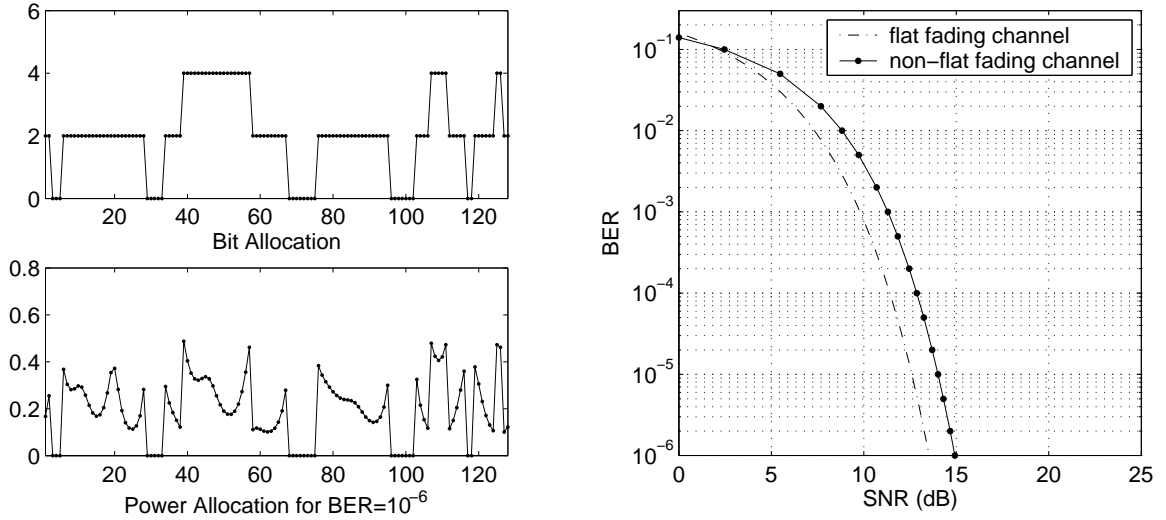
Figure 1.3: Example of bit and power allocation for a non-flat fading channel

Generally speaking, in order to exploit the full potential of a resource allocation scheme in OFDM system, the transmitter should have a complete and perfect knowledge of the CSI. In wireline communication systems, this condition may be satisfied since the wireline channel is static or extremely slow-varying, which allows the receiver to achieve perfect channel estimation and feed back the complete CSI to the transmitter. However, for most of the wireless communication systems, this assumption is not realistic because the physical channel is time-varying and achieving perfect channel estimation is almost impossible. Moreover, in case of time-varying channels, the extra signalling overhead become overwhelming since the CSI need to be to transmitted back to the receiver. Therefore, in the scenario of time-varying wireless channels, imperfect CSI is assumed to be used for resource allocation. In this dissertation, both resource allocation methods assuming perfect and imperfect CSI have been addressed.

1.4 Introduction to the Multiband Keying UWB System

Multiband Keying, which is also known as Spectral Keying [2], is a novel modulation scheme optimized for UWB systems. It proposes to divide the whole UWB band into multiple subbands having a bandwidth greater than 500MHz. For each subband, a specifically designed pulse signal can be used to transmit data through this subband. Figure 1.4 shows an example of such pulse signal associated with the subband having a center frequency of 4GHz. In the time domain, a complete Multiband Keying symbol consists of a "pulse time" and a "guard time", where multiple phase-modulated pulses like that of Figure 1.4 are transmitted during the pulse time, and where no

---

[2]Spectral Keying[TM] is a registered trademark of General Atomics

8
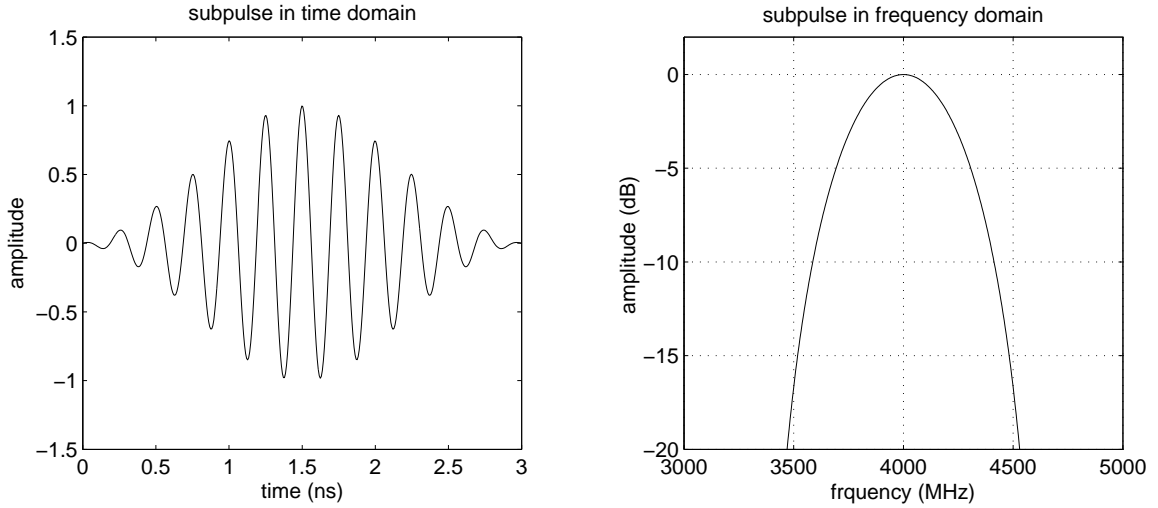
Figure 1.4: Pulse signal used for the Multiband Keying UWB system

transmission occurs during guard time for the purpose of avoiding ISI. Figure 1.5 illustrates in details the structure of a typical Multiband Keying signal. It is noted from this figure that, the pulse time in each symbol is divided into several non-overlapping subpulses, within which the modulated signals from *different* subbands are transmitted. Clearly, the Multiband Keying scheme can be viewed as a special form of fast frequency hopping (FH).

An important property of the Multiband Keying system is that, for each symbol, the transmitted subpulses are chosen from different subbands. As a result, pulse signals from the same subband are separated with at least one guard time, which is larger than the delay spread of the channel, and this prevents ISI. Although there exists interference among subpulses from different subbands, they can be eliminated at the receiver using a bank of bandpass filters (BPF) tuned for different subbands. In other words, the problem caused by ISI is negligible in Multiband Keying systems. Moreover, a RAKE receiver without extra hardware can be used in this system to capture much of the signal power [44, 45].

The main drawback of Multiband Keying systems is the difficulty of achieving high data rate due to its low duty cycle with the application of zero-padded guard intervals. For example, when used for a short range indoor UWB system, the duty cycle of the Mutiband Keying signals are generally limited to be less than 50%. In order to mitigate this problem, in each symbol, information bits is not only modulated on to the phases of subpulses but also on to the *sequences of subbands* associated with these subpulses. In other words, the sequences of bands during pulse time of each symbol is also encoded by data, which increases the number of information bits conveyed by each symbol. However, this approach also increases the complexity of demodulation, especially when a maximum likelihood (ML) detection is required. The

9
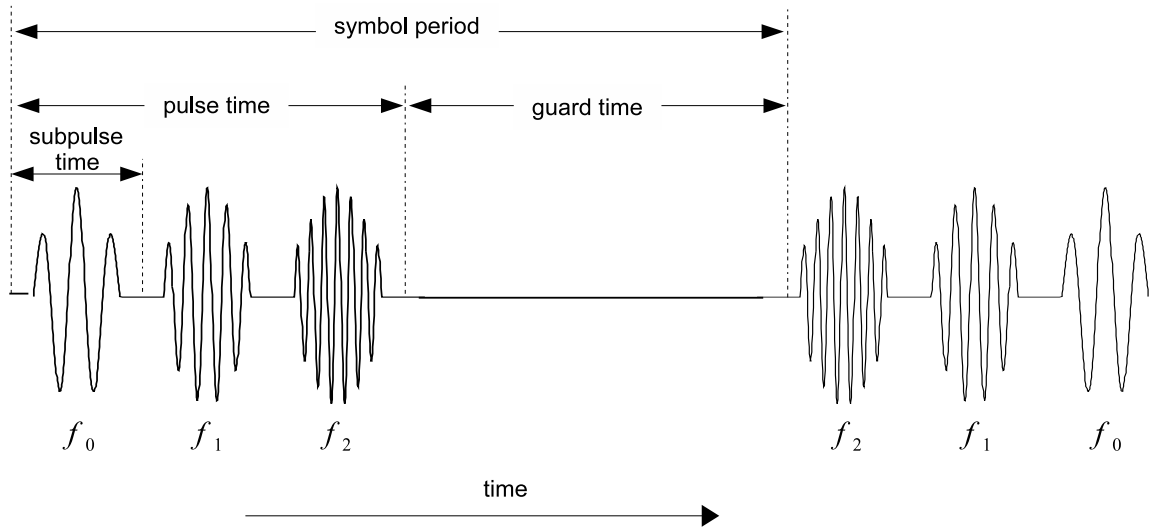
Figure 1.5: Basic structure of the Multiband Keying symbols

complexity issue of the ML receiver of Multiband Keying signals will be discussed in this dissertation.

1.5 Organization of the Dissertation

This dissertation is organized as follows. In Chapter 1, a brief introduction to the OFDM system is presented with a focus on its properties over quasi-stationary frequency-selective fading channels. Furthermore, the problem of high bit error in un-coded OFDM systems has been highlighted as a motivation for resource allocation. Subsequently, an introduction to the Multiband Keying modulation scheme used for UWB systems is also covered in this chapter.

Chapter 2 investigates parametric modeling of wideband and ultra wideband wire-less channels in frequency domain, where, by uniform sampling of the channel frequency response, an equivalent discrete channel can be obtained. It is shown that the parametric modeling in the frequency domain is possible, if and only if the uni-formly spaced CFR samples satisfy the wide-sense stationary (WSS) condition that is equivalent to the uncorrelated scattering (US) condition for the discrete CIR. This new WSS-US condition is fulfilled if the underlying continuous-time wideband or ul-tra wideband channel is WSSUS with independent path gains and arrival times. It is also shown that there exists an analytic relationship between the power spectral density (PSD) of the uniformly spaced CFR samples and the power profile of the discrete CIR that satisfies the WSS-US condition. Based on these results, it is shown from analysis and simulation that the wideband and ultra wideband channels can be adequately modelled by low order autoregressive (AR) and/or autoregressive moving average (ARMA) models in the frequency domain.

In Chapter 3, the problem of resource allocation for multiuser OFDM systems has been considered assuming perfect knowledge of the CSI. This problem has been considered by many researchers, and there exist different solutions to this problem in the literature. The main goal of Chapter 3 is to find a method with nearly optimal performance and lower complexity than the methods reported previously. In order to achieve a numerically efficient solution, the problem is divided into two separate optimization problems: one for subcarrier allocation and one for bit and power allocation. Heuristic algorithms are then developed for each problem. The performance and the computational complexity of the proposed algorithms are compared with existing methods from extensive simulation.

In Chapter 4, we extend the scope of resource allocation in OFDM systems to the time-varying channels, where only imperfect knowledge of the CSI is assumed. The bit and power allocation scheme proposed in Chapter 3, which assumes perfect CSI, is shown to experience significant performance loss when the channel is actually time-varying. The error in CSI caused by the delayed channel estimates has been recognized as the main reason for this problem. The relationship between channel variation rate and the accuracy of CSI denoted by normalized mean square error (NMSE) has been analyzed in this chapter. To solve this problem, we propose to first reduce errors in CSI using *channel prediction*, then exploit a bit and power allocation scheme, which is robust to the imperfect CSI. The channel predictors based on Wiener filter and adaptive filters have been discussed in Chapter 4. Different resource allocation schemes based on imperfect CSI are also investigated. Simulation results have confirmed that, at least for slowly time-varying Rayleigh fading channels, the spectral efficiency of the proposed system can be very close to that of the system with perfect CSI knowledge.

In Chapter 5, we concern the Multiband Keying system using M-ary Phase Shift Keying (MPSK) in the subpulses of each symbol. The optimal receiver for Multiband Keying signals over AWGN channel and the associated ML decision rule have been developed in this chapter. The performance of the ML receiver has been evaluated through analysis and simulation. Then, a computationally efficient suboptimal algorithm based on a depth-first search (DFS) is introduce to simplify the demodulation of Multiband Keying signals.

Finally, in Chapter 6, we draw conclusions and suggest some prospective topics for future research.

CHAPTER 2. PARAMETRIC MODELING OF WIDEBAND AND ULTRA WIDEBAND CHANNELS IN FREQUENCY DOMAIN[1]

2.1 Introduction

It is known that most modern technologies are model based. Due to the randomly varying nature of the wireless channel with respect to time, it is necessary to develop statistical models with a minimum number of parameters to regenerate or predict the measured channel behavior accurately. This is entailed not only by computer simulations for wireless channels, but also by channel estimation in wireless communications. For this reason modeling of wireless channels has received considerable attention. The early work of Bello [3] on randomly time variant channels is representative in characterizing the wide-sense stationary (WSS) channel, uncorrelated scattering (US) channel, and WSSUS channel. Such characterizations are obtained for the radio propagation gains based on time domain measurements. Since then statistical modeling of the radio channels has been an important research topic. Indeed a statistical model is proposed in [20] for urban mobile radio where the measurement data were collected from a global experiment in a research laboratory. For indoor multipath propagation, a different statistical model is proposed in [18] that has its roots in the earlier model in [20]. Specifically, the model in [18] assumes that the paths arrive in clusters and both paths and clusters form Poisson processes. See also [9, 15, 16] on channel measurements and modeling.

While the time domain approach for modeling wireless channels is more direct and has been effective, it requires more parameters to describe the wideband and ultra wideband channels. A more interesting development in channel modeling is the low order AR (autoregressive) model in frequency domain as proposed in [12] for wideband indoor radio propagation. Similar AR models in frequency domain are also employed more recently to model ultra wideband channels in [10, 11, 19]. Based on the large amount of experimental measurement data and extensive computer simulations, these papers show that the uniformly spaced samples of the CFR (channel frequency response) for wideband and ultra wideband channels can be modeled very accurately by low order AR processes. Recall that uniform sampling of the CFR results in an equivalent discretized channel with the discrete CIR (channel impulse response) obtained from the inverse DFT (discrete Fourier transform) of the CFR samples. Because of the low order, the AR model in the frequency domain requires many fewer parameters to represent the channel than its time domain counterpart.

It has additional advantages in that the frequency domain measurement system provides coherent measurements and the frequency domain model can be simulated on the computer considerably more easily. However the channel modeling results in [11, 12, 19] also raise a natural question: why can the CFR samples of the wideband and ultra wideband channels be described by low order AR models? Such a question is fundamental but difficult to answer through the experimental method and deserves further investigation. Our goals in this chapter are to present a theoretical justification for the low order AR modeling and to derive an equivalent condition on the feasibility of low order parametric modeling in frequency domain. An important contribution of this chapter is the development of periodic random processes which help to deepen our understanding of the wireless channels and enable us to derive new results in modeling of wideband and ultra wideband channels in the frequency domain. It is shown that the parametric modeling in the frequency domain is possible, if and only if the discretized wireless channel fulfills the WSS-US (wide-sense stationary and uncorrelated scattering) condition. It is also shown that there exists an analytic relation between the PSD (power spectral density) of the CFR samples and the power delay profile of the discrete CIR for wireless channels that satisfy the WSS-US condition. The results in this chapter provide new insights in channel modeling and answer the question of why low order AR models are adequate in modeling wideband and ultra wideband channels in the frequency domain.

2.2   Preliminaries on Channel Modeling

Nearly all radio channels of interest are more or less time-variant and time dispersive in nature. For wideband channels, they are characterized by multipath propagation where a number of reflected or scattered radio rays arrive at the receiver end. A widely used channel model is the following continuous-time CIR:

$$c(t; \tau) = \sum_{k=0}^{L-1} c_k(t)\delta\left(\tau - \tau_k(t)\right) \tag{2.1}$$

where $\delta(\cdot)$ is the Dirac delta function and time t is real valued. The finite delay sequence $\{\tau_k(t)\}_{k=0}^{L-1}$ is strictly increasing with respect to k for all time t and is given by

$$\tau_k(t) = \tau_p(t) + \tau_{d_k}(t), \quad 0 \le k < L, \tag{2.2}$$

with $\tau_p(t)$ the propagation delay and $\tau_{d_k}(t)$ the instantaneous differential delay [57]. The early work on radio channels indicates that the kth path gain $c_k(t)$ is a WSS random process for each integer k, and $\{c_k(t)\}_{k=0}^{L-1}$ are uncorrelated or US at all time t [3]. This gives rise to WSSUS channels.

While the CIR in (2.1) is only an approximation to the continuous-time radio channel due to the use of Dirac delta functions, it encompasses many practical channel models including (a) Rayleigh fading (wideband) channels [59] of which the amplitude

$|c_k(t)|$ has Rayleigh distribution and the phase $\angle c_k(t)$ is uniformly distributed over $[0, 2\pi)$, and (b) ultra wideband channels [18] in which the power gain for each ray is log-normal distributed and paths arrive in clusters: the arrival times of clusters and path delays within each cluster form two independent Poisson processes. Both channel models will be the focus of this chapter. Channel modeling in the time domain notwithstanding, more parameters are required in describing the wideband and ultra wideband channels. A more interesting development is the frequency domain approach in [11, 12, 19] where the uniformly spaced CFR samples are shown to satisfy some low order AR models based on large amounts of experimental measurement data for wideband and ultra wideband channels that is contrast to the time domain approach. In this section we give a preliminary analysis on the uniformly spaced CFR samples before proceeding to our main results on low order parametric modeling in the frequency domain.

For wideband and ultra wideband wireless channels, both $\{c_k(t)\}_{k=0}^{L-1}$ and $\{\tau_k(t)\}_{k=0}^{L-1}$ of the continuous-time CIR in (2.1) normally change very slowly. This holds true especially for indoor channels. For this reason, we assume that $c_k(t) = c_k$ and $\tau_k(t) = \tau_k$ through the duration of interest for $0 \le k < L$. Applying the continuous-time Fourier transform to the CIR in (2.1) yields the following CFR:

$$C(f) = \sum_{k=0}^{L-1} c_k e^{-j2\pi\tau_k f}, \quad j = \sqrt{-1}. \tag{2.3}$$

Taking uniformly spaced samples over the channel bandwidth as $f_i = f_L + if_{\mathrm{BW}}/N$ for $0 \le i < N$ where f_L is the low frequency edge and f_{BW} is the bandwidth. Then we obtain the uniformly spaced N-point CFR samples as follows:

$$
\begin{aligned}
H_N(i) &= C(f_i) = \sum_{k=0}^{L-1} c_k e^{-j2\pi\tau_k(f_L + if_{\mathrm{BW}}/N)} \\
&= \sum_{k=0}^{L-1} \left[c_k e^{-j2\pi\tau_k f_L} \right] e^{-j2\pi i \tau_k f_{\mathrm{BW}}/N}.
\end{aligned}
\tag{2.4}
$$

Suppose that $N >> L$ so that $\{\lfloor \tau_k f_{\mathrm{BW}} \rfloor\}_{k=0}^{L-1}$ are all distinct and strictly bounded by N where $\lfloor x \rfloor$ takes the integer part of x. Let

$$
h_{\ell_k} = \begin{cases} c_k e^{-j2\pi\tau_k f_L}, & \text{if } \tau_k f_{\mathrm{BW}} = \ell_k + \varepsilon_{\ell_k}, \\ 0, & \text{elsewhere} \end{cases}
\tag{2.5}
$$

where $0 \le \varepsilon_{\ell_k} < 1$, $\ell_k = \lfloor \tau_k f_{\mathrm{BW}} \rfloor$, and $0 \le \ell_k < N$. Let $W_N = e^{-j2\pi/N}$. Then we have a new expression for the N-point uniformly spaced CFR samples:

$$
\begin{aligned}
H_N(n) &= \sum_{\ell_k=0}^{N-1} h_{\ell_k} W_N^{n\ell_k} W_N^{n\varepsilon_{\ell_k}} \\
&= \sum_{\ell_k=0}^{N-1} h_{\ell_k} W_N^{n(\ell_k + \varepsilon_{\ell_k})}, \quad 0 \le n < N.
\end{aligned}
\tag{2.6}
$$

The above discretizes the continuous-time channel in the frequency domain. Computing N-point inverse DFT for $\{H_N(n)\}_{n=0}^{N-1}$ gives

$$
\begin{aligned}
h_N(m) &= \tfrac{1}{N} \sum_{n=0}^{N-1} H_N(n) W_N^{-mn} \\
&= \sum_{\ell_k=0}^{N-1} h_{\ell_k} \left[\tfrac{1}{N} \sum_{n=0}^{N-1} W_N^{-n(m-\ell_k-\varepsilon_{\ell_k})} \right], \\
& \qquad 0 \le m < N.
\end{aligned}
\tag{2.7}
$$

Hence $\{h_N(m)\}_{m=0}^{N-1}$ can be regarded as an equivalently discretized CIR. Note that $h_N(m) \ne h_m$ in general and more importantly $\{h_N(m)\}$ are uniformly spaced in the time domain but $\{h_{\ell_k}\}$ are not.

It is noted that the discrete samples of the CFR such as in (2.6) can be experimentally determined. Indeed in [11, 12, 19], the uniformly spaced CFR samples are measured for wideband channels and ultra wideband channels and are treated as random processes with respect to the frequency index. Moreover these reports show that the uniformly spaced CFR samples satisfy low order (1st order or 2nd order) AR models. That is, there exists some constant α or (α_1, α_2) such that

$$
H_N(n) = \alpha H_N(n-1) + V_N(n) \quad \text{or} \tag{2.8}
$$

$$
H_N(n) = \alpha_1 H_N(n-1) + \alpha_2 H_N(n-2) + V_N(n) \tag{2.9}
$$

for some AWGN (additive white Gaussian noise) process $\{V_N(n)\}_{n=0}^{N-1}$. A natural question is: why can uniformly spaced CFR samples for wideband and ultra wideband channels be described by low order AR models? Let f_1 and f_2 be two samples of the CFR such that $(f_1 - f_2) = (n_1 - n_2)f_{\text{BW}}/N = nf_{\text{BW}}/N$ with $n = (n_1 - n_2)$ integer. Denote $\text{E}\{\cdot\}$ as the operation of expectation and $\bar{\cdot}$ as complex conjugate. By assuming independence of $\{c_k\}$ and $\{\tau_k\}$, it is easy to verify that

$$
\begin{aligned}
\text{E}\left\{ C(f_1)\bar{C}(f_2) \right\} &= \sum_{k=0}^{L-1} \sigma_{c_k}^2 \, \text{E}\left\{ e^{-j2\pi(f_1-f_2)\tau_k} \right\} \\
&= \sum_{k=0}^{L-1} \sigma_{c_k}^2 \, \text{E}\left\{ W_N^{n(\ell_k+\varepsilon_{\ell_k})} \right\} \\
&= \sum_{\ell_k=0}^{N-1} \sigma_{h_{\ell_k}}^2 \, \text{E}\left\{ W_N^{n(\ell_k+\varepsilon_{\ell_k})} \right\} \\
&=: R_H(n).
\end{aligned}
\tag{2.10}
$$

Therefore CFR samples are WSS processes that can be modeled as output of some linear time-invariant system driven by some WSS white noises. However being WSS processes alone does not imply that the CFR samples $\{H_N(n)\}$ are low order AR processes. A theoretical proof is entailed to justify the low order AR modeling for uniformly spaced CFR samples.

We are motivated by the channel modeling results in [11, 12, 19] to investigate why and under what condition the low order parametric modeling is possible for wideband and ultra wideband channels. To accomplish this goal we note that the CFR samples in (2.6) have finite length N. With the use of DFT and inverse DFT, it is possible to extend the uniformly spaced CFR samples in (2.6) and the discretized CIR samples in (2.7) to periodic sequences with period N. Hence both become periodic random processes. We will first investigate the periodic random processes in the next section and then apply the results on periodic random processes to model the uniformly spaced CFR samples. Our results on channel modeling in the frequency domain shed some new light on the results reported in [11, 12, 19] and provide a theoretical justification for low order parametric modeling of wideband and ultra wideband channels in the frequency domain.

2.3 Periodic Random Processes

In this section, we will first introduce periodic random processes, and then study dynamic systems whose inputs and outputs are periodic sequences. A periodic random process, with period M and denoted by $\{v_M(k)\}$, is the periodic extension of the random variables $\{v_M(k)\}_{k=0}^{M-1}$. For convenience, in the sequel we assume that all random processes and random variables are zero-mean. The process $\{v_M(k)\}$ is said to be periodic uncorrelated, if

$$\mathrm{E}\{v_M(k)v_M(i)^*\} = \mathrm{E}\{|v_M(k)|^2\}\delta_M(k-i), \qquad (2.11)$$

where superscript * denotes complex conjugate and transpose, and $\delta_M(k)$ is the periodic Kronekar delta function, i.e.,

$$\delta_M(n) = \begin{cases} 1, & \text{if } n = \ell M, \\ 0, & \text{if } n \neq \ell M, \end{cases} \qquad (2.12)$$

for any integer ℓ. The periodic random sequence $\{v_M(k)\}$ is called periodic WSS, if

$$R_M^{(v)}(n) = \mathrm{E}\{v_M(k)v_M(k-n)^*\} \qquad (2.13)$$

is independent of k. A periodic WSS sequence $\{v_M(k)\}$ is said to be periodic uncorrelated if

$$R_M^{(v)}(n) = \mathrm{E}\{v_M(k)v_M(k-n)^*\} = R_v\delta_M(n), \qquad (2.14)$$

for some $R_v > 0$. Suppose that the transfer function $G(z)$ is given by

$$G(z) = \sum_{k=0}^{\infty} g(k)z^{-k}, \qquad \sum_{k=0}^{\infty} |g(k)| < \infty. \qquad (2.15)$$

Then $G(z)$ represents a causal and stable dynamic system. For a periodic random process $\{v_M(k)\}$ as input, its output $\{y_M(k)\}$ is also periodic, and there holds

$$
\begin{aligned}
y_M(k) &= \sum_{s=0}^{\infty} g(s) v_M(k-s) \\
&= \sum_{\ell=0}^{\infty} \sum_{i=0}^{M-1} g(\ell M + i) v_M(k - i - \ell M) \\
&= \sum_{i=0}^{M-1} \left(\sum_{\ell=0}^{\infty} g(\ell M + i) \right) v_M(k-i) \\
&= \sum_{i=0}^{M-1} g_M(i) v_M(k-i) \\
&= : g_M(k) \circledast v_M(k)
\end{aligned}
\tag{2.16}
$$

which is the periodic convolution of the input, and the periodic impulse response, given by

$$
g_M(i) = \sum_{k=0}^{\infty} g(kM + i), \quad i = 0, 1, \cdots, M-1.
\tag{2.17}
$$

Because of the stability assumption, $g_M(i)$'s are bounded for each i. Furthermore it can be shown that $\{g_M(k)\}_{k=0}^{M-1}$ is the M-point inverse DFT of $\{G(W_M^{-i})\}_{i=0}^{M-1}$. That is, $\{g_M(k)\}_{k=0}^{M-1}$ and $\{G(W_M^{-i})\}_{i=0}^{M-1}$ form a DFT pair. Applying the M-point DFT on both sides of (2.16) yields

$$
Y_M(i) = G(W_M^{-i}) V_M(i), \quad i = 0, 1, \cdots, M-1,
\tag{2.18}
$$

where $\{V_M(i)\}_{i=0}^{M-1}$ and $\{Y_M(i)\}_{i=0}^{M-1}$ are the M-point DFT's of the input and output, respectively. We have the following theorem.

Theorem 2.1 *Suppose that $\{y_M(k)\}$ is a periodic random process with zero mean. Then*

1. *The process $\{y_M(k)\}$ is periodic WSS if and only if its M-point DFT $\{Y_M(i)\}$ is periodic uncorrelated.*

2. *Let ACS (autocorrelation sequence) and PSD (power spectral density) of $\{y_M(k)\}$ be defined by*

$$
R_M^{(y)}(n) = \mathrm{E}\{y_M(k) y_M(k-n)^*\}, \quad and
\tag{2.19}
$$

$$
\Phi_M^{(y)}(i) = \sum_{n=0}^{M-1} R_M^{(y)}(n) W_M^{ni},
\tag{2.20}
$$

respectively. Then

$$
\Phi_M^{(y)}(i) = \frac{1}{M} \mathrm{E}\{|Y_M(i)|^2\}, \quad i = 0, 1, \cdots, M-1.
\tag{2.21}
$$

3. If the ACS and PSD are estimated via

$$\hat{R}_M^{(y)}(n) = \frac{1}{M} \sum_{k=0}^{M-1} y_M(k) y_M(k-n)^*, \quad and \tag{2.22}$$

$$\hat{\Phi}_M^{(y)}(i) = \sum_{n=0}^{M-1} \hat{R}_M^{(y)}(n) W_M^{ni}, \tag{2.23}$$

respectively, then

$$\hat{\Phi}_M^{(y)}(i) = \frac{1}{M} |Y_M(i)|^2, \quad i = 0, 1, \cdots, M-1. \tag{2.24}$$

Proof: We prove the three statements in the theorem as follows.

1. If the periodic random process $\{y_M(k)\}$ is periodic WSS, then we have

$$E\{Y_M(i) Y_M(i-k)^*\}$$
$$= \sum_{s=0}^{M-1} \sum_{\ell=0}^{M-1} E\{y_M(s) y_M(\ell)^*\} W_M^{is} W_M^{-\ell(i-k)}$$
$$= \sum_{s=0}^{M-1} \sum_{\ell=0}^{M-1} R_M^{(y)}(s-\ell) W_M^{(s-\ell)i} W_M^{\ell k}.$$

Setting $n = s - \ell$ and using the periodicity property we get

$$E\{Y_M(i) Y_M(i-k)^*\}$$
$$= \sum_{n=0}^{M-1} R_M^{(y)}(n) W_M^{in} \sum_{\ell=0}^{M-1} W_M^{\ell k} \tag{2.25}$$
$$= \left(M \sum_{n=0}^{M-1} R_M^{(y)}(n) W_M^{in} \right) \delta_M(k),$$

where we have used the identity

$$\frac{1}{M} \sum_{\ell=0}^{M-1} W_M^{\ell k} = \delta_M(k). \tag{2.26}$$

It follows from (2.25) that the DFT of any periodic WSS process is periodic uncorrelated. Conversely suppose $\{Y_M(i)\}$ has zero mean and is periodic uncorrelated. Then direct calculation yields

$$E\{y_M(k) y_M(k-n)^*\}$$
$$= \frac{1}{M^2} \sum_{i=0}^{M-1} \sum_{\ell=0}^{M-1} E\{Y_M(i) Y_M(\ell)^*\} W_M^{-ik} W_M^{\ell(k-n)}$$
$$= \frac{1}{M} \sum_{i=0}^{M-1} \left(\frac{1}{M} E\{|Y_M(i)|^2\} \right) W_M^{-in} = R_M^{(y)}(n),$$

which is indeed periodic WSS.

18

2. The above and (2.25) also show that for $i = 0, 1, \cdots, M-1$,

$$\Phi_M^{(y)}(i) = \sum_{n=0}^{M-1} R_M^{(y)}(n) W_M^{in} = \frac{1}{M} \text{E}\{|Y_M(i)|^2\},$$

which establishes (2.20). By the inverse DFT of $\{\Phi_y(i)\}$ at $k = 0$, we have

$$R_M^{(y)}(0) = \text{E}\{|y_M(n)|^2\} = \frac{1}{M} \sum_{i=0}^{M-1} \Phi_M^{(y)}(i).$$

Therefore $\{\Phi_M^{(y)}(i)\}$ is indeed the PSD of $\{y_M(k)\}$ distributed over M spectral samples.

3. For the estimated ACS and PSD in (2.24), by direct calculation we have,

$$
\begin{aligned}
\hat{\Phi}_M^{(y)}(i) &= \sum_{n=0}^{M-1} \hat{R}_M^{(y)}(n) W_M^{ni} \\
&= \frac{1}{M} \sum_{n=0}^{M-1} \sum_{k=0}^{M-1} y_M(k) y_M(k-n)^* W_M^{ni} \\
&= \frac{1}{M} \sum_{k=0}^{M-1} y_M(k) W_M^{ki} \times \\
&\qquad \left(\frac{1}{M} \sum_{n=0}^{M-1} y_M(k-n) W_M^{(k-n)i} \right)^* \\
&= \frac{1}{M} |Y_M(i)|^2, \quad i = 0, 1, \cdots, M-1,
\end{aligned}
$$

which establishes (2.24). ∎

It is important to learn that for a zero-mean periodic random process to be periodic WSS, it is both necessary and sufficient for its DFT to be periodic uncorrelated. This fact impacts the channel modeling in the next section, and reveals the reason why low order parametric modeling is possible for uniformly spaced CFR samples in the case of wideband and ultra wideband channels [11, 12, 19]. The next result is also important in that it shows that any periodic zero-mean Gaussian WSS process can be generated by filtering a periodic zero-mean and unit-variance independent identically-distributed (i.i.d.) Gaussian process. By convention, q^{-1} is used to denote the delay operator.

Theorem 2.2 *Suppose that $\{y_M(k)\}$ is a periodic WSS Gaussian process with zero mean. Then there exists a stable ARMA model $G(q)$ such that $\{y_M(k)\}$ is the output of the ARMA model $G(q)$ for some input $\{v_M(k)\}$, which is a periodic i.i.d. Gaussian process with zero mean and unit variance.*

Proof: We note that if $\{y_M(k)\}$ is a periodic WSS Gaussian process with zero mean, then its PSD is given by (2.20), and there exists a continuous PSD function of bounded variation

$$\Psi(e^{j2\pi\phi}) = \sum_{k=-\infty}^{\infty} R_k e^{-j2k\pi\phi} \geq 0 \quad \forall\, \phi \in [0,\ 2\pi],$$

such that $\Psi(W_M^{-i}) = \Phi_M^{(y)}(i)$ for $i = 0, 1, \cdots, M - 1$ in light of the well-known Weierstrass Theorem in approximation theory. In fact the degree of $\Psi(z)$ can be made finite. Performing spectral factorization on $\Psi(z)$ yields $\Psi(z) = G(z)[G(z^{*^{-1}})]^*$ where $G(z)$ has all its poles strictly inside the unit circle and avoids zeros outside the unit circle. It follows that $G(q)$ is a stable ARMA model, satisfying $|G(W_M^{-i})|^2 = \Phi_M^{(y)}(i)$ for $i = 0, 1, \cdots, M - 1$. Let $\{v_M(k)\}$ be a periodic i.i.d. Gaussian random process with zero mean and unit variance. It follows that for $k = 0, 1, \cdots, M - 1$,

$$\widehat{y}_M(k) = g_M(k) \circledast v_M(k) = \sum_{i=0}^{M-1} g_M(i)v_M(k - i)$$

is a periodic WSS Gaussian process with zero mean, whose first and second order statistics are identical to those of $\{y_M(k)\}$ since $|G(W_M^{-i})|^2 = \Phi_M^{(y)}(i)$ for each i. Thus the process $\{y_M(k)\}$ can be generated by passing $\{v_M(k)\}$ through a stable ARMA filter. ∎

The results on periodic random processes developed in this section are closely parallel to those of aperiodic random processes. However, not every result in this section has its correspondence in the conventional theory of random processes.

2.4   Channel Modeling in Frequency Domain

We are now ready to answer the question raised earlier in the chapter: why can wideband and ultra wideband channels be described by low order AR models in the frequency domain? The following is the main result of this section.

Theorem 2.3 *Let $\{H_N(n)\}_{n=0}^{N-1}$ be the N-point uniformly spaced CFR samples as in (2.6) and its N-point inverse DFT be $\{h_N(m)\}_{m=0}^{N-1}$ that is the discretized CIR as given in (2.7). Then $\{H_N(n)\}_{n=0}^{N-1}$ and $\{h_N(m)\}_{m=0}^{N-1}$ form a DFT pair and can be extended into periodic sequences. Suppose that $\{H_N(n)\}_{n=0}^{N-1}$ is a zero-mean periodic WSS process. Define its discrete ACS and PSD by*

$$R_H(k) = \mathrm{E}\{H_N(n)H_N(n - k)^*\}, \quad and \qquad (2.27)$$

$$\Phi_H(W_N^{-m}) = \sum_{k=0}^{M-1} R_H(k)W_N^{km}, \qquad (2.28)$$

respectively. Then

$$\Phi_H(W_N^{-m}) = N\mathrm{E}\{|h_N(N-m)|^2\}, \quad m = 1, 2, \cdots, N. \tag{2.29}$$

Furthermore, if the ACS and PSD of $\{H_N(n)\}$ are estimated by

$$\hat{R}_H(k) = \frac{1}{N} \sum_{n=0}^{N-1} \{H_N(n)H_N(n-k)^*\}, \qquad and \tag{2.30}$$

$$\hat{\Phi}_H(W_N^{-m}) = \sum_{k=0}^{N-1} \hat{R}_H(k)W_N^{-mk}, \tag{2.31}$$

respectively, then

$$\hat{\Phi}_H(W_H^{-m}) = N|h_N(N-m)|^2, \quad m = 1, 2, \cdots, N. \tag{2.32}$$

Proof: The zero-mean periodic WSS assumption on $\{H_N(n)\}_{n=0}^{N-1}$ implies that $\{h_N(m)\}_{m=0}^{N-1}$, its inverse DFT, is periodic uncorrelated in light of Theorem 2.1. The expressions of ACS $\{R_H(n)\}$ and PSD $\{\Phi_H(W_N^{-i})\}$ as in (2.27) lead to

$$
\begin{aligned}
&\Phi_H(W_N^{-m})\\
=\ & \sum_{n=0}^{N-1} \mathrm{E}\left\{H_N(n)H_N(n-k)^*\right\} W_N^{km}\\
=\ & \mathrm{E}\left\{H_N(n) \sum_{k=0}^{N-1} H_N(n-k)^* W_N^{km}\right\}\\
=\ & \mathrm{E}\left\{H_N(n)W_N^{mn} \left(\sum_{n=0}^{N-1} H_N(n-k)W_N^{m(n-k)}\right)^*\right\}\\
=\ & \mathrm{E}\left\{H_N(n)W_N^{mn} \left(\sum_{k=0}^{N-1} H_N(k)W_N^{mk}\right)^*\right\}\\
=\ & \mathrm{E}\left\{NH_N(n)W_N^{mn} \left(\frac{1}{N}\sum_{k=0}^{N-1} H_N(k)W_N^{-(N-m)k}\right)^*\right\}\\
=\ & N\mathrm{E}\left\{H_N(n)h_N(N-m)^*\right\} W_N^{mn}\\
=\ & N \sum_{k=0}^{N-1} \mathrm{E}\left\{h_N(k)h_N(N-m)^*\right\} W_N^{n(k+m)}\\
=\ & N\mathrm{E}\{|h_N(N-m)|^2\}
\end{aligned}
$$

for $m = 1, 2, \cdots, N$ by the periodic uncorrelated property of $\{h_N(k)\}$ which establishes (2.29). Similarly we have that the estimated PSD at $\lambda_m = W_N^{-m}$ is given

by

$$\hat{\Phi}_H(\lambda_m)$$

$$= \frac{1}{N} \sum_{k=0}^{N-1} \sum_{n=0}^{N-1} H_N(n) H_N(n-k)^* W_N^{km}$$

$$= \frac{1}{N} \sum_{n=0}^{N-1} H_N(n) W_N^{mn} \times$$

$$\sum_{k=0}^{N-1} \left(H_N(n-k) W_N^{m(n-k)} \right)^*$$

$$= N \sum_{n=0}^{N-1} H_N(n) W_N^{mn} \left(\frac{1}{N} \sum_{k=0}^{N-1} H_N(k) W_N^{km} \right)^*$$

$$= N \left(\frac{1}{N} \sum_{n=0}^{N-1} H_N(n) W_N^{-n(N-m)} \right) \times$$

$$\left(\frac{1}{N} \sum_{k=0}^{N-1} H_N(k) W_N^{-k(N-m)} \right)^*$$

$$= N |h_N(N-m)|^2,$$

which establishes (2.32). ■

Theorem 2.3 characterizes the PSD of the uniformly spaced CFR samples in terms of the power delay profile of the discretized CIR given in (2.7). By assuming independence of the path gains $\{c_k\}$ and the arrival times $\{\tau_k\}$ in the continuous-time CIR, the uniformly spaced CFR samples are periodic WSS as shown in (2.10) which is equivalent to that the discrete channel CIR coefficients $\{h_N(m)\}$ are US. This new WSS-US condition is the very reason why the uniformly spaced CFR samples can be modeled by low order AR models for wideband and ultra wideband channels [11, 12, 19]. Specifically assume that the sequence of the uniformly spaced CFR samples $\{H_N(k)\}$ is periodic WSS and Gaussian. Then it can be generated by passing a periodic i.i.d. Gaussian process through some ARMA model with transfer function $T(\lambda)$ of finite order in light of Theorem 2.2. Here we have used λ, instead of z, in the transfer function to emphasize that the CFR samples, not the time domain data, are the output. In this case $E\{|h_N(m)|^2\}$, the power delay profile of the discretized channel, corresponds to the sampling of some smooth function $|T(\lambda)|^2$ at $\lambda_m = W_N^{-m}$ for $0 \le m < N$. That is, the power delay profile of the discretized channel can be regarded as the "spectrum" of the uniformly spaced CFR samples that justifies the parametric modeling for wideband and ultra wideband channels in the frequency domain. It remains to show that the transfer function $T(\lambda)$ can be taken as an AR model and its order can be as low as one or two.

In light of the expression in (2.7), the power delay profile of the discrete channel is given by

$$
\mathrm{E}\{|h_N(m)|^2\}
$$

$$
= \mathrm{E}\left\{\left|\sum_{\ell_k=0}^{N-1} h_{\ell_k}\left[\frac{1}{N}\sum_{n=0}^{N-1} W_N^{-n(m-\ell_k-\varepsilon_k)}\right]\right|^2\right\} \tag{2.33}
$$

$$
= \sum_{\ell_k=0}^{N-1} \sigma_{h_{\ell_k}}^2 \mathrm{E}\left\{\left|\frac{1}{N}\sum_{n=0}^{N-1} W_N^{-n(m-\ell_k-\varepsilon_k)}\right|^2\right\} \tag{2.34}
$$

$$
= \sum_{k=0}^{L-1} \sigma_{c_k}^2 \mathrm{E}\left\{\left|\frac{1}{N}\sum_{n=0}^{N-1} W_N^{-n(m-\ell_k-\varepsilon_k)}\right|^2\right\}
$$

which is an interpolation of $\{\sigma_{c_k}^2\}$, namely the power delay profile of the continuous-time channel. For the indoor environment, the variability of the arrival times is relatively small and the propagation delays are dependent more on the distance from the transmitter to the receiver than on the locations of the receiver. Hence the power delay profile of the discrete channel $\{\mathrm{E}[|h_N(m)|^2]\}$ exhibits similar peaks and valleys to those of typical wideband and ultra wideband channels versus integer index m. Let $\tau_{\mathrm{m}} = \max\{\tau_k\}$ be the maximum excess delay and $N = \lfloor \tau_{\max}f_{\mathrm{BW}}\rfloor \geq L$. Then for some wideband channels, it is very likely that the power delay profile $\{\mathrm{E}[|h_N(m)|^2]\}$ has only one peak as m changes from 0 to N. In this case a first order AR model with the pole close to the unit circle is adequate to describe the uniformly spaced CFR samples. For some other wideband and ultra wideband channels, more than one peak may exist that requires more than one pole to model them. However if $N \gg \lfloor \tau_{\max}f_{\mathrm{BW}}\rfloor \geq L$, then all peaks of $\mathrm{E}\{|h_N(m)|^2\}$ are suppressed to the beginning values of m with essentially a single or at most two peaks, and the power delay profile decays to zero quickly as m increases towards N. Consequently a first order or second order AR model is adequate to describe the uniformly spaced CFR samples $\{H_N(n)\}$ for sufficiently large N. Moreover the poles of $T(\lambda)$ for the AR model are in the fourth quadrant of the complex plane because of the reversed index for the PSD in (2.29). This coincides with the results in [11, 12, 19].

Remark 2.1 Theorem 2.3 shows that accurate modeling for wideband and ultra wideband channels in frequency domain requires the knowledge of the power delay profile $\mathrm{E}\{|h_N(m)|^2\}$ which has to be estimated from the experimental measurements. Let $\hat{h}_N^{(k)}(m)$ be obtained in the kth independent experiment. An unbiased estimate for $\mathrm{E}\{|h_N(m)|^2\}$ is given by

$$
\hat{\sigma}_{m,K}^2 = \frac{1}{K}\sum_{k=1}^{K}|h_N^{(k)}(m)|^2, \quad 0 \leq m \leq N-1. \tag{2.35}
$$

That is, $\mathrm{E}\{\hat{\sigma}_{m,K}^2\} = \sigma_m^2$. The question is how large K should be in order to have a reasonable estimate for $\sigma_m^2 = \mathrm{E}\{|h_N(m)|^2\}$. By the Chebyshev inequality, for any

$\epsilon > 0$ there holds

$$\begin{aligned}
\mathrm{Prob}\left\{\left|\hat{\sigma}^2_{m,K} - \sigma^2_m\right| \geq \epsilon\right\} &\leq \frac{\mathrm{Var}\left\{\hat{\sigma}^2_{m,K}\right\}}{\epsilon^2}\\
&= \frac{\mathrm{E}\{|h^{(k)}_N(m)|^4\} - \sigma^4_m}{K\epsilon^2}\\
&= \frac{\sigma^4_m}{K\epsilon^2}.
\end{aligned} \qquad (2.36)$$

Hence given any error tolerance $\epsilon > 0$ in estimation of the discretized power delay profile, the probability for the estimation error to exceed ϵ can be made arbitrarily small by choosing K sufficiently large. ∎

It is noted that σ^2_m is unknown. Thus $\hat{\sigma}^2_{m,K}$ has to be used in the right hand side of the inequality (2.36). But if the real and imaginary parts of $h_N(m)$ are independent of each other, and both are Gaussian distributed with zero mean and variance $\sigma^2_m/2$, then $X_{m,K} = \frac{2K\hat{\sigma}^2_{m,K}}{\sigma^2_m/2}$ is a random variable with χ^2-distribution of degree $2K$ [55] (page 119). In this case the probability on the left hand side of (2.36) can be evaluated through integration of the χ^2 PDF (probability density function) that is a function of K. Hence K, the number of experiments, can be determined to ensure a reasonably good estimate for the discretized power delay profile.

Remark 2.2 For ultra wideband channels, f_{BW}, the bandwidth of the channel can be very large. If $N \approx \lfloor \tau_{\max} f_{\mathrm{BW}} \rfloor \geq L$, then low order AR models may not be adequate to model the uniformly spaced CFR samples due to many peaks and valleys of the discrete CIR, inherited from the continuous-time CIR. In this case high order ARMA models are more appropriate in describing the uniformly spaced CFR samples. ∎

2.5 Simulation Study for Parametric Modeling

In this section we investigate the parametric modeling in frequency domain through numerical simulations. We adopt two time domain channel models as our benchmarks for the wideband and ultra wideband channels. One is the typical outdoor channel model used for macrocellular applications and the other is the indoor channel model introduced by Saleh and Valenzuela [18], which is also validated for the UWB channel [17]. Both models generate the continuous-time CIRs that can be described by (2.1). The N-point uniform samples of the corresponding CFRs are obtained from (2.4). We will show that these discrete CFRs can indeed be described accurately by low order parametric models.

2.5.1 Benchmark Time Domain Channel Models

We begin with the outdoor wideband wireless channel. Figure 2.1 illustrates the continuous-time model for a multipath mobile radio channel. The received signal is

comprised of L paths with time delays $\tau_0, \tau_1, \cdots, \tau_{L-1}$. For path k, $k = 0, 1, \cdots, L-1$, the attenuation $A_k g_k(t)$ is attributed to the Doppler frequency shift and admits the Rayleigh fading property with average power gain A_k^2. We use the 12-ray power delay profile listed in Table 2.1, which is recommended in the COST207 study for a typical urban area [6]. It is assumed that the path attenuations are uncorrelated. This model is solely determined by the power delay profiles and the maximum Doppler frequency shift [59]. By assuming a quasi-stationary channel, the CIR of the continuous-time channel is given by

$$C(t) = \sum_{k=0}^{L-1} A_k g_k \delta(t - \tau_k). \tag{2.37}$$

For the indoor ultra wideband channel, we adopt the model from [18]. The time domain measurements reveal that, for indoor wireless channels, the path arrivals tend to occur in clusters. In light of [18], the impulse response of the channel is given by

$$h(t) = \sum_{i=0}^{\infty} \sum_{k=0}^{\infty} \beta_{k,i} e^{j\theta_{k,i}} \delta(t - T_i - \tau_{k,i}) \tag{2.38}$$

where T_i denotes the arrival time of the ith cluster, and $\tau_{k,i}$ denotes the excess delay of the kth multipath component in the ith cluster relative to T_i. The T_i's and $\tau_{k,i}$'s are modeled as the arrival times of two independent Poisson processes with arrival rates Λ and λ, respectively. The average power gain of each ray satisfies the double-exponential decaying property, manifested by the following expression [18]:

$$\mathrm{E}\{\beta_{k,i}^2\} = \mathrm{E}\{\beta_{0,0}^2\} e^{-T_i/\Gamma} e^{-\tau_{k,i}/\gamma}. \tag{2.39}$$

The clustering of the multipath components has been reported for UWB channels in [5]. The model in (2.38) has also been validated in [8] for the UWB channel with bandwidth ranging from 2 GHz to 8 GHz under the assumption that $\{\beta_{k,i}\}$ have log-normal distribution, and $\{\theta_{k,i}\}$ are independent uniform random variables over $[0, 2\pi)$ [17]. Furthermore the power variance

$$\sigma^2 = \mathrm{E}\left\{ \left(\beta_{k,i}^2 - \mathrm{E}\{\beta_{k,i}^2\} \right)^2 \right\} \quad \forall\, i, k \geq 0 \tag{2.40}$$

is assumed to be constant [8]. It follows that this model is determined by the parameters Λ, λ, Γ, γ and σ^2. The parameters we choose in our simulation are as follows: $\Lambda = 0.4$ ns^{-1}, $\lambda = 1.0$ ns^{-1}, $\Gamma = 5.2$ ns, $\gamma = 6.5$ ns and $\sigma = 4.8$ dB. According to [17], these parameters correspond to the case of none line-of-sight (NLOS) situation, and the separation between the transmitter and receiver is $0 \sim 4$ meters.

As mentioned earlier, the discrete CFR is obtained through uniform sampling over the bandwidth of interest. For the outdoor channel, the low frequency edge, f_L, is set to be 900 MHz and the bandwidth is $f_{BW} = 10.24$ MHz. The total number of samples is $N = 512$. So the frequency offset between the neighboring samples is $f_{BW}/N = 20$ KHz. For the indoor channel, we set $f_L = 5$ GHz, $f_{BW} = 1.024$ GHz and $N = 512$. So the frequency offset is 2MHz in this case. It is indeed clear that the outdoor channel considered here is wideband and the indoor channel is ultra wideband.
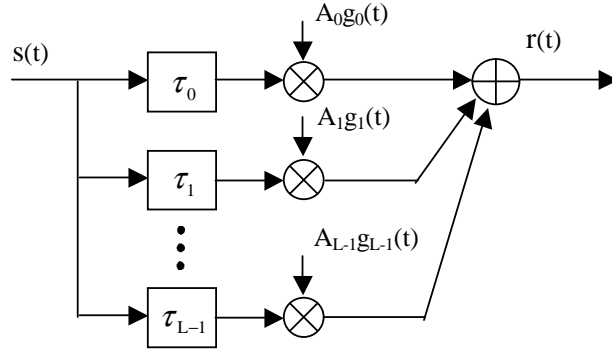
Figure 2.1: Outdoor mobile radio propagation model

Table 2.1: Typical macrocellular urban 12-ray power delay profile

Index	Delay (μs)	Fractional power	Index	Delay (μs)	Fractional power
k	τ_k	$A_k^2/\sum_l A_l^2$	k	τ_k	$A_k^2/\sum_l A_l^2$
1	0.0	0.092	7	0.5	0.127
2	1.3	0.046	8	3.1	0.032
3	0.1	0.115	9	0.8	0.115
4	1.7	0.074	10	3.2	0.018
5	0.3	0.231	11	1.1	0.074
6	2.3	0.051	12	5.0	0.025

2.5.2 Parametric Modeling for the Discrete CFRs

It can be seen that running the time domain model once generates one CFR sequence, which is comprised of N samples. In this section, we will show that every CFR sequence produced by the two benchmark models can be modeled as a low order ARMA process. In order to identify the coefficients of the ARMA process corresponding to each CFR sequence, we first compute an estimate of its ACS using (2.30) that is the same as frequency autocorrelation function (ACF). The channel orders, namely r_a for the AR part, and r_b for the MA part, are estimated subsequently. Several methods exist for order estimation [54, 8]. Once the AR and MA orders are determined, estimation of the ARMA coefficients is performed using the two-stage least-squares method [14, 63]. We would like to point out that while other algorithms (such as Levinson-Durbin [14, 63] for the AR models) are available the two-stage least-squares method is the most effective for the more general ARMA models.

In order to have a more complete view about the parametric modeling, we first evaluate the modeling quality for parametric models of different orders by comparing the normalized prediction error (NPE) defined as follows:

$$\text{NPE} = \frac{\text{E}\left\{\sum_{n=0}^{N-1}|H_N(n) - T(q)V_N(n)|^2\right\}}{\sum_{n=0}^{N-1}|H_N(n)|^2} \tag{2.41}$$

where $\{H_N(n)\}$ is the given CFR sequence, $T(q)$ is the transfer function determined by the estimated AR and/or ARMA model coefficients, and $\{V_N(n)\}$ denotes a periodic i.i.d. Gaussian process with zero mean and variance σ_V^2. In practice, the expectation is replaced by averaging. By running the outdoor and indoor models for 1000 times, we generated 1000 independent CFR sequences for each channel model. In each channel realization, we obtained the associated NPEs for different AR and MA orders. Table 2.2 illustrates the NPEs each was averaged over 1000 channel realizations. It can be seen that the prediction errors decrease dramatically with the increase of the AR order. Moreover for $r_a = 2$ and $r_b = 0$, the NPE is already quite small for both outdoor and indoor channels. Figure 2.2 illustrates the scatter plots of the two poles in the complex plane associated with different channel realizations where $r_a = 2$ and $r_b = 0$ are fixed. It can be seen that for both channels the first poles are densely situated close to the unit circle, while the second poles are scattered more and are not so close to the unit circle. This suggests that the first pole is more dominant than the second, and if a higher order ARMA model is used, the higher order poles will not reduce the modeling errors significantly.

In Figure 2.3, the cumulative distributive functions (CDFs) of the noise processes $\{V_N(n)\}$ in the ARMA model are plotted for both the outdoor and indoor channels.

The CDFs are computed based on the histogram of the simulation results under one channel realization in both cases, where the model orders are fixed to be $r_a = 2$ and $r_b = 0$. The theoretical CDFs of the Gaussian random variables are also plotted

27

Table 2.2: NPEs with respect to the model orders

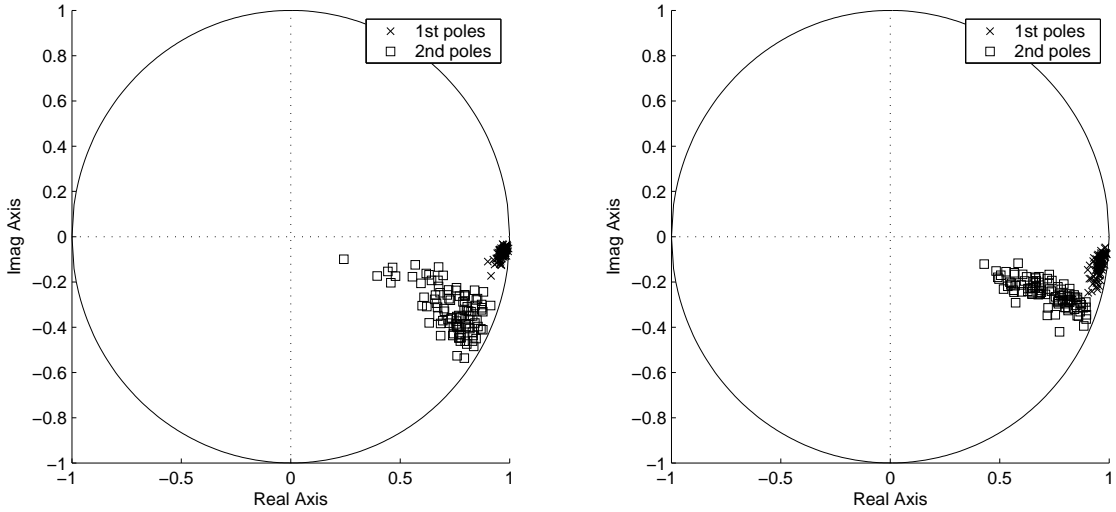| Outdoor Channel			Indoor Channel		
MA order	AR order	Average NPE	MA order	AR order	Average NPE
	1	0.0168		1	0.0113
0	2	5.57×10^{-4}	0	2	2.835×10^{-4}
	3	1.35×10^{-5}		3	7.0634×10^{-6}
	1	0.0167		1	0.0113
1	2	4.93×10^{-4}	1	2	2.8136×10^{-4}
	3	1.366×10^{-5}		3	7.1047×10^{-6}

Figure 2.2: Pole distributions for the outdoor channel (left) and the indoor channel (right)

Table 2.3: Parameters for the 2nd-order AR models

Parameters	Outdoor channel	Indoor channel
α_1	$-1.7047 + 0.3488j$	$-1.7681 + 0.2681j$
α_2	$0.7029 - 0.3302j$	$0.7678 - 0.2450j$
σ_V^2	0.008729	0.006306

for reference. It can be seen that the distribution of the noise process the matches Gaussian distribution very closely in both cases.

In summary, the simulation results presented in this section suggest that a second order AR model is capable of reproducing each CFR sequence generated by our chosen benchmark models.

2.5.3 Performance of the Second Order Frequency Domain AR Model

Consider a second order AR model whose coefficients α_1 and α_2 are constant complex values. We will examine its performance as a frequency domain model by applying at input an i.i.d. Gaussian process with zero mean and variance σ_V^2. The length of the input sequence is N and the output represents the CFR samples. If the difference equation (2.8) is adopted, the N CFR samples can be generated by applying the white Gaussian noise input periodically with period N. The simulation can also be carried out by computing N-point DFT of the input and its product with the uniformly sampled transfer function which is solely determined by α_1, α_2, and σ_V^2. The CFR samples can then be obtained by taking N-point inverse DFT of the product which is one realization of the channel corresponding to the above noise sequence. It will be shown that by correct estimation of α_1, α_2, and σ_V^2, this low order AR model is capable of capturing the main statistical properties of the benchmark channels.

Using the same parameters as in Subsection 2.5.1 for the two benchmark models, we first generated 1000 sequences of CFR samples for each of the two. In order to validate the 2nd order AR model for channel modeling in frequency domain, we computed 1000 CIR sequences via inverse DFT of the corresponding 1000 sequences of CFR samples, and then obtained 1000 power delay profiles based on which the AR parameters (α_1, α_2, σ_V^2) were estimated. Recall the theoretical results in Section 2.4. These AR parameters are listed in Table 2.3. We then generated 1000 CFR sequences with this second order AR model for both outdoor and indoor channels by exciting the AR model with the 1000 sets of i.i.d. Gaussian random variables (length N). The statistical properties of these discrete CFR's are compared side by side with that of the benchmark models.

It is noted that the empirical frequency domain autocorrelation functions (ACF)

29
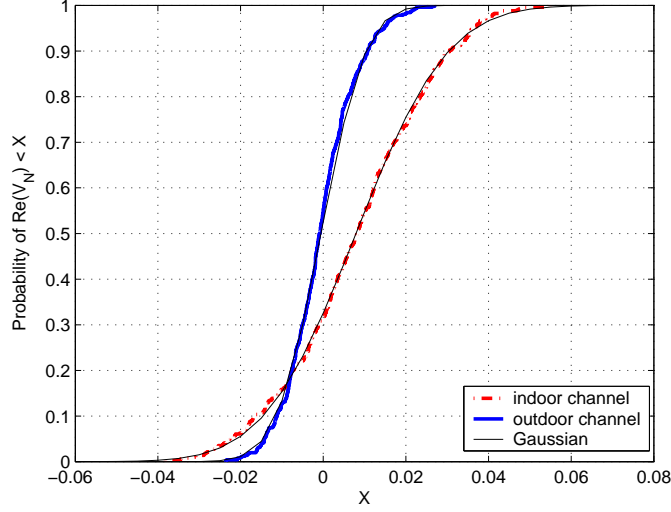
Figure 2.3: CDFs of the periodic noise processes vs. Gaussian CDF

for these two models can be calculated by

$$\overline{R}_H(k) = \frac{1}{1000} \sum_{i=1}^{1000} \hat{R}_H^{(i)}(k), \quad k = 0, \pm 1, \pm 2, \cdots \tag{2.42}$$

where $\hat{R}_H^{(i)}(k)$, given by (2.30), is the estimate of the ACS for the ith channel realization. In general, the frequency domain ACS may depend on not only the index difference but also the index itself, as given below

$$\hat{R}_H(n; k) \approx \frac{1}{1000} \sum_{i=1}^{1000} H^{(i)}(n) H^{(i)^*}(n-k) \tag{2.43}$$

$$n \in \{0, \cdots, N-1\}; \quad (n-k) \in \{0, \cdots, N-1\}$$

where $\{H^{(i)}(n)\}$ is the CFR sequence for the ith channel realization, in which WSS is not assumed. In Figure 2.4 the real and imaginary parts of the general ACS defined in (2.43) have been plotted with respect to k for $n = 140$ and 200. It can be observed that the benchmark models and the second order AR models match well in terms of the frequency domain ACS. On the other hand, different values of n yield almost the same ACS. Furthermore, the real part of ACS tends to be an even function and the imaginary part is approximately odd in all cases. These observations hold true for other values of n and k that are not plotted here. This implies that the CFR sequences generated by the benchmark models and the AR models can be viewed as WSS.

Similar to [12] we have compared the distributions of 3dB width of the frequency correlation functions for the AR models and the benchmark models. Figure 2.5 illustrates the CDF plots of 3dB width for various channel models, where the mean

Figure 2.4: Frequency domain ACS for AR models and benchmark models

Figure 2.5: Distribution of 3dB width for frequency correlation functions

Figure 2.6: Distribution of RMS delay spread

Figure 2.7: Comparison of power delay profile for outdoor (left) and indoor (right) channels

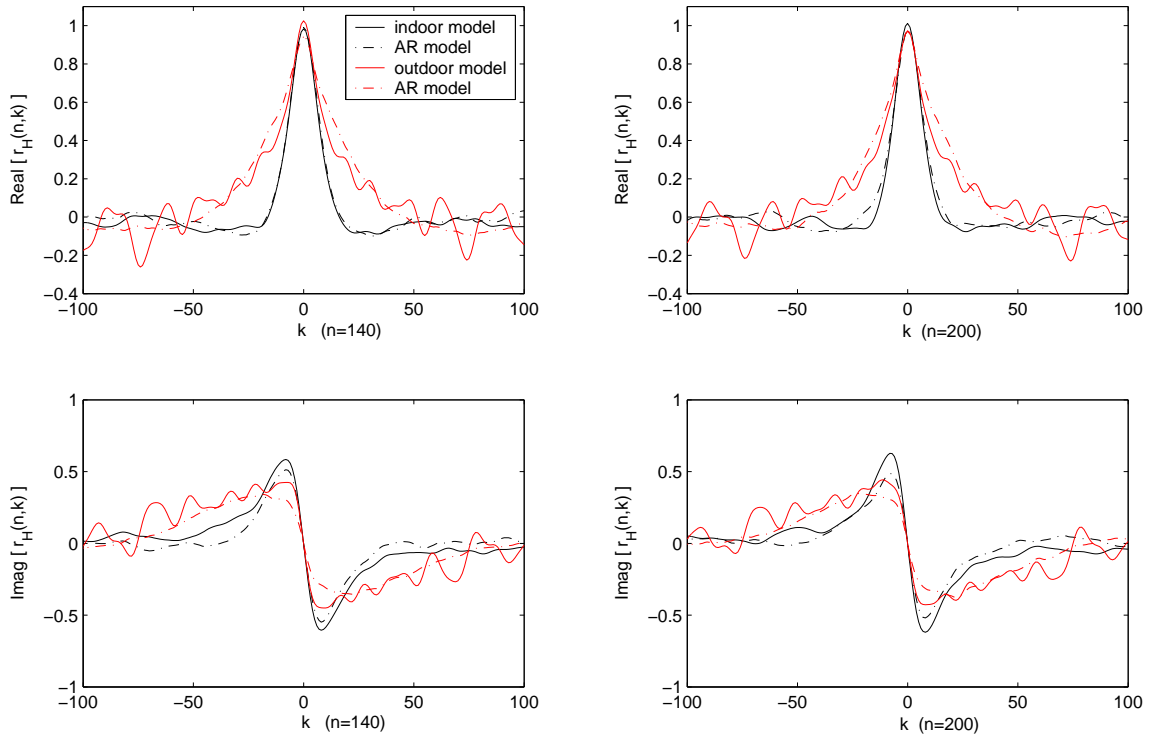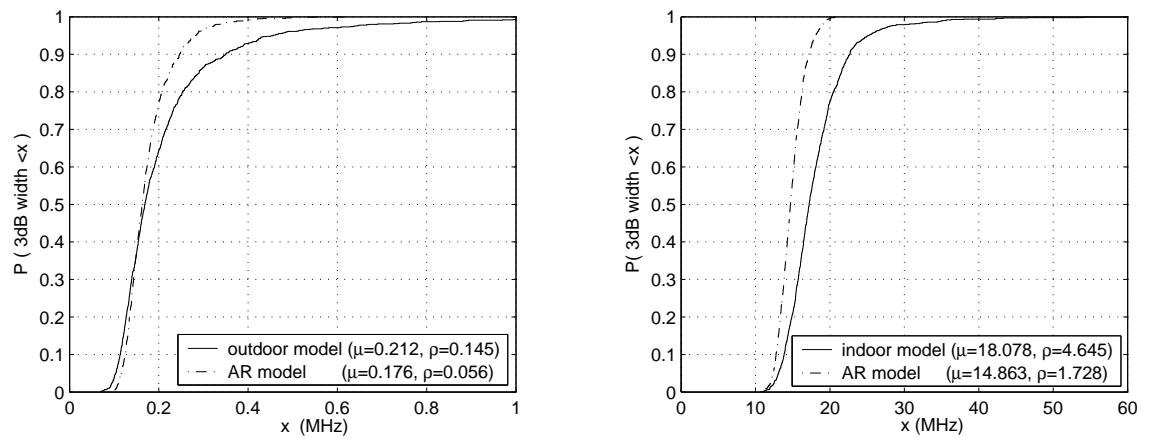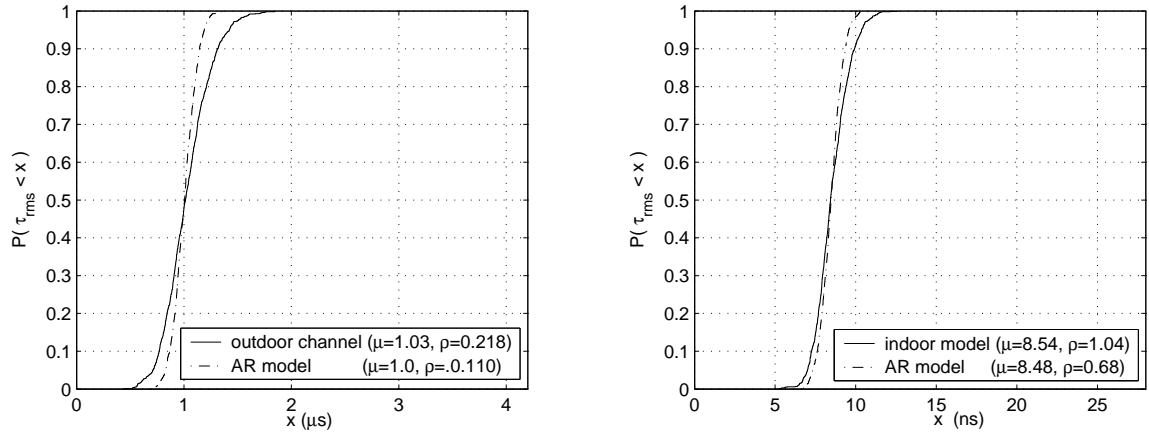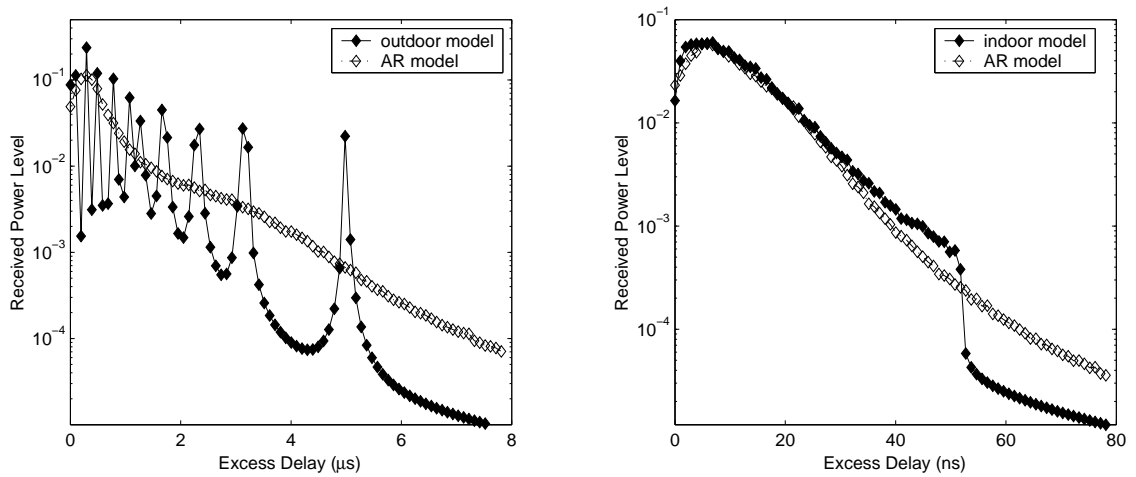values (μ) and standard deviations (ρ) have been listed as well. Although the 3dB width associated with the AR models tend to be less dispersed than that of the benchmark models, especially for the case of indoor channel, the mean values match well. Further study shows that the 3dB width for the AR models and benchmark channels follow the same type of distributions.

Another important metric for wireless channel models is the *rms delay spread* (τ_{RMS}). Given discrete CIR, the rms delay spread of the channel can be calculated following the same steps as in [12]. In our simulation, the discrete CIRs are obtained by taking N-point IDFT of the CFR samples generated by each channel model. The CDF plots for the rms delay spread of different channel models are shown in Figure 2.6. For the indoor channel, the second order AR model matches perfectly the time domain model in terms of rms delay spread. However, for the outdoor channel, there are noticeable differences between the AR model and the benchmark model in terms of the rms delay spread.

Figure 2.7 illustrates the power delay profile for the AR models and benchmark time domain channel models. It can be observed that they match very well in the case of indoor UWB channel. As for outdoor channel, the AR model only resembles the average power delay profile of the time domain model.

Remark 2.3 Our simulation results confirm that the proposed second order AR model reproduces the CFRs of the indoor UWB channel model accurately. However some noticeable differences between the outdoor benchmark model and the second AR model are observed, especially in Figures 2.4 and 2.7. The main reason for such discrepancies is that the path delays are fixed in the 12-ray outdoor channel model and we have employed $N \approx \lfloor \tau_{\max} f_{\mathrm{BW}} \rfloor$. Hence in light of Remark 2.2, more than two significant peaks exist in the associated power delay profile, which is closely related to the PSD of the ARMA process of order higher than 2, in accordance with our analysis. In this case, an AR model with higher order is necessary to yield a better match. ∎

2.6 Chapter Summary

Channel modeling in frequency domain has been investigated for wideband and ultra wideband channels. The periodic random processes are introduced to facilitate the parametric modeling. Our main results show that the sampled CFR is periodic WSS, if and only if the discrete CIR is periodic uncorrelated. It follows that the parametric modeling in frequency domain is possible, if and only if the uniformly spaced CFR samples are WSS that is equivalent to that the discrete CIR are US. This new WSS-US condition is shown to hold under some mild assumption that answers the question why wideband and ultra wideband channels can be modeled in the frequency domain as proposed and studied in [10, 11, 19]. In addition, the PSD of the uniformly spaced CFR samples is derived that explains why low order AR models are adequate

for channel modeling in frequency domain. Our simulation study investigated two wireless channels, one outdoor wideband and the other indoor ultra wideband, which shows the effectiveness of the parametric modeling in frequency domain. Narrowband channels are not studied because they do not involve frequency-selective fading.

It is important to note that uniformly spaced sampling for CFR over the channel bandwidth converts the wireless channel into an equivalent OFDM (orthogonal frequency division multiplexing) system such as the one studied in [7] in which the CFR samples can be shown to be periodic WSS. Hence the results in this chapter are applicable to such wideband OFDM channels. However for more general wideband OFDM channels where matched filters are used, the WSS assumption for the CFR does not hold in general. We would like to comment that for a non-WSSUS wireless channel, its uniformly spaced CFR samples are unlikely to be WSS, and thus parametric modeling is less effective in frequency domain because the time-invariant models are inapplicable. Time-varying AR or ARMA models have to be employed that has its own independent interest for which not all multipath gains are resolvable. Consequently the corresponding discretized channel does not satisfy the WSSUS assumption. This specific modeling problem deserves further investigation.

CHAPTER 3. COMPUTATIONALLY EFFICIENT RESOURCE ALLOCATION FOR MULTI-USER OFDM SYSTEMS

3.1 Introduction

Orthogonal frequency division multiplexing has been regarded as one of the most effective techniques for broadband wireless communication systems. OFDM converts the frequency selective fading channel into a number of parallel narrowband flat fading subchannels thereby eliminating the need for complex equalizers at the receiver. The flexibility of subcarrier management in OFDM systems provides an attractive multiple access control mechanism for systems supporting multiple users. Through judicious assignment of subcarriers to users, one can not only eliminate multiuser interference but also improve the system power and spectral efficiency. System performance can be further enhanced by employing resource allocation techniques which optimize the power and bit allocation for each subcarrier in response to the channel state information.

Many authors have recently considered the problem of subcarrier, bit and power allocation in multiuser OFDM (MU-OFDM) systems [25, 27, 29]. In these studies it is assumed that the base station (BS) knows the channel state information (CSI) for all the users and, using the CSI, dynamically assigns a subset of subcarriers to each user and allocates the power and modulation scheme for each subcarrier. In general, a constrained optimization problem is formulated wherein the object is to minimize the total transmit power (resp. maximize the total data rate) for the entire OFDM block while satisfying some constraints for the average bit-error-rate (BER) and the data rate of each user (resp. the total transmit power).

The optimal subcarrier, bit and power allocation is a challenging task and its complexity is prohibitive in practical communication systems [24, 26]. To avoid this difficulty a tractable approach is to divide this problem into two separate problems: first find the optimal allocation for subcarriers to users, next, given the assignment of subcarriers, find the optimal allocation of bit and transmit power for each user. While the first step exploits the multiuser diversity, the second step makes use of the frequency diversity for each user. Although this approach does not result in the optimal solution for joint subcarrier, bit and power allocation, it is possible to achieve a close-to-optimal performance in most cases [25, 26]. The bit and power allocation problem has been investigated in [21, 22, 23, 24]. Several suboptimal solutions for subcarrier allocation have also been proposed in [25, 27, 29]. The main difficulty with the algorithms proposed in these references is their high computational complexity. While these algorithms may be applicable in wireline applications where the CSI remains static for extended periods of time, they are not suitable for the wireless

environment where, even in the case of slowly fading channels, the CSI needs to be updated (and the solution recalculated) after several OFDM blocks.

In this chapter we present a novel method for subcarrier, bit and power allocation. We also consider the problem in two steps: subcarrier allocation to all the users followed by bit and power allocation for each user. Our algorithm achieves a near optimal solution with considerably less computational complexity than the optimal solution. The remainder of this chapter is organized as follows. In Section 3.2 we present the framework for our study and describe the optimal allocation problem for a multi-user OFDM system. In Section 3.3 we present an efficient bit and power allocation scheme for a single user system. The subcarrier allocation algorithm is described in Section 3.4 and numerical results are presented in Section 3.5. Finally conclusions are drawn in Section 3.6.

3.2 Framework

Consider a MU-OFDM system with K users and N subcarriers. We are concerned with the downlink channel where data is transmitted from the base station to the mobile stations. The base station and all mobile stations are presumed to have single transmit and receive antennas. Assuming that the frequency offset between adjacent subcarriers is much less than the channel coherence bandwidth, that the channel delay spread is less than the cyclic prefix, and perfect block and symbol synchronization, the frequency selective channels from the BS to these users may be represented by a series of NK flat fading subchannels. Thus the received symbol for subcarrier n and user k, denoted $Y_{n,k}$, is given by

$$Y_{n,k} = \rho_{n,k}H_{n,k}S_{n,k} + \sum_{j \neq k} \rho_{n,j}H_{n,j}S_{n,j} + V_{n,k}; \ n = 1, \cdots, N; \ k = 1, \cdots, K. \quad (3.1)$$

where $S_{n,k}$ is the input symbol for subcarrier n and user k, $H_{n,k}$ is the channel frequency response (CFR) for the nth subcarrier of the kth user and $\{V_{n,k}\}$ is an *iid* sequence of zero-mean Gaussian random variables with variance σ_V^2. Moreover, $\rho_{n,k}$ denotes the multiplexing factor of subcarrier n and user k. If not specified, the real and imaginary parts of the CFR are assumed to be arbitrary real numbers.

It is shown in [28] that in the optimal allocation scheme a single subcarrier should be assigned to a single user. Thus $\rho_{n,k}$ is either 1 or 0 where $\rho_{n,k} = 1$ implies that the nth subcarrier has been assigned to the kth user. Accordingly Equation (3.1) can be simplified as

$$Y_{n,k} = H_{n,k}S_{n,k} + V_{n,k}; \ \text{for all } n \text{ assigned to user } k; \ k = 1, \cdots, K. \quad (3.2)$$

The transmitted signal $S_{n,k}$ is the modulated symbol from a discrete constellation (e.g., PSK or QAM) whose average power, assuming unit duration of symbol transmit time, is denoted by $P_{n,k} = E\left[|S_{n,k}|^2\right]$. Let β_n denote the number of bits assigned

to the nth subcarrier of an OFDM block. In this case β_n bits are mapped into a complex-valued symbol chosen from the modulation alphabet of size 2^{β_n}. Suppose $\beta_n \in \Omega$, where $\Omega = \{0, b_1, b_2, \cdots, b_L\}$ is the collection of all possible number of bits that can be transmitted through one subcarrier. We assume that b_i's are integers and $0 < b_1 < b_2 < \cdots < b_L$.

In this chapter we consider a system where each user has a predetermined QoS requirement. The QoS requirement of user k is specified in terms of its target average BER ε_k and data rate R_k, where R_k denotes the total number of bits transmitted for user k in each OFDM block.

For a given modulation class (e.g., QAM, PSK, FSK) the bit error probability of the optimal demodulator is a function of the signal-to-noise ratio (SNR), as well as the size of the signal constellation (e.g., the number of bits β_n in that subcarrier). Let $f(\beta, \varepsilon)$ denote the minimum SNR required to ensure that the target BER ε is met when the size of the constellation is 2^β. For any given signal constellation $f(\beta, \varepsilon)$ is either given in closed form or can be well approximated in closed form. It is clear that f is monotone decreasing with respect to ε and monotone increasing with respect to β.

The problem of optimal subcarrier, bit and power allocation can be formulated as follows.

$$\min_{\{\rho_{n,k}, \beta_{n,k}, P_{n,k}\}} \quad \sum_{k=1}^{K} \sum_{n=1}^{N} \rho_{n,k} P_{n,k} \tag{3.3}$$

$$\text{subject to:} \quad \sum_{n=1}^{N} \rho_{n,k} \beta_{n,k} \geq R_k, \quad \forall k \in \{1, 2, \cdots, K\} \tag{3.4}$$

$$P_{n,k} \geq \frac{\sigma_V^2}{|H_{n,k}|^2} f(\beta_{n,k}, \varepsilon_k), \quad \forall n, k \text{ such that } \rho_{n,k} = 1 \tag{3.5}$$

$$\beta_{n,k} \in \Omega, \ P_{n,k} \geq 0, \ \rho_{n,k} \in \{0, 1\}, \ \sum_{k=1}^{K} \rho_{n,k} = 1 \tag{3.6}$$

The following lemma somewhat simplifies the optimal subcarrier, bit and power allocation.

Lemma 3.1 *If* $\{\rho_{n,k}^*, \beta_{n,k}^*, P_{n,k}^*\}$ *is the solution to the optimization problem (3.3) - (3.6), then*

$$P_{n,k}^* = \begin{cases} 0 & \text{if } \rho_{n,k}^* = 0 \\ \frac{\sigma_V^2}{|H_{n,k}|^2} f(\beta_{n,k}^*, \varepsilon_k) & \text{if } \rho_{n,k}^* = 1 \end{cases} \tag{3.7}$$

Proof: The case for $\rho_{n,k}^* = 0$ is trivial. For arbitrary n and k and $\rho_{n,k}^* = 1$, assume to the contrary that $P_{n,k}^* > \frac{\sigma_V^2}{H_{n,k}^2} f(\beta_{n,k}, \varepsilon_k)$. Then by setting $P_{n,k}^* = \frac{\sigma_V^2}{H_{n,k}^2} f(\beta_{n,k}^*, \varepsilon_k)$ while all other variables are fixed a better solution for (3.3) - (3.6) can be obtained. ∎

Lemma 3.1 shows that given the subcarrier assignment, the optimal power allocation can be solely determined by the optimal bit allocation. Thus, the optimal subcarrier, bit and power allocation problem can be reduced to a problem of subcarrier and bit allocation. The original optimization problem can now be described as follows.

$$\min_{\{\rho_{n,k},\beta_{n,k}\}} \quad \sum_{k=1}^{K} \sum_{n=1}^{N} \rho_{n,k} \frac{\sigma_V^2}{|H_{n,k}|^2} f(\beta_{n,k}, \varepsilon_k) \tag{3.8}$$

$$\text{subject to:} \quad \sum_{n=1}^{N} \rho_{n,k}\beta_{n,k} \geq R_k, \quad \forall k \in \{1, 2, \cdots, K\} \tag{3.9}$$

$$\beta_{n,k} \in \Omega, \ \rho_{n,k} \in \{0, 1\}, \text{ and } \sum_{k=1}^{K} \rho_{n,k} = 1 \tag{3.10}$$

In the following sections we first derive an efficient algorithm for bit and power allocation by assuming all subcarriers have been allocated to users and then propose a simple method for assigning subcarriers to users. In practice, the allocation of subcarriers is performed first.

3.3   An Efficient Algorithm for Bit and Power Allocation

In this section we temporarily ignore the problem of subcarrier allocation and assume that all the subcarriers have been pre-allocated to users. As a result the total number of subcarriers and the associated channel frequency response will be fixed for every user. The optimal bit and power allocation can now be solved for a single user. Thus in the rest of this section we drop the subscript k and use N to denote the total number of subcarriers assigned to the individual user of interest.

Following Lemma 3.1, the optimal bit and power allocation problem for a single user is actually a bit allocation problem, which can be stated as follows.

$$\min_{\{\beta_n\}} \sum_{n=1}^{N} \frac{\sigma_V^2}{|H_n|^2} \cdot f(\beta_n, \varepsilon) \tag{3.11}$$

$$\text{subject to:} \quad \sum_{n=1}^{N} \beta_n \geq R \tag{3.12}$$

$$\beta_n \in \Omega, \ \forall n = 1, 2, \cdots, N. \tag{3.13}$$

The above is a mixed integer programming (MIP) problem requiring an exhaustive search with high computational complexity. In [21] the authors proposed a greedy method to assign bits iteratively until the target data rate is reached. During each iteration one more bit is added by searching for the smallest additional power necessary to guarantee the target BER. Although this method can achieve the optimal solution, its computational complexity is $O(N^2)$ making it prohibitive when N is large. In [22]

another algorithm is introduced whose complexity is $O\left(I \times N + 2N\right)$ where I is the number of iterations. However, each iteration calls for N operations of logarithm calculation and division, requiring a great deal of processing time. A new algorithm is presented in [23] which eliminates the need for logarithm calculations from each iteration but still needs to perform N logarithms outside of the iterations. In this section we propose a novel iterative algorithm to achieve the optimal bit allocation by simply using comparison operations within each iteration.

3.3.1 Problem Analysis

It is well known that for the modulation techniques of interest the function $f(\beta, \varepsilon)$ can be well approximated by a function with a closed form which is differentiable and convex with respect to β [24]. In the sequel we replace f by this approximation. We further relax the constraint in (3.13) by allowing β_n's to take non-negative real values. In this way the original optimization problem reduces to a convex optimization problem with a closed form solution.

Theorem 3.1 *Suppose $\{\beta_n^\dagger\}_{n=1}^N$ is the solution to the relaxed optimization problem (3.11), (3.12) and (3.14) below.*

$$\beta_n \in \Re^+, \ \forall n = 1, 2, \cdots, N \tag{3.14}$$

where $\Re^+$ is the set of non-negative real numbers. If for any $\varepsilon > 0$, the function $f(\beta, \varepsilon)$ is differentiable, convex and strictly monotone increasing with respect to β, then

$$\beta_n^\dagger = \max\left\{0, \mathcal{F}_\varepsilon^{-1}\left(\frac{|H_n|^2}{\sigma_V^2}\Lambda^\dagger\right)\right\} \quad \forall n = 1, 2, \cdots, N \tag{3.15}$$

where $\mathcal{F}_\varepsilon(\beta) = \frac{\partial}{\partial \beta} f(\beta, \varepsilon)$ and $\mathcal{F}_\varepsilon^{-1}$ is the inverse function of $\mathcal{F}_\varepsilon$. The parameter $\Lambda^\dagger$ is a unique solution to the following equation

$$\sum_{n=1}^N \max\left\{0, \mathcal{F}_\varepsilon^{-1}\left(\frac{|H_n|^2}{\sigma_V^2}\Lambda^\dagger\right)\right\} = R \tag{3.16}$$

Proof: The optimization problem specified by (3.11), (3.12) and (3.14) is a non-linear programming problem with differentiable convex objective and constraint functions. We can show that *strong duality* holds for this problem and the optimal solution can be obtained using the *Karush-Kuhn-Tucker* (KKT) conditions [61].

Introducing Lagrange multipliers $\Lambda^\dagger \in \Re$ for the constraint in (3.12) and $\lambda^\dagger \in \Re^N$ for the constraint in (3.14), the KKT conditions are given by

$$\beta_n^\dagger \geq 0 \ \forall n, \ \sum_{n=1}^N \beta_n^\dagger \geq R, \ \lambda_n^\dagger \geq 0 \ \forall n, \ \Lambda^\dagger \geq 0, \ \lambda_n^\dagger \beta_n^\dagger = 0 \ \forall n,$$

$$\Lambda^\dagger (\sum_{n=1}^N \beta_n^\dagger - R) = 0, \ \frac{\sigma_V^2}{|H_n|^2}\mathcal{F}_\varepsilon(\beta_n^\dagger) - \lambda_n^\dagger - \Lambda^\dagger = 0 \ \forall n.$$

It is clear that $\sum_{n=1}^{N} \beta_n^\dagger = R$. Otherwise the last two conditions above imply $\lambda_n^\dagger = \frac{\sigma_V^2}{|H_n|^2}\mathcal{F}_\varepsilon(\beta_n^\dagger) > 0$ for all n because f is strictly monotone increasing. Since : $\lambda_n^\dagger \beta_n^\dagger = 0$ for all n then $\beta_n^\dagger = 0 \ \forall n$ and this violates (3.12).

By eliminating $\lambda^\dagger$ the KKT conditions above can be simplified as

$$\beta_n^\dagger \geq 0 \ \forall n, \ \sum_{n=1}^{N} \beta_n^\dagger = R, \ 0 \leq \Lambda^\dagger \leq \frac{\sigma_V^2}{|H_n|^2}\mathcal{F}_\varepsilon(\beta_n^\dagger), \ \beta_n^\dagger\left(\frac{\sigma_V^2}{|H_n|^2}\mathcal{F}_\varepsilon(\beta_n^\dagger) - \Lambda^\dagger\right) = 0 \ \forall n.$$

While f is convex $\mathcal{F}_\varepsilon(\cdot)$ is monotone increasing, which, since $\beta_n^\dagger$ is non-negative, implies that $\mathcal{F}_\varepsilon(\beta_n^\dagger) \geq \mathcal{F}_\varepsilon(0)$ for all n. Three cases are considered.

1. If $\Lambda^\dagger < \frac{\sigma_V^2}{|H_n|^2}\mathcal{F}_\varepsilon(0)$, then $\left(\frac{\sigma_V^2}{|H_n|^2}\mathcal{F}_\varepsilon(\beta_n^\dagger) - \Lambda^\dagger\right) > \left(\frac{\sigma_V^2}{|H_n|^2}\mathcal{F}_\varepsilon(0) - \Lambda^\dagger\right) > 0$, and the last simplified KKT condition implies $\beta_n^\dagger = 0$.

2. If $\Lambda^\dagger > \frac{\sigma_V^2}{|H_n|^2}\mathcal{F}_\varepsilon(0)$, then the third condition implies $\mathcal{F}_\varepsilon(\beta_n^\dagger) > \mathcal{F}_\varepsilon(0)$ and therefore $\beta_n^\dagger > 0$. Consequently from the last condition we get $\beta_n^\dagger = \mathcal{F}_\varepsilon^{-1}\left(\frac{|H_n|^2}{\sigma_V^2}\Lambda^\dagger\right)$.

3. If $\Lambda^\dagger = \frac{\sigma_V^2}{|H_n|^2}\mathcal{F}_\varepsilon(0)$ then either $\beta_n^\dagger = 0$ or $\mathcal{F}_\varepsilon(\beta_n^\dagger) = \mathcal{F}_\varepsilon(0)$. However, the latter also implies that $\beta_n^\dagger = 0$. Thus in this case $\beta_n^\dagger = 0$.

In summary, if $\Lambda^\dagger \leq \frac{\sigma_V^2}{|H_n|^2}\mathcal{F}_\varepsilon(0)$ then $\beta_n^\dagger = 0$. Otherwise $\beta_n^\dagger = \mathcal{F}_\varepsilon^{-1}\left(\frac{|H_n|^2}{\sigma_V^2}\Lambda^\dagger\right)$. ∎

If the value of $\Lambda^\dagger$ is known, then a solution of the relaxed bit allocation problem is at hand in closed form. Unfortunately the calculation of $\Lambda^\dagger$ is in itself computationally intensive. In the following we first assume that the value of $\Lambda^\dagger$ is known and thus the solution given by (3.15) is available. Next we will address the solution method without the knowledge of $\Lambda^\dagger$.

In general, $\{\beta_n^\dagger\}_{n=1}^{N}$ is not a legitimate solution to the optimization problem (3.11) - (3.13) since the satisfaction of (3.13) is not guaranteed. A straightforward method of obtaining an integer-valued solution from $\{\beta_n^\dagger\}_{n=1}^{N}$ is to quantize these values. A vector $\{\beta_n\}_{n=1}^{N}$ can be obtained from $\{\beta_n^\dagger\}_{n=1}^{N}$ by letting $\beta_n = Q(\beta_n^\dagger)$ where $Q : \Re \longrightarrow \Omega$ denotes a scalar quantization function. To ensure that the data rate of the quantized solution $\{\beta_n\}_{n=1}^{N}$ remains close to that of $\{\beta_n^\dagger\}_{n=1}^{N}$, we choose Q so as to minimize $E\left[\left|\sum_{n=1}^{N} \beta_n^\dagger - \sum_{n=1}^{N} \beta_n\right|\right]$. Now

$$E\left[\left|\sum_{n=1}^{N} \beta_n^\dagger - \sum_{n=1}^{N} \beta_n\right|\right] \leq \sum_{n=1}^{N} E[|\beta_n^\dagger - \beta_n|]$$

The quantizer that minimizes the absolute error $E[|\beta_n^\dagger - \beta_n|]$ has threshold values $T_1, T_2, \cdots, T_L$ given by

$$T_i = \frac{b_{i-1} + b_i}{2}, \ i = 1, 2, \cdots, L. \tag{3.17}$$

where $b_0 = 0$. Based on these threshold values, the proposed quantization process is represented by the following equation.

$$\beta_n = \mathrm{Q}(\beta_n^\dagger) = \begin{cases} 0, & \text{if } \beta_n^\dagger < T_1 \\ b_1, & \text{if } T_1 \leq \beta_n^\dagger < T_2 \\ \vdots & \vdots \\ b_L, & \text{if } \beta_n^\dagger \geq T_L \end{cases} \quad \forall n \tag{3.18}$$

Let T be an arbitrary positive real number. Then the following statements can be easily verified from (3.15).

$$\beta_n^\dagger > T \iff |H_n|^2 > \frac{\sigma_V^2}{\Lambda^\dagger} \mathcal{F}_\varepsilon(T) \tag{3.19}$$

$$\beta_n^\dagger = T \iff |H_n|^2 = \frac{\sigma_V^2}{\Lambda^\dagger} \mathcal{F}_\varepsilon(T) \tag{3.20}$$

$$\beta_n^\dagger < T \iff |H_n|^2 < \frac{\sigma_V^2}{\Lambda^\dagger} \mathcal{F}_\varepsilon(T) \tag{3.21}$$

The above shows that the proposed quantization process can be applied directly to the sequence of channel power gains. In other words, the suboptimal bit allocation $\{\beta_n\}_{n=1}^N$ may be obtained by quantizing $\{|H_n|^2\}_{n=1}^N$ as follows

$$\beta_n = \tilde{\mathrm{Q}}(|H_n|^2) = \begin{cases} 0, & \text{if } |H_n|^2 < G_1 \\ b_1, & \text{if } G_1 \leq |H_n|^2 < G_2 \\ \vdots & \vdots \\ b_L, & \text{if } |H_n|^2 \geq G_L \end{cases} \quad \forall n \tag{3.22}$$

where
$$G_i = \frac{\sigma_V^2}{\Lambda^\dagger} \cdot \mathcal{F}_\varepsilon(T_i) \quad \forall\, i = 1, 2, \cdots, L. \tag{3.23}$$

It should be noted that the threshold values $\{G_i\}_{i=1}^L$ can be easily pre-computed from (3.17) and (3.23).

So far we have developed an adaptive bit allocation scheme assuming the value of $\Lambda^\dagger$ is known. As mentioned previously, intensive computations are required to obtain the value of $\Lambda^\dagger$ from (3.16). In addition, even when $\Lambda^\dagger$ is calculated, the bit-allocation solution obtained from (3.22) may not satisfy (3.12). In the next section, we propose an algorithm based on the scheme developed in this section which circumvents these difficulties.

3.3.2 Algorithm Description and Complexity Analysis

In this section we introduce an algorithm to obtain the values of $G_1, G_2, \cdots, G_L$ such that the result of the quantization process developed in the previous section satisfies (3.12) as well. We start with the following.

Lemma 3.2 *Let* $\delta = \max_{i \in \{1,2,\cdots,L\}} \{b_i - b_{i-1}\}$. *Then the solution* $\{\beta_n^*\}_{n=1}^N$ *for the optimization problem (3.11) - (3.13) satisfies*

$$R \leq \sum_{n=1}^N \beta_n^* \leq R + \delta \tag{3.24}$$

Proof: Assume to the contrary that $\sum_{n=1}^N \beta_n^* > R + \delta$. Clearly there exists $n_0 \in \{1, 2, \cdots, N\}$ such that $\beta_{n_0}^* > 0$. Suppose $\beta_{n_0}^* = b_i$ for some $i \in \{1, 2, \cdots, L\}$. Since $b_{i-1} \in \Omega$, by changing the value of $\beta_{n_0}^*$ to b_{i-1} we obtain a new bit allocation satisfying constraints (3.12) and (3.13) with less transmit power than the optimal solution. This contradicts the optimality of the original solution. ∎

The condition in (3.24) will be used in our search algorithm as the condition for the termination of the algorithm. From (3.23) we get

$$\frac{G_i}{G_1} = \frac{\mathcal{F}_\varepsilon(T_i)}{\mathcal{F}_\varepsilon(T_1)} \quad \forall i \in \{2, 3, \cdots, L\} \tag{3.25}$$

This shows that we only need to determine the value of one of the G_i's (say G_1). The remaining threshold values can be computed from (3.25).

It is obvious that R must be no larger than Nb_L, otherwise (3.12) and (3.13) can not be both satisfied. According to the definition of δ, it is trivial to consider the problem of bit and power allocation for R between $(Nb_L - \delta)$ and Nb_L. Instead, the value of interest for R is $0 < R < (Nb_L - \delta)$. Define $b_{i_0} = \sup\{b \in \Omega | b < \frac{R}{N}\}$ and $b_{i_1} = \inf\{b \in \Omega | b > \frac{R+\delta}{N}\}$. It can be seen the existence of b_{i_0} and b_{i_1} is guaranteed for any R of interest. Furthermore $b_{i_0} \in \Omega \setminus \{b_L\}$ and $b_{i_1} \in \Omega \setminus \{0\}$. Let $\mathcal{H}_{max} = \max_{n \in \{1,2,\cdots,N\}} \{|H_n|^2\}$ and $\mathcal{H}_{min} = \min_{n \in \{1,2,\cdots,N\}} \{|H_n|^2\}$. The following theorem specifies a range of values for G_1.

Theorem 3.2 *Suppose for a value of* G_1 *we generate the vector* $\mathbf{G} = [G_1, G_2, \cdots, G_L]$ *from (3.25) and use* $\mathbf{G}$ *to obtain a bit allocation* $\{\beta_n\}_{n=1}^N$ *from (3.22). If* $\{\beta_n\}_{n=1}^N$ *satisfies (3.24) then the following must be true*

$$\underline{G}_1 < G_1 \leq \overline{G}_1 \tag{3.26}$$

where

$$\underline{G}_1 = \mathcal{H}_{min} \cdot \mathcal{F}_\varepsilon(T_1)/\mathcal{F}_\varepsilon(T_{i_1}) \tag{3.27}$$

$$\overline{G}_1 = \mathcal{H}_{max} \cdot \mathcal{F}_\varepsilon(T_1)/\mathcal{F}_\varepsilon(T_{i_0+1}) \tag{3.28}$$

Proof: Since $b_{i_0} \in \Omega \setminus \{b_L\}$ and $b_{i_1} \in \Omega \setminus \{0\}$ then $(i_0 + 1), i_1 \in \{1, 2, \cdots, L\}$. Thus both T_{i_0+1} and T_{i_1} exist, i.e., $\overline{G_1}$ and $\underline{G_1}$ are well defined.

Suppose $\mathcal{H}_{max} < G_{i_0+1}$. Then the power gain of all subcarriers are below the threshold value G_{i_0+1}, which implies $\beta_n \leq b_{i_0}$ for all n. Therefore $\sum_{n=1}^{N} \beta_n \leq N b_{i_0} < N \cdot \left(\frac{R}{N}\right) < R$, which violates (3.24). Thus $\mathcal{H}_{max} \geq G_{i_0+1}$. According to (3.25), this is equivalent to $G_1 \leq \mathcal{H}_{max} \frac{\mathcal{F}_\varepsilon(T_1)}{\mathcal{F}_\varepsilon(T_{i_0+1})} = \overline{G_1}$. Similarly it can be shown that $G_1 > \underline{G_1}$. ∎

The upper and lower bounds on G_1 established above will be used in searching for the value of G_1. An important observation is that if we increase the value of G_1 all threshold values increase, and thus the total number of bits allocated by the quantization process decreases, and vice versa. The following algorithm uses this observation to obtain the optimal value of G_1 and in this way solves the bit allocation problem.

Adaptive Bit and Power Allocation (ABPA) Algorithm

Step 1: Calculate the power gains $\{|H_n|^2\}_{n=1}^{N}$, find $\mathcal{H}_{max}$ and $\mathcal{H}_{min}$.
Step 2: Calculate $\underline{G_1}$ and $\overline{G_1}$ from (3.27) and (3.28),
   let $G_1 = \frac{\overline{G_1} + \underline{G_1}}{2}$, $\Delta = \frac{\overline{G_1} - \underline{G_1}}{4}$ and $I = 0$.
Step 3: Determine $G_2 \sim G_L$ from (3.25) and compute β_n from (3.22) for each n.
Step 4: If $\sum_{n=1}^{N} \beta_n < R$ and $I \leq MaxCount$, then $G_1 = G_1 - \Delta$;
   else if $\sum_{n=1}^{N} \beta_n > R + \delta$ and $I \leq MaxCount$, then $G_1 = G_1 + \Delta$;
   otherwise, go to Step 6.
Step 5: Let $\Delta = \Delta/2$, $I = I + 1$ and go to Step 3.
Step 6: For each n, calculate $P_n = \frac{\sigma_V^2}{|H_n|^2} f(\beta_n, \varepsilon)$.

In the above algorithm Steps 1 and 6 each require operations of order N, and Step 3 needs to perform N quantizations during each iteration. These operations dominate the complexity of the proposed algorithm since N is usually much larger than L for practical systems. So the computational complexity of the proposed algorithm is $O(I \times N + 2N)$, where I denotes the number of iterations. It can be seen that the complexity of the proposed algorithm has the same expression as that in [22] and [23]. However, the actual complexity, when the algorithm is implemented in DSP chips, is much lower. This is due to the fact that the operations performed during each iteration only include comparisons required by the quantization process whereas the logarithm and/or division operations are necessary in [22] and [23]. Moreover, the performance of the proposed method is almost the same as that of the greedy approach in [21] and is better than [22] and [23].

3.4 An Efficient Subcarrier Allocation Method

As mentioned previously the optimal allocation of subcarriers requires the solution of the constrained optimization problem (3.3) - (3.6) which is computationally pro-

hibitive. To get around the complexity issue, the problem of subcarrier allocation may be studied without involving bit and/or power allocation.

In [28] it is shown that if the constraint in (3.4) is removed, then the optimal subcarrier allocation is to assign each subcarrier to the user whose power gain is the largest in that subcarrier. This approach, however, is unfair as it penalizes users whose channel power gains are small. It is clear that any subcarrier allocation method that satisfies (3.4) must also satisfy

$$\sum_{n=1}^{N} \rho_{n,k} \geq \left\lceil \frac{R_k}{b_L} \right\rceil \quad \forall k = 1, 2, \cdots, K \tag{3.29}$$

In other words (3.29) is a necessary condition so that the data rate requirement of all users is satisfied.

Several algorithms [27, 25, 30, 31] have been proposed in the literature to perform subcarrier allocation while satisfying (3.29). In [27] the bit allocation has been assumed to be uniform for all users and the target BER is identical for different users as well. The proposed algorithm tries to minimize the objective function $\sum_{n,k} \rho_{n,k} \frac{1}{|H_{n,k}|^2}$. Specifically, it first attains an initial allocation under the constraint of (3.29). Then improves it following a greedy approach. The performance of this algorithm is very good. In fact it performs so well for subcarrier allocation that the subsequent adaptive bit allocation yields little performance improvement. However, this algorithm has a high computational complexity of the order of $O(KN \log N + N^2)$ [29]. We describe our algorithm for subcarrier allocation next.

3.4.1 Algorithm Description

The algorithm presented below inspects all N subcarriers in a step by step fashion. In each step it allocates the corresponding subcarrier to a user who requires the least increase in transmit power among a subset of all users. The subset of users chosen for comparison during each step is designed to satisfy (3.29).

To evaluate the increases in transmit power we use the *normalized* power gains defined by

$$g_{n,k} := \frac{|H_{n,k}|^2}{\sum_n |H_{n,k}|^2} \quad \forall n = 1, 2, \cdots, N, \ \forall k = 1, 2, \cdots, K \tag{3.30}$$

During the mth step, if the corresponding subcarrier is assigned to the kth user then the increase of transmit power for that user is given by

$$\Delta P_k(m) = \frac{\sigma_V^2 f(\beta_0, \varepsilon_k)}{g_{m,k}} \tag{3.31}$$

where, to simplify the algorithm, we assume that the number of bits assigned to each subcarrier is a constant given by

$$\beta_0 := \frac{\sum_k R_k}{N} \tag{3.32}$$

Subcarrier Allocation (SA) Algorithm

Step 1: Calculate $\{g_{n,k}\}$ from (3.30). Let $\Theta_0 = \{1, \cdots, K\}$ and $\Theta_1 = \Phi$, where Φ denotes the null set. Let $s_k = 0$ for $k = 1, 2, \cdots, K$.

Step 2: For m from 1 to N, performs the following:

If $\Theta_0 \neq \Phi$, assign the mth subcarrier to user $\hat{k} = \arg\min_{k \in \Theta_0} \Delta P_k(m)$;

$s_{\hat{k}} = s_{\hat{k}} + 1$;

if $s_{\hat{k}} \geq \left\lceil \frac{R_k}{b_L} \right\rceil$, let $\Theta_0 = \Theta_0 - \left\{\hat{k}\right\}$,

if $s_{\hat{k}} < \left\lceil \frac{R_k}{\beta_0} \right\rceil$, then $\Theta_1 = \Theta_1 + \left\{\hat{k}\right\}$.

Otherwise, assign the mth subcarrier to user $\hat{k} = \arg\min_{k \in \Theta_1} \Delta P_k(m)$.

$s_{\hat{k}} = s_{\hat{k}} + 1$;

if $s_{\hat{k}} \geq \left\lceil \frac{R_k}{\beta_0} \right\rceil$, then $\Theta_1 = \Theta_1 - \left\{\hat{k}\right\}$.

The proposed subcarrier allocation algorithm terminates after at most N steps. In each step the number of users chosen for comparison is determined by the size of Θ_0 or Θ_1, which is less than or equal to K. So the complexity of the proposed algorithm is no greater than $O(N \times K)$. For each user chosen for comparison, calculating the increase of transmit power requires only one division operation since the numerator of (3.31) has been given and can be calculated beforehand. It can be seen that the proposed algorithm is computationally more efficient than the subcarrier allocation schemes presented in [25], [27] and [29].

3.5 Numerical Results

In this section we examine the performance of the proposed ABPA algorithm and SA algorithm through simulation. The simulated OFDM system has $N = 128$ subcarriers with the frequency offset between adjacent subcarriers equals to $\Delta F = 20$KHz. The modulation schemes that are considered are QPSK, 16QAM and 64QAM. Thus $\Omega = \{0, 2, 4, 6\}$. According to [24], the function f associated with this system may be written as

$$f(\beta, \varepsilon) = \frac{\left(2^{\beta} - 1\right)\left(\ln c_1 - \ln \varepsilon\right)}{c_2} \tag{3.33}$$

where $c_1 = 0.2$ and $c_2 = 1.6$.

3.5.1 Performance of the ABPA Algorithm

We have generated 1,000 independent realizations of CFR using a 9-path outdoor channel model similar to the COST207 model [59]. The power delay profile for the simulated channel model is exponentially decaying with the maximum excessive delay of $5\mu s$ [59]. Specifically, the delay of these 9 rays are randomly generated within the

$5\mu s$ interval while their amplitudes undergo independent Rayleigh fading. The CFR is generated by taking N-point discrete Fourier transform (DFT) for the samples of channel impulse response, where the sampling rate is $N\Delta F = 2.56\text{MHz}$. For the purpose of simplicity, the CFR has been *normalized* such that $\frac{\sum_{n=1}^{N} |H_n|^2}{N} = 1$ for all channel realizations. The proposed ABPA algorithm is then performed for a given target BER ε and data rate requirement R.

The resulting total receive power for all the subcarriers is calculated from the algorithm for each CFR realization and then averaged over the 1,000 realizations to obtain $P_{\text{ave}}(\varepsilon, R)$. The average SNR is then calculated as

$$\bar{\nu} = 10 \log_{10} \frac{P_{\text{ave}}(\varepsilon, R)}{N \sigma_V^2} \quad (\text{dB}). \tag{3.34}$$

Two values of $R = 256$ and $R = 512$ were used. Figure 3.1 illustrates the simulation results where BER ε is plotted vs. the SNR $\bar{\nu}$. In this figure the performance of the proposed ABPA algorithm is compared with that of the greedy method in [21] which is labelled as "optimal". For comparison the results for the non-adaptive OFDM system, where bit and power allocation is identical for all subcarriers has also been plotted. From Figure 3.1 we can see that the performance of the proposed ABPA algorithm is almost the same as the optimal method of [21] and is at least 10dB better than the non-adaptive system for BER 10^{-3}. The complexity of our algorithm is, however, significantly lower than that of the optimal solution. The number of iterations required for the ABPA algorithm to terminate is less than 7 in most cases. The worst case we observed involved only 14 iterations.

The complexity of the proposed algorithm has been compared with that of the method in [23], which is one of the most efficient bit and power allocation algorithms in the literature. For each value of N, 1000 independent realizations of CFR have been generated following the approach described previously. Both algorithms are applied to each channel realization for $R = 4N$ and BER 10^{-3}. The numbers of various operations including comparison, addition, multiplication, division and logarithm have been counted and averaged in category. We assume that each logarithm operation requires 16 clock cycles to finish and the division operation needs 8 clock cycles. All other operations are assumed to take only one clock cycle. Figure 3.2 illustrates the average number of clock cycles for both algorithms as a function of N. We can see they both increase linearly with respect to N. However, the proposed ABPA algorithm is significantly faster than the method of [23] for large N. Figure 3.3 shows the performance of both methods for the same parameters as in Figure 3.1 for $R = 512$. It can be seen that the ABPA algorithm is about 0.3dB better for all values of SNR.
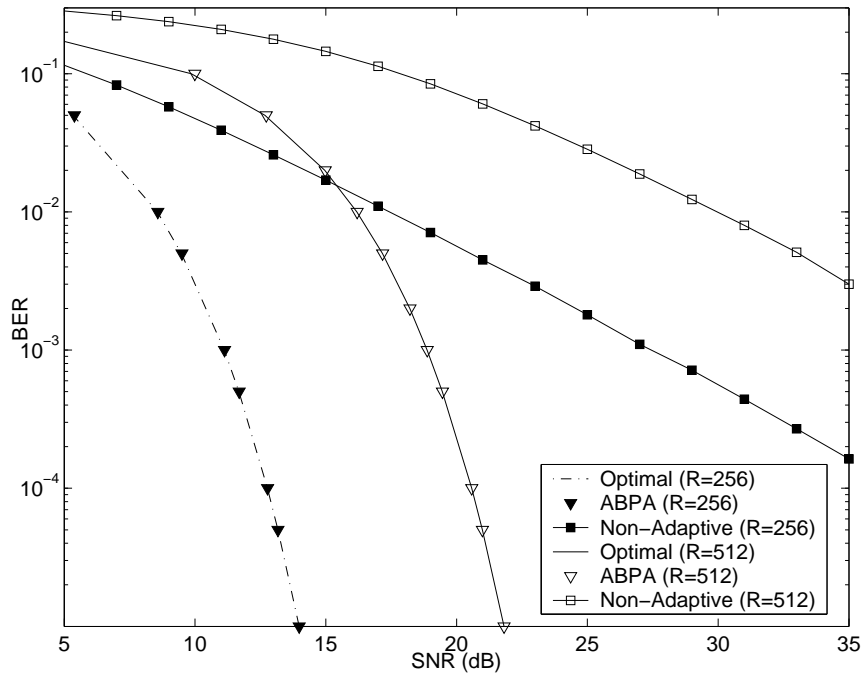
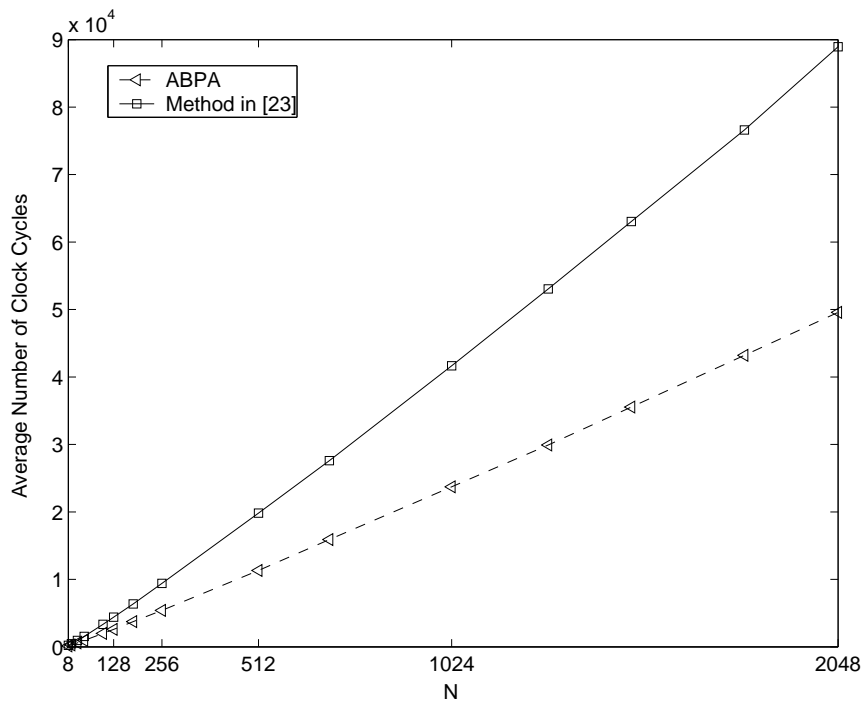Figure 3.1: Performance of the ABPA algorithms

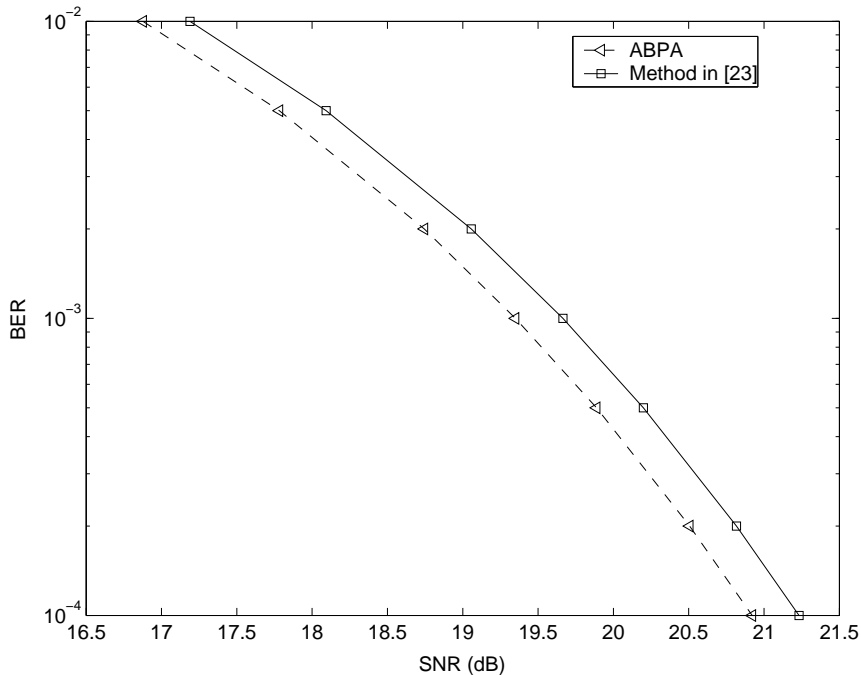Figure 3.2: Complexity of the ABPA algorithm

47

Figure 3.3: Performance comparison: ABPA vs method in [23]

3.5.2 Performance of the SA Algorithm

We now consider a MU-OFDM system with $K = 5$ users. The CFR for these users are randomly selected from the aforementioned channel realizations. The target BER for all users are set to the same value ε. For various users the target data rates and the average channel power gain given by $\sum_n |H_{n,k}|^2$ can be different. We have simulated two cases whose configurations are given in Table 3.1. In both cases we compare three different subcarrier allocation schemes. One is the algorithm presented in [27] and it is denoted by "WSA". Another is our proposed subcarrier allocation algorithm which is referred to as "SA". The third is a rate proportional FDMA scheme which yields a fixed subcarrier allocation, and is denoted by "FSA" [25].

After performing subcarrier allocation a bit and power allocation algorithm must be employed for each user to ensure that their data rate and BER requirements are satisfied. One method we use is the proposed ABPA algorithm. The other one is denoted by "UBA", which uniformly allocates bits to the subcarriers assigned to the same user according to the data rate requirement for that user. Moreover, the corresponding transmit power is adjusted such that the BER requirement for that user is satisfied as well.

Figures 3.4 and 3.5 illustrate the simulation results for both cases where the power of white noise are assumed to be identical for all five mobile stations. The system SNR is calculated from equation (3.34) by replacing $P_{\text{ave}}(\varepsilon, R)$ with the average transmit

Table 3.1: User and channel configurations for the MU-OFDM system

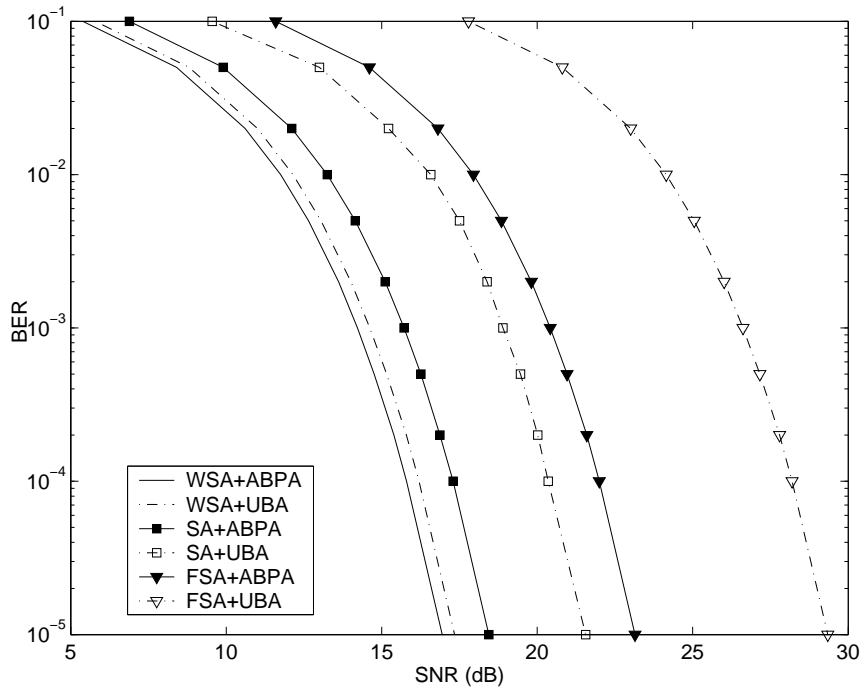|	Case 1			Case 2	
User (k)	R_k	Average Power Gain	R_k	Average Power Gain
1	100	0dB	24	0dB
2	100	0dB	24	+2dB
3	100	0dB	128	-4dB
4	100	0dB	128	+6dB
5	100	0dB	208	-8dB

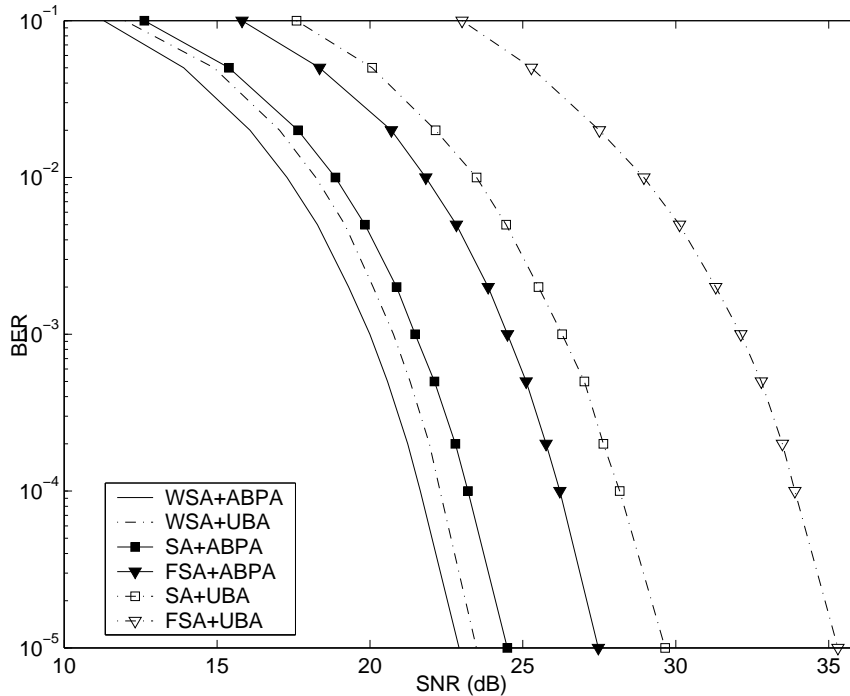Figure 3.4: Performance of the Subcarrier Allocation algorithm (case 1)

Figure 3.5: Performance of the Subcarrier Allocation algorithm (case 2)

power of the BS. We can see that when the WSA algorithm is employed the difference between using UBA or ABPA is negligible although the latter yields a better performance. Moreover, the performance of the system using both SA and ABPA is close (within 1.5dB) to the "WSA+ABPA" case whose performance is nearly optimal [27]. It is clear that the complexity for the proposed SA algorithm along with the ABPA algorithm is much lower than the WSA method making it more favorable for the wireless OFDM systems.

3.6   Chapter Summary

The optimal subcarrier, bit and power allocation problem for MU-OFDM systems has been investigated. The optimal bit and power allocation problem is first formulated as a mixed integer programming problem. This problem is then relaxed to a constraint optimization problem and solved using the Karush-Kuhn-Tucker conditions. Guided by the insights gained from this solution we develop a computationally efficient iterative algorithm to obtain a near-optimal solution for the original bit and power allocation problem. An efficient suboptimal algorithm is also presented for the subcarrier allocation problem. Numerical results illustrate the low computational complexity and nearly optimal performance of the algorithms making them suitable for wireless MU-OFDM systems.

CHAPTER 4. ON THE BIT AND POWER ALLOCATION FOR OFDM SYSTEMS WITH TIME-VARYING CHANNELS

4.1   Introduction

Adaptive modulation has been recognized as an effective technique for improving the performance of wide-band communication systems over frequency-selective fading channels. When applied to OFDM systems, this scheme proposes to select for each subcarrier a proper size of modulation signal set and transmit power according to the instantaneous frequency response of the channel such that the desired quality of service (QoS) can be achieved with the maximum spectral efficiency [24, 22, 32, 33]. Intuitively, in order to exploit the full potential of an adaptive modulation scheme, the transmitter should have *complete* and *perfect* knowledge of channel state information (CSI). However, this condition is too optimistic to be satisfied in practice due to the following reasons: 1) CSI is obtained by the receiver through channel estimation and the noise in the received signal may cause estimation errors; 2) the physical channel is often time-varying and thus transmission and processing delay will make the CSI estimates outdated. Previous works [36, 39, 40, 41] have confirmed that the performance of most adaptive modulation schemes assuming perfect knowledge of CSI will degrade significantly even with moderate errors in the estimated CSI. While the errors in the estimated CSI can be considerably suppressed using recently proposed efficient channel estimation techniques, the difficulties caused by the outdated CSI estimates in time-varying channels remains. For OFDM systems this problem is more pronounced due to a greater symbol duration than single-carrier systems with similar bandwidth, as well as the large processing and transmission delay inherent in OFDM systems.

In this chapter, we focus on the problem of resource allocation based on the noisy and outdated knowledge of the CSI. An earlier study in [42] shows that the state of a frequency-flat fading channel can be reliably predicted from the outdated observations across a long range of time. This motivates the prediction of frequency-selective channels for the OFDM system since, using OFDM, the wide-band channel is transformed into a number of flat-fading sub-channels. We adopt the idea of CSI prediction and propose to perform resource allocation based on the predicted CSI.

This chapter is organized as follows. The channel model used in this chapter is first introduced in Section 4.2, in which we also motivate channel prediction by showing the effect of delayed CSI estimation in the time-varying channel. In Section 4.3, different channel predictors using Wiener filter or adaptive filters are discussed and their performance are compared. Bit and power allocation based on the predicted CSI is discussed in Section 4.4, where, by taking the remaining errors in channel predictions

into account, the proposed allocation schemes guarantee to meet the target BER. Finally, simulation results are presented in Section 4.5. We draw some conclusions in Section 4.6.

4.2 Preliminary Analysis

4.2.1 Channel Model

In general, the equivalent lowpass impulse response of a time-varying, frequency-selective multipath fading channel can be written as [58, 59]

$$c(\tau;t) = \sum_{i=0}^{D-1} \alpha_i e^{-j\phi_i(t)} \delta(\tau - \tau_i),$$

where

$$\phi_i(t) = 2\pi\{(f_c + f_{d,i})\tau_i - f_{d,i}t\}$$

and where D denotes the number of paths, τ_i, α_i and $f_{d,i}$ are, respectively, the propagation delay, the attenuation factor and Doppler frequency spread for the ith path, $\delta(\cdot)$ is the Dirac delta function, and f_c is the carrier frequency. Let $r_i(t) = \alpha_i e^{-j\phi_i(t)}$. Then

$$c(\tau;t) = \sum_{i=0}^{D-1} r_i(t)\delta(\tau - \tau_i) \tag{4.1}$$

where we assume that the path gains $r_i(t)$ are uncorrelated wide-sense stationary random processes (wide-sense stationary, uncorrelated scattering (WSS-US) condition) [58, 59]. The WSS-US assumption implies that

$$E[r_i(t_1)r_j^*(t_2)] = \begin{cases} 0 & i \neq j \\ E[|r_i|^2]\rho(t_1 - t_2) & i = j \end{cases} \tag{4.2}$$

where $\rho(t)$ denotes the normalized autocorrelation function of $\{r_i(t)\}$.

Now consider an N-tone OFDM system transmitted over the channel defined by (4.1). The size of the cyclic prefix (CP) used in this system is denoted by L, and the sampling time is T_S. It is assumed that, when compared with the rate of the OFDM blocks, the variation of $r_i(t)$ is slow for all i. Thus, in this case, the inter-carrier interference (ICI) can be ignored, and the OFDM system can be simply represented by $y_{n,k} = h_{n,k}x_{n,k} + v_{n,k}$ for all $n = 0, 1, \cdots, N-1$ and $k = \cdots, 1, 2, \cdots$, where $x_{n,k}$ and $y_{n,k}$ are, respectively, the nth transmitted and received complex symbols of the kth block. Meanwhile, the sequence $\{h_{n,k}\}_{n=0}^{N-1}$ represents the channel frequency response (CFR) and $\{v_{n,k}\}_{n=0}^{N-1}$ is a sequence of *iid* complex Gaussian random variables with zero mean and fixed variance σ_v^2 for all k and n. Let $\mathbf{h}(k) = [h_{0,k}, \cdots, h_{N-1,k}]^T$. Then it is known that $\mathbf{h}(k) = \mathbf{F}_L \mathbf{g}(k)$ for all k, where $\mathbf{F}_L$ is the first L columns of the

N-point DFT transform matrix and $\mathbf{g}(k) = [g_{0,k}, \cdots, g_{L-1,k}]^T$ is the channel impulse response (CIR) for block k in the discrete time domain. $\mathbf{g}(k)$ is determined by the realization of $c(\tau; t)$ at the time $t = kT_B$, where $T_B = (N+L)T_S$. Let $p(\tau)$ denote the composite impulse response of the analog components in the OFDM system including DAC, ADC, analog filters, power amplifiers, etc. It is shown in Chapter 1 that

$$g_{l,k} = \sum_{i=0}^{D-1} r_i(kT_B)p(lT_S - \tau_i), \ \forall l = 0, 1, \cdots, L-1, \tag{4.3}$$

for all k. It is inferred from (4.3) that, although $r_i(t)$ are uncorrelated for different i, the elements of $\mathbf{g}(k)$ are correlated. Therefore, in order to achieve optimal channel prediction, all elements of the outdated CIRs should be used to predict each element of the current CIR.

4.2.2   Motivation

In this section we illustrate the effect of outdated channel state information and motivate the need for channel prediction. As mentioned previously, it is not feasible to obtain perfect knowledge of $\mathbf{g}(k)$ or $\mathbf{h}(k)$ for resource allocation of the kth OFDM block. A straightforward approach is to take the *most recent* estimation of CSI from the receiver, which is not only noisy but also outdated, as a prediction of the current CSI. In other words, let

$$\tilde{\mathbf{g}}(k) := \hat{\mathbf{g}}(k-d) = \mathbf{g}(k-d) + \mathbf{e}(k-d),$$

where $\hat{\mathbf{g}}(k-d)$ is the estimated CIR at time $k-d$, $\tilde{\mathbf{g}}(k)$ is our prediction of CIR at time k and dT_B is the associated delay and $\mathbf{e}(k-d)$ is the channel estimation error. The normalized mean square error (NMSE), which is defined by $\text{NMSE}_{\tilde{\mathbf{g}}(k)} := E(\|\tilde{\mathbf{g}}(k) - \mathbf{g}(k)\|^2)/E(\|\mathbf{g}(k)\|^2)$, is used to measure the difference between $\mathbf{g}(k)$ and $\tilde{\mathbf{g}}(k)$, where $\|\cdot\|$ is the L_2-norm and $E(\cdot)$ denotes expectation. From the relationship between CIR and CFR one can show that $\text{NMSE}_{\tilde{\mathbf{h}}(k)} = \text{NMSE}_{\tilde{\mathbf{g}}(k)}$. Using the WSS assumption of the channel, the NMSE of the outdated CIR can be calculated as follows

$$
\begin{aligned}
\text{NMSE}_{\tilde{\mathbf{g}}(k)} &= E\left[\|\mathbf{g}(k-d) + \mathbf{e}(k-d) - \mathbf{g}(k)\|^2\right]/E\left[\|\mathbf{g}(k)\|^2\right] \\
&= \frac{2E(\|\mathbf{g}\|^2) + E(\|\mathbf{e}\|^2) - 2\text{Re}\left[\sum_{l=0}^{L-1} E(g_{l,k-d}^* g_{l,k})\right]}{E(\|\mathbf{g}\|^2)}
\end{aligned}
\tag{4.4}
$$

Using (4.2) it can be shown that

$$
\begin{aligned}
E[g_{l,k-d}^* g_{l,k}] &= \sum_{i=0}^{D-1}\sum_{j=0}^{D-1} E[r_i^*((k-d)T_B)r_j(kT_B)p^*(lT_S - \tau_i)p(lT_S - \tau_j) \\
&= \rho(dT_B)\sum_{i=0}^{D-1} E[|r_i|^2]\,|p(lT_S - \tau_i)|^2 \\
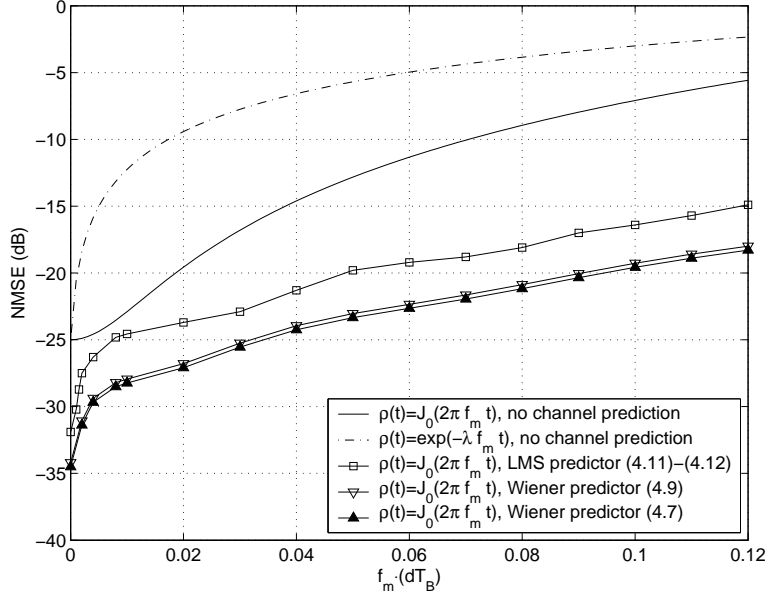&= \rho(dT_B)E[g_{l,k}^* g_{l,k}]
\end{aligned}
\tag{4.5}
$$

Figure 4.1: Performance of channel prediction in terms of NMSE

Using (4.4) and (4.5) we can write

$$\mathrm{NMSE}_{\tilde{\mathbf{g}}(k)} = 2\left[1 - \mathrm{Re}(\rho(dT_B))\right] + E(\|\mathbf{e}\|^2)/E(\|\mathbf{g}\|^2) \qquad (4.6)$$

Equation (4.6) shows that if the outdated channel estimate is used as a prediction of the current CSI, the associated NMSE is not only determined by the signal to noise ratio (SNR) of the channel estimation method, but also the autocorrelation function $\rho(\cdot)$. It turns out that in this case the effect of the channel autocorrelation function is more significant than that of the estimation error.

For Rayleigh fading channels, it is well known that $\rho(t) = J_0(2\pi f_m t)$ [59], where $J_0(\cdot)$ is the zeroth-order Bessel function of the first kind and f_m denotes the maximum Doppler frequency shift. Another commonly used autocorrelation function is $\rho(t) = e^{-\lambda f_m t}$. For $\lambda \approx 2.8634$ this model has the same coherence time[1] as the Rayleigh fading model. The NMSEs calculated from (4.6) using these two correlation functions have been plotted with respect to $f_m dT_B$ in Figure 4.1, where the SNR in the CIR estimation, namely the value of $E(\|\mathbf{e}\|^2)/E(\|\mathbf{g}\|^2)$, has been fixed to be 25dB. This figure illustrates that, when a delayed version of the estimated CIR is used for future CIR prediction, a small delay may result in large errors in CIR prediction even in cases where the estimation error is at an acceptable level (SNR=25dB). For comparison, in the same figure, we show the results of the CIR prediction using different predictors, which will be discussed in the next section.

---

[1]The time over which the correlation coefficient is above 0.5

4.3 Channel Prediction

Channel prediction can be performed for either CFR or CIR. There are two advantages in performing channel prediction in the time domain (CIR). First, the length of CFR sequence (N) is often much larger than that of CIR (L) resulting in much higher complexity for the predictor. Secondly, there exist several well established models for the autocorrelation function of CIR [58, 59]. Recently, new autoregressive models for the CFR of wideband channels have been proposed [12, 35], which may be exploited for the prediction of CFR. However, the first point on the higher complexity of CFR prediction remains.

4.3.1 Wiener Channel Prediction

As mentioned previously, due to the correlation between channel coefficients, a vector predictor should be used to achieve optimal performance. Let $\hat{\mathbf{g}}(k-d), \hat{\mathbf{g}}(k-2d), \cdots, \hat{\mathbf{g}}(k-Md)$ be the CIR estimations available to the transmitter. Due to the limited capacity of the feedback channel, it is assumed that only a down-sampled version (by a ratio of d) of the CIR estimates at the receiver are fed back to the transmitter. So, d is usually an integer number larger than 1. The objective is to find an optimal estimation of $\mathbf{g}(k)$ based on these outdated samples. We rearrange all elements of these vectors into a single LM-by-1 vector $\mathbf{u}(k) := [\mathbf{u}_{0,k}^T, \cdots, \mathbf{u}_{L-1,k}^T]^T$, where $\mathbf{u}_{l,k} = [\hat{g}_{l,(k-d)}, \cdots, \hat{g}_{l,(k-Md)}]^T$. Then the optimal linear prediction of $\mathbf{g}(k)$, which will result in the minimum mean-squared error (MSE), is given by the Wiener-Hopf equation as follows

$$\tilde{\mathbf{g}}_{opt}(k) = \left(\mathbf{R}_{\mathbf{uu}}^{-1}\mathbf{P}_{\mathbf{ug}}\right)^H \mathbf{u}(k) \tag{4.7}$$

where $\mathbf{R}_{\mathbf{uu}} = E[\mathbf{u}(k)\mathbf{u}(k)^H]$, $\mathbf{P}_{\mathbf{ug}} = E[\mathbf{u}(k)\mathbf{g}^H(k)]$, and $(\cdot)^H$ and $(\cdot)^{-1}$ denote, respectively, the matrix transpose conjugate and matrix inversion operations [60]. The definition of $\mathbf{u}(k)$ implies that $\mathbf{R}_{\mathbf{uu}} = [\mathbf{A}(l_1, l_2)]_{0 \leq l_1, l_2 \leq L-1}$, where $\mathbf{A}(l_1, l_2) = E[\mathbf{u}_{l_1,k}\mathbf{u}_{l_2,k}^H]$ is a square matrix. Similarly, $\mathbf{P}_{\mathbf{ug}} = [\mathbf{b}(l_1, l_2)]_{0 \leq l_1, l_2 \leq L-1}$, in which $\mathbf{b}(l_1, l_2) = E[\mathbf{u}_{l_1,k}g_{l_2,k}^*]$ is a column vector. The minimum MSE associated with this predictor is given by

$$\text{NMSE}_{opt} = 1 - \text{Tr}(\mathbf{P}_{\mathbf{ug}}^H \mathbf{R}_{\mathbf{uu}}^{-1} \mathbf{P}_{\mathbf{ug}})/E[\|\mathbf{g}\|^2] \tag{4.8}$$

where $\text{Tr}(\mathbf{A})$ is the trace of the matrix $\mathbf{A}$. In order to implement this predictor and evaluate its performance, it is necessary to have $\mathbf{A}(l_1, l_2)$ and $\mathbf{b}(l_1, l_2)$ for all $l_1, l_2 \in \{0, \cdots, L-1\}$. While these can, in principle, be calculated from (4.3), the implementation of the predictor requires the inversion of a matrix of size $LM \times LM$. This is computationally prohibitive and makes this predictor impractical.

In many cases, when $l_1 \neq l_2$, the cross-correlation between g_{l_1,k_1} and g_{l_2,k_2} is relatively small and can be ignored. Thus, assuming $E(g_{l_1,k_1}g_{l_2,k_2}^*) = 0$ for all $l_1 \neq l_2$, the matrices $\mathbf{R}_{\mathbf{uu}}$ and $\mathbf{P}_{\mathbf{ug}}$ can be rewritten as $\mathbf{R}_{\mathbf{uu}} = \text{diag}\{\mathbf{A}(0,0), \cdots, \mathbf{A}(L-1, L-1)\}$

and $\mathbf{P_{ug}} = \text{diag} \{\mathbf{b}(0,0), \cdots, \mathbf{b}(L-1, L-1)\}$. Accordingly, (4.7) and (4.8) can be significantly simplified as follows

$$\tilde{\mathbf{g}}_{sub}(k) = \left\{\mathbf{b}^H(l,l)\mathbf{A}^{-1}(l,l)\mathbf{u}_{l,k}\right\}_{l=0}^{L-1} \tag{4.9}$$

$$\text{NMSE}_{sub} = 1 - \sum_{l=0}^{L-1} \mathbf{b}^H(l,l)\mathbf{A}^{-1}(l,l)\mathbf{b}(l,l)/E[\|\mathbf{g}\|^2] \tag{4.10}$$

where the subscript "*sub*" indicates a *suboptimal* predictor when neglecting the cross-correlation of coefficients of the CIR. On the other hand, (4.9) reveals a channel predictor structure different from that of (4.7). Instead of lumping all entries of the M outdated CIR estimations to perform a complicated vector predictor, (4.9) suggests to use L independent scalar predictors. This structure is computationally much more efficient and will be adopted in the remainder of this chapter.

4.3.2 Adaptive Channel Prediction

Using the L predictors in (4.9) requires the matrices $\{\mathbf{A}(l,l)\}_{l=0}^{L-1}$ and the vectors $\{\mathbf{b}(l,l)\}_{l=0}^{L-1}$. However, for a time-varying channel, frequent computation of these will be unrealistic. In this case, a more realistic approach is to use an adaptive filter such as least mean-square (LMS) filter, recursive least-squares (RLS) filter or a Kalman filter, to replace each of the L Wiener filters in (4.9). In this case, the filter coefficients can be computed recursively. More importantly, an adaptive channel predictor has the ability of tracking the variation of channel statistics. Take the LMS predictor for example, the processing of the lth branch of the predictor can be represented by

$$\tilde{g}_{l,k} = \mathbf{w}_{l,k}^H \mathbf{u}_{l,k} \tag{4.11}$$

$$\mathbf{w}_{l,k+d} = \mathbf{w}_{l,k} + \nu \left(\hat{g}_{l,k-d} - \mathbf{w}_{l,k}^H \mathbf{u}_{l,k-d}\right)^* \mathbf{u}_{l,k-d} \tag{4.12}$$

where $\mathbf{w}_{l,k}$ denotes the filter coefficients of the lth branch at time $t = kT_B$, and ν is a positive constant denoting the step size. The choice of ν greatly affects the convergence properties and the performance of this predictor and this has been thoroughly discussed in [60]. It should be noted that, in (4.12), the prediction error for block k is evaluated by the difference between the latest channel estimation $\hat{g}_{l,k-d}$ and the predicted value $\tilde{g}_{l,k-d} = \mathbf{w}_{l,k}^H \mathbf{u}_{l,k-d}$ using the current filter coefficients.

Figure 4.1 also shows the performance of the optimal and suboptimal Wiener predictors ((4.7), (4.9)) and the LMS predictor ((4.11)-(4.12)) in terms of NMSE assuming a 12-ray channel model following (4.1), i.e., $D = 12$. The path delays $\{\tau_i\}$, which are spaced within the interval of $[0, 5]$ μsec, are provided in [59] (Table 2.1 of page 96) and remain constant throughout the simulation. All paths are assumed to undergo Rayleigh fading and have the normalized autocorrelation function $\rho(t) = J_0(2\pi f_m t)$. The power gain for each path has also been listed in Table 2.1 in [59]. The OFDM parameters used are $N = 64$, $L = 16$, $T_S = 0.625\mu s$ ($T_B = 50\mu s$), and

$p(\tau)$ is set to be the raised-cosine function with a roll-off factor of 0.35. The SNR of CIR estimation is set to 25dB, as in Section 4.2.2. In this case, d is set to 10 and the Doppler frequency f_m varies between 0Hz and 240Hz. It is clear that, the two Wiener predictors have very close performance and are better than the LMS predictor. Moreover, even the LMS predictor has significant performance improvement over that of using outdated CSI. It should be noted that, when f_m is small the performance of the predicted CIR can be better than that of the estimated CIR. This is because the considered channel estimation is performed for only one OFDM block, while the channel predictor can take estimations from M blocks whose CIRs can be strongly correlated with the current CIR.

4.4   Bit and Power Allocation Based on CSI Predictions

In this section we consider the problem of optimal bit and power allocation for OFDM systems using the predicted values of CIR. Since the discussion is focused on a single block, the subscript indicating the block number will be dropped. Let P_n and β_n, respectively, denote the power and the number of bits allocated to subcarrier n. The size of the modulation signal set for this subcarrier is then 2^{β_n}. The objective is to minimize the power allocated to the entire block while satisfying the requirement on system BER (ε_{target}) and data rate (R_{target} bits per block). In this section the prediction error is treated as additive noise and is measured by NMSE. We first show that if the prediction error in CIR is assumed to have a Gaussian distribution, then the resource allocation problem can be transformed into an equivalent problem of bit and power allocation with perfect CSI. Another approach to resource allocation will be presented in a subsequent section for general distributions of the channel prediction error.

4.4.1   Resource Allocation with Gaussian Prediction Error

We assume that the CIR prediction error $\mathbf{e} = (\tilde{\mathbf{g}} - \mathbf{g})$ is a complex-valued Gaussian random vector such that $E[\mathbf{e}] = \mathbf{0}_{L \times 1}$ and $E[\mathbf{e}\mathbf{e}^H] = \sigma_e^2 \mathbf{I}_{L \times L}$. This assumption is justified in light of the fact that the predictor is linear and that all fading components of the channel are assumed to follow a Gaussian distribution. In [33], we discussed the problem of bit and power allocation for the case of perfect CSI (i.e., $\sigma_e^2 = 0$). In this section, this is extended to the case of $\sigma_e^2 \neq 0$.

The instantaneous bit error probability for subcarrier n can be written as

$$\text{BER}_n = c_1 \exp\left[-P_n |h_n|^2 q(\beta_n)\right] \tag{4.13}$$

where $q(\cdot)$ is a known function of β_n [24]. For example, for QAM, $q(\beta_n) = \frac{c_2}{(2^{\beta_n}-1)\sigma_v^2}$, where c_1 and c_2 are known constants. It should be noted that the BER in (4.13) is evaluated using the channel CFR $\{h_n\}$, whereas the bit and power allocation is

performed using the predicted values of CFR, namely $\{\tilde{h}_n\}$, which in turn is obtained from an N-point DFT of CIR predictions $\{\tilde{g}_n\}$. For $\sigma_e^2 = 0$, i.e., $(\tilde{h}_n = h_n)$, setting $\text{BER}_n = \varepsilon_{target}$ results in a closed form relationship between P_n and β_n. This significantly simplifies the problem of bit and power allocation, which can then be solved using some computationally efficient algorithm, such as that in [33, 34]. On the other hand for $\sigma_e^2 \neq 0$, h_n and thus BER_n are random variables. In this case, a constraint regarding system BER requirement is proposed as follows:

$$E(\text{BER}_n | \tilde{h}_n) = \varepsilon_{target}, \ \forall n = 0, \cdots, N-1. \tag{4.14}$$

Based on the assumption on the distribution of the channel prediction error, it can be shown that, given $\tilde{h}_n$, h_n is a complex-valued Gaussian random variable with mean $\tilde{h}_n$ and variance $L\sigma_e^2$. Using (4.13), (4.14) can be rewritten as:

$$\frac{c_1}{1 + L\xi_n\sigma_e^2} \exp\left[-\frac{|\tilde{h}_n|^2 \xi_n}{1 + L\xi_n\sigma_e^2}\right] = \varepsilon_{target}, \ \forall n = 0, 1, \cdots, N-1, \tag{4.15}$$

where $\xi_n = q(\beta_n)P_n$. Thus, (4.15) also offers an analytical relationship between P_n and β_n. The left hand side of (4.15) is monotone decreasing in ξ_n. Thus for a given ε_{target}, there exists a unique ξ_n^* satisfying (4.15). Define $|h_n^\dagger|^2 := \ln(\frac{c_1}{\varepsilon_{target}})/\xi_n^*$. It can be shown that P_n and β_n satisfy (4.15) if and only if

$$c_1 \exp[-P_n|h_n^\dagger|^2 q(\beta_n)] = \varepsilon_{target}.$$

Consequently $|h_n^\dagger|^2$ can be defined as the *effective power gain* of subcarrier n, and can be calculated as follows:

$$|h_n^\dagger|^2 = L^2\sigma_e^4 \ln\left(\frac{c_1}{\varepsilon_{target}}\right) / \left[\frac{|\tilde{h}_n|^2}{\Psi^{-1}\left\{\frac{\varepsilon_{target}}{c_1}\Psi\left[\frac{|\tilde{h}_n|^2}{L\sigma_e^2}\right]\right\}} - L\sigma_e^2\right] \tag{4.16}$$

where $\Psi(x) = xe^x$ and $\Psi^{-1}(\cdot)$ is the inverse function of $\Psi(x)$. The effective power gain calculated from (4.16) has been plotted versus $|\tilde{h}_n|^2$ in Figure 4.2, for $\varepsilon_{target} = 10^{-3}$, $c_1 = 0.2$, and $L\sigma_e^2 = 1$. This figure show that, when the channel-to-noise ratio (CNR) $|\tilde{h}_n|^2/L\sigma_e^2$ is more than 15dB, the effective power gain is very close to the predicted value. For lower CNR, the effective power gain can be much smaller than the originally predicted value. Moreover, the effective value tends to be a very small constant as CNR approaches zero.

By treating $|h_n^\dagger|^2$ as the perfect power gain for sub-channel n, the bit and power allocation problem can be solved using known algorithms developed for the case of perfect CSI. However, unlike the approach of directly using $|\tilde{h}_n|^2$, the proposed method guarantees that the average BER satisfies the requirement in (4.14). The complete bit and power allocation method for $\sigma_e^2 \neq 0$ is implemented as follows.
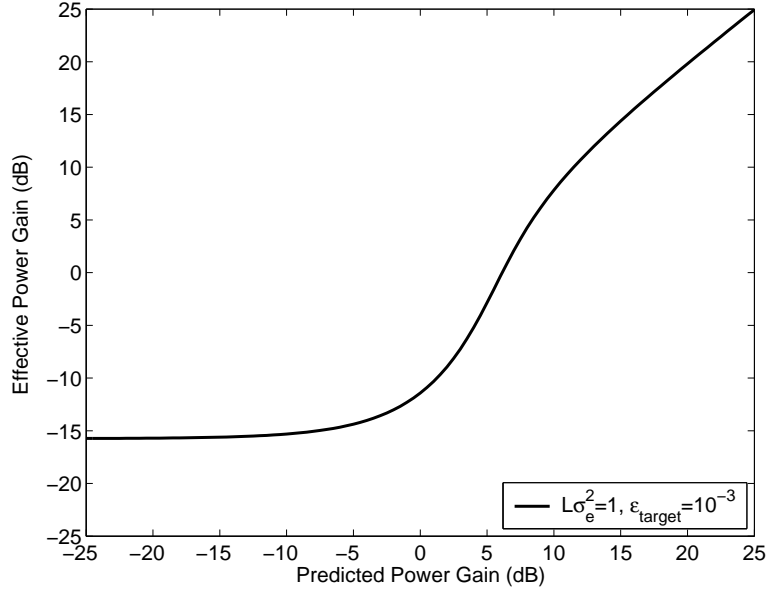
Figure 4.2: Effective channel power gain with errors in CFR

1. Use (4.16) to calculate $|h_n^\dagger|^2$ for all n.

2. Use the bisection method proposed in [33] or [34] to find the cutoff power gain for all modulation signal sets.

3. For all n, determine β_n by comparing $|h_n^\dagger|^2$ with the cutoff points obtained in the previous step.

4. Calculate P_n from β_n using (4.15).

4.4.2 Resource Allocation with Arbitrary Channel Prediction Error

Our discussion in the previous section assumed that $\{h_n\}$, the values of CFR at all subcarriers, are predicted. However, in bit and power allocation algorithm it is $\{|h_n|^2\}$, the channel power gain, (or more specifically the SNR of each subcarrier) that is required. As argued in [41], using the square magnitude of $\tilde{h}_n$ as a prediction of the channel power gain underestimates the true power and results in a biased estimate. Consequently in [41], an unbiased quadratic power prediction method from [37] has been used for optimal rate and power allocation.

In this section we consider the problem of optimal bit and power allocation in OFDM assuming an arbitrary distribution for the channel CFR. In particular let $X_n := |h_n|^2$ and $Y_n := |\tilde{h}_n|^2$. It is assumed that the joint PDF of X_n and Y_n, denoted by $f_{X_n,Y_n}(x,y)$, is known, whether $\tilde{h}_n$ or $|\tilde{h}_n|^2$ is obtained through channel prediction.

For all n, both X_n and Y_n are viewed as complex random variables. As before, P_n and β_n are, respectively, the power and the number of bits allocated to the nth subchannel.

In the optimal bit and power allocation P_n and β_n are determined by the value of Y_n. Since BER also depends on the value of X_n, (see (4.13)), as in the previous section the BER constraint is considered as follows.

$$E\left(\text{BER}_n|Y_n = y\right) = \int_0^\infty c_1 e^{-q(\beta_n)P_n x} f_{X_n|Y_n}(x;y) dx = \varepsilon_{target}, \ \forall n = 1, \cdots, N. \quad (4.17)$$

Define

$$Z_n(z;y) = \int_0^\infty e^{-zx} f_{X_n|Y_n}(x;y) dx$$

Then, for each y, $Z_n(z;y)$ is a monotone decreasing function of z. Let $Z_n^{-1}(\cdot;y)$ denote its inverse function such that $Z_n(Z_n^{-1}(x;y);y) \equiv x$. Thus (4.17) can be rewritten as

$$P_n = \frac{1}{q(\beta_n)} Z_n^{-1}\left(\frac{\varepsilon_{target}}{c_1};y\right) \quad (4.18)$$

Given the channel power prediction $Y_n = y$, (4.18) describes a relationship between P_n and β_n. By using this relationship we ensure that the BER constraint is satisfied as well as significantly simplify the problem by reducing it to a bit (or power) allocation problem.

Let $\Omega = \{b_0, b_1, \cdots, b_{\mathcal{M}}\}$ be the set of integers that β_n can assume. In other words, Ω is the number of bits transmitted over each subcarrier in one block. In other words, $\beta_n \in \Omega$ for all n. Our proposed algorithm is the following. Divide the interval $[0,\infty)$ into $\mathcal{M}$ consecutive subintervals with the boundary points $0 = \varphi_{0,n} < \varphi_{1,n} < \cdots < \varphi_{\mathcal{M},n} < \varphi_{\mathcal{M}+1,n} = \infty$. Then, let $\beta_n = b_m$ if the value of Y_n falls in the interval $(\varphi_{m,n}, \varphi_{m+1,n}]$. Finally, calculate P_n from (4.18) with $\beta_n = b_m$. The same procedure will be performed for all n to obtain resource allocation for the entire block. From (4.18), the transmit power of the OFDM block is given by

$$\begin{aligned}
\bar{P} &= \sum_{n=1}^{N} \int_0^\infty \frac{1}{q(\beta_n)} Z_n^{-1}\left(\frac{\varepsilon_{target}}{c_1};y\right) f_{Y_n}(y) dy \\
&= \sum_{n=1}^{N} \sum_{m=1}^{\mathcal{M}} \frac{1}{q(b_m)} \int_{\varphi_{m,n}}^{\varphi_{m+1,n}} Z_n^{-1}\left(\frac{\varepsilon_{target}}{c_1};y\right) f_{Y_n}(y) dy, \quad (4.19)
\end{aligned}$$

and the data rate is given by

$$\bar{R} = \sum_{n=1}^{N} \sum_{m=1}^{\mathcal{M}} b_m \int_{\varphi_{m,n}}^{\varphi_{m+1,n}} f_{Y_n}(y) dy = R_{target} \quad (4.20)$$

The bit and power allocation algorithm attempts to minimize the total power assigned to an OFDM block subject to the constraints on the BER and the data rate per OFDM

block. It can be shown that there exist optimal boundary values $\varphi_{m,n}^*$ such that the transmit power in (4.19) can be minimized subject to (4.17) and rate constraint in $\bar{R} = R_{total}$. This problem can be solved using the method of Lagrange multipliers. The Lagrange cost function is

$$
J(\varphi_{1,1},\cdots,\varphi_{\mathcal{M},N}) = \sum_{n=1}^{N}\sum_{m=1}^{\mathcal{M}} \frac{1}{q(b_m)} \int_{\varphi_{m,n}}^{\varphi_{m+1,n}} Z_n^{-1}\left(\frac{\varepsilon_{target}}{c_1};y\right) f_{Y_n}(y)dy
$$
$$
+ \Lambda \left[\sum_{n=1}^{N}\sum_{m=1}^{\mathcal{M}} b_m \int_{\varphi_{m,n}}^{\varphi_{m+1,n}} f_{Y_n}(y)dy - R_{target}\right] \qquad (4.21)
$$

where Λ is the Lagrange multiplier. The necessary conditions for optimality are given by

$$
\left.\frac{\partial J}{\partial \varphi_{m,n}}\right|_{\varphi_{m,n}=\varphi_{m,n}^*} = 0, \ \ \forall m,n \qquad (4.22)
$$

which yield

$$
Z_n^{-1}\left(\frac{\varepsilon_{target}}{c_1};\varphi_{m,n}^*\right) = -\frac{\Lambda(b_m - b_{m-1})}{\left[\frac{1}{q(b_m)} - \frac{1}{q(b_{m-1})}\right]} \qquad (4.23)
$$
$$
\text{for } n = 1,\cdots,N; \ \ m = 1,\cdots,\mathcal{M}.
$$

For a given value of Λ, we can obtain $\{\varphi_{m,n}^*\}$ by solving the above equations. For a given set of thresholds $\{\varphi_{m,n}^*\}$ we can obtain the value of Λ, from (4.20). In practice, a recursive numerical method can be used to solve for $\{\varphi_{m,n}^*\}$ and Λ. We should point out that further information on the convexity of $\bar{P}$ and $\bar{R}$ is required to ensure the optimality of the solution. We also note that the proposed algorithm can be applied in conjunction with an arbitrary channel prediction method as long as $f_{X_n|Y_n}$ and f_{Y_n} can be determined a priori. We provide the following two examples to illustrate the effectiveness of the proposed method.

Example 4.1 Suppose that the prediction of channel power gain is perfect, i.e., $Y_n = X_n$ for all n. In this case, $f_{X_n|Y_n}(x;y) = \delta(x-y)$ and $Z_n(z;y) = e^{-zy}$. Thus (4.23) can be reduced to

$$
\varphi_{m,n}^* = \frac{\ln(\frac{\varepsilon_{target}}{c_1})}{\Lambda} \left[\frac{\frac{1}{q(b_m)} - \frac{1}{q(b_{m-1})}}{b_m - b_{m-1}}\right], \ \ \forall m, \ n. \qquad (4.24)
$$

Equation (4.24) shows that the ratio of the optimal threshold values are fixed. A result which coincides with earlier results in [33, 34]. Moreover, the values given by (4.24) are the same as those obtained in [34], where these optimal threshold values are derived using a different approach. ∎

Example 4.2 Suppose $\tilde{h}_n = h_n + \eta_n$, where h_n and η_n are independent complex Gaussian random variables satisfying $h_n \sim \mathcal{CN}(0, \theta^2)$ and $\eta_n \sim \mathcal{CN}(0, \sigma_\eta^2)$, where θ^2 and σ_η^2 are given. When conditioned on $\tilde{h}_n$, h_n is a complex-valued Gaussian random variable with mean $\tilde{h}_n$ and variance σ_η^2. It is clear that given $Y_n = |\tilde{h}_n|^2$, $X_n = |h_n|^2$ has a *noncentral* chi-square distribution with two degrees of freedom. Accordingly, $f_{X_n|Y_n}(x; y)$ can be written as

$$f_{X_n|Y_n}(x; y) = \frac{1}{\sigma_\eta^2} \exp\left(-\frac{x+y}{\sigma_\eta^2}\right) I_0\left(\frac{\sqrt{xy}}{\sigma_\eta^2/2}\right) \tag{4.25}$$

where $I_0(\cdot)$ denotes the zeroth order modified Bessel function of the first kind. For the conditional distribution defined in (4.25), the function Z_n can be rewritten as follows:

$$Z_n(z; y) = \frac{\exp\left[-\left(\frac{yz}{1+\sigma_\eta^2 z}\right)\right]}{1 + \sigma_\eta^2 z} \tag{4.26}$$

In this case, (4.23) can be simplified as

$$\varphi_{m,n}^* = \left[\frac{1}{\Lambda\Delta_m} + \sigma_\eta^2\right] \ln\left(\frac{c_1/\varepsilon_{target}}{1 + \Lambda\sigma_\eta^2\Delta_m}\right) \tag{4.27}$$
$$\text{for all } n = 1, \cdots, N; \; m = 1, \cdots, \mathcal{M}.$$

where $\Delta_m = -(b_m - b_{m-1})/(\frac{1}{q(b_m)} - \frac{1}{q(b_{m-1})})$. It is observed that for $\sigma_\eta^2 = 0$, (4.27) reduces to (4.24). In general, the Lagrange multiplier Λ is determined by the constraint in (4.20). Specifically, if σ_η^2 and θ^2 are identical for all n, then (4.20) can be rewritten as follows:

$$\sum_{m=1}^{\mathcal{M}} \frac{b_m}{\theta^2}\left(e^{-\varphi_m^*/\theta^2} - e^{-\varphi_{m+1}^*/\theta^2}\right) = \frac{R_{target}}{N} \tag{4.28}$$

■

4.5   Simulation Study

In this section, we first illustrate through simulation the efficacy of the resource allocation schemes proposed in Section 4.4. For simplicity, we neglect the details of channel predictor by assuming its output is a (Gaussian) noisy version of the CIR with known NMSE. Meanwhile, the 12-ray channel model described in Section 4.3.2 has been used in this simulation, where f_m=200Hz. The noisy CIR used for resource allocation is generated by adding to $\mathbf{g}(k)$, which is calculated using (4.3), a sequence of iid complex-valued Gaussian random variables, whose variance is determined by NMSE. Moreover, the system parameters are the same as those in Section 4.3.2.
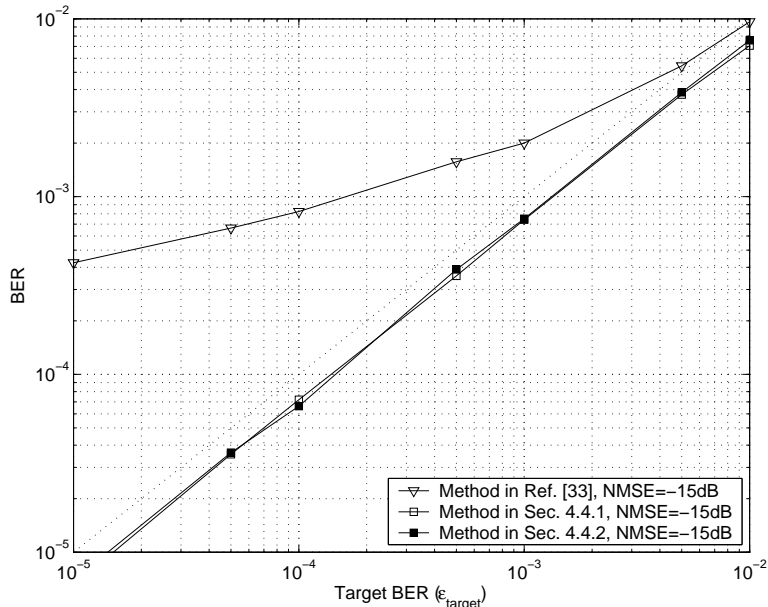
Figure 4.3: Comparison between the measured BER and the target BER

The set of modulation schemes used in this case are QPSK, 16QAM, 64QAM and 256QAM, and the target data rate is $R_{target} = 4N$.

Let NMSE be -15dB. The allocation methods proposed in Section 4.4.1 and Section 4.4.2 are compared with the results in [33] assuming perfect knowledge of the CSI. We should point out that the method in [33] is in fact optimal if the knowledge of CSI is indeed perfect. For these three approaches, the BERs measured from simulation are plotted with respect to the target values in Figure 4.3. It is clear that both methods in Section 4.4 meet the BER requirement while the approach in [33] can not.

The efficiency of the above three allocation methods is compared in Figure 4.4, where the results corresponding to the perfect CSI case (NMSE=-∞ dB) is also plotted. For the method in Section 4.4.1, since the effective power gain $|h_n^\dagger|^2$ in (4.16) equals the predicted value $|\tilde{h}_n|^2$ in the case of perfect CSI, then the scheme in Section 4.4.1 is equivalent to that in [33]. Thus, only two curves exist in the case of perfect CSI. Moreover, in this case, the approach in Section 4.4.2 outperforms that in Section 4.4.1. This can be explained as follows: the method in Section 4.4.1 requires each OFDM block to transmit R_{target} bits, while the method in Section 4.4.2 has a more relaxed condition (4.20) and should result in higher efficiency. However, it should be noted that the scheme in Section 4.4.1 is easier to implement. For this reason, we use this method in the following simulation. On the other hand, for the case of imperfect CSI (NMSE=-15dB), the resource allocation scheme in Section 4.4.1 has about 2.5dB improvement over the method in [33] for $\varepsilon_{target} = 10^{-4}$, and the method in Section 4.4.2 is about 1dB better than the method in Section 4.4.1.

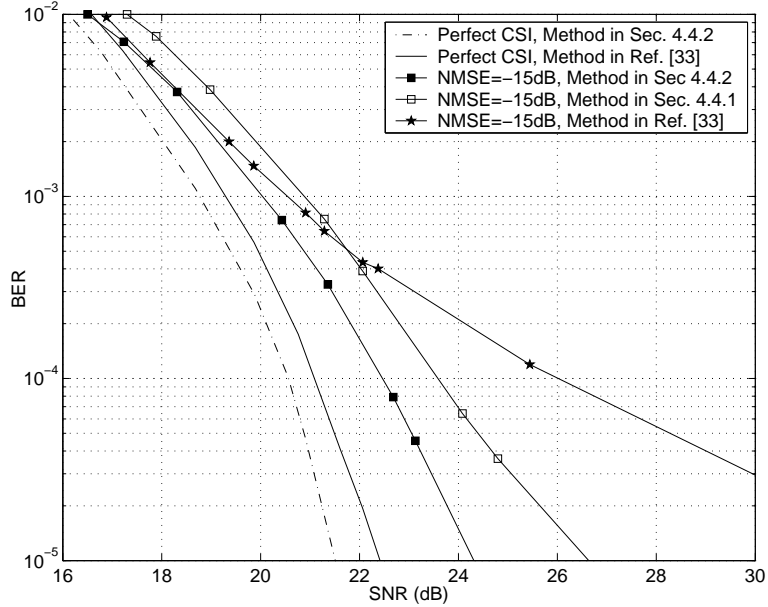A complete OFDM system using both channel prediction and resource allocation

63

Figure 4.4: Performance of resource allocation schemes for imperfect CSI

is shown by the block diagram in Figure 4.5. The same channel model and system parameters as those in previous simulations have been used in this system, where the range of Doppler frequency is 0∼150Hz and $R_{target} = 2N$. For every 20 OFDM blocks, one channel estimation is sent back to the transmitter, i.e., $d = 20$. Consequently, the rate of CFR updating is 1000Hz. In Figure 4.5, a bit allocation vector (BAV) and power allocation vector (PAV) have been used to control modulation and demodulation for every OFDM symbol, and they are determined by the resource allocation scheme in Section 4.4.1. The channel predictor used here is the LMS predictor (4.11)-(4.12) with M=5.

Figure 4.6 illustrates simulation results for the above OFDM system. A reference system without either the proposed channel prediction or resource allocation methods, which uses the most recent channel estimation and treats it as perfect, has also been simulated. The results corresponding to the reference system have been labelled as "non-pred." in Figure 4.6. The system having channel prediction and the proposed resource allocation clearly outperforms the reference system under all Doppler frequencies. In this case, the efficiency of the proposed system is almost as good as the perfect CSI case for Doppler frequencies up to 100Hz, which corresponds to a mobile speed of 73.8mph for a carrier frequency of 900MHz. On the other hand, the reference system suffers tremendous performance loss even if f_m is 50Hz. For $\varepsilon_{target} = 10^{-3}$, the proposed system results 2dB improvement from the reference system in f_m=50Hz, 8dB improvement in 100Hz, and 10dB improvement in 150Hz.
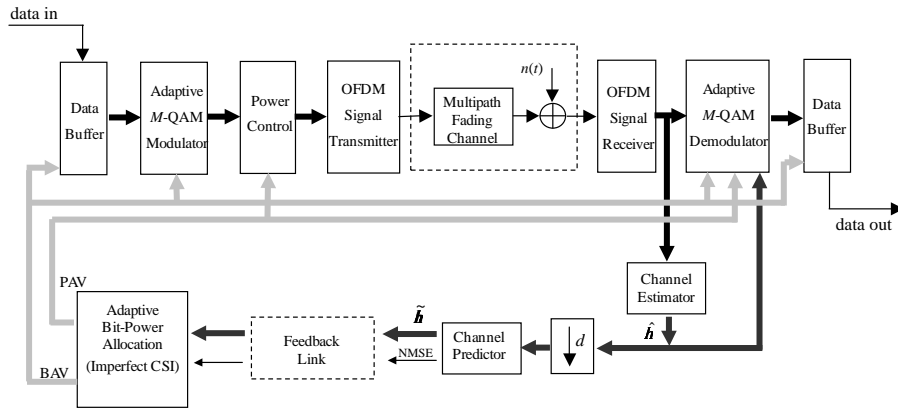
Figure 4.5: OFDM system using channel prediction and resource allocation
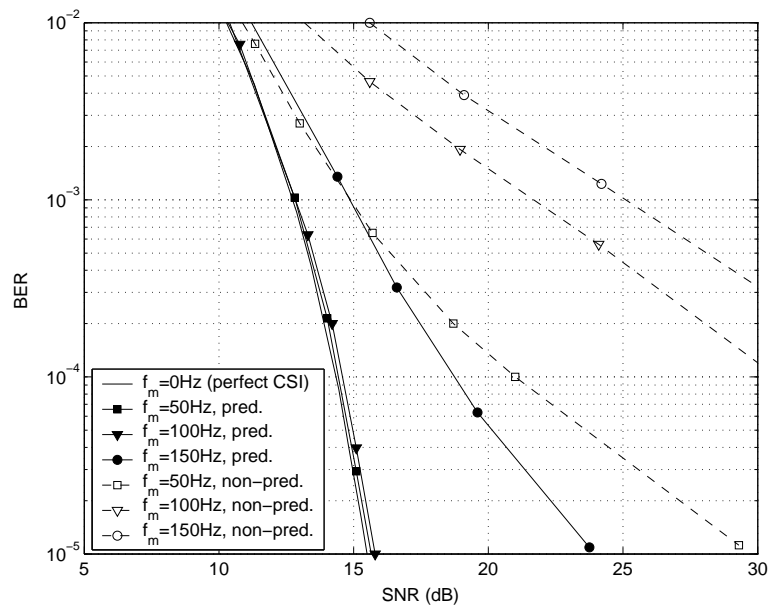

Figure 4.6: Performance of the OFDM system in Figure 4.5

4.6   Chapter Summary

The problem of resource allocation with imperfect CSI has been considered for OFDM systems for time-varying channels. The outdated CSI is identified as the main difficulty for achieving performance enhancement promised by resource allocation. With the aid of channel prediction, a bit and power allocation scheme has been proposed to overcome this difficulty. The simulation results confirm that, using the proposed method, the system performance for slowly time-varying channels (e.g., $f_m \leq 100$Hz in our simulation) can be very close to that of the static channel case.

CHAPTER 5. MAXIMUM LIKELIHOOD RECEIVER FOR THE MULTIBAND KEYING SIGNALS IN THE AWGN CHANNEL

5.1 Introduction

Ultra Wideband (UWB) communication is now receiving a great deal of attention from the research community. The FCC has allocated a band of several gigahertz (3.1GHz – 10.6GHz) for the prospective UWB systems. According to FCC, a signal is qualified to be a UWB signal when it occupies a -10dB bandwidth which exceeds 500MHz or 20% of its center frequency [43]. Several techniques have been proposed to modulate information bits into UWB signals including OFDM [2], DS-CDMA [46], Frequency Hopping [47] and Multiband Keying modulation [44] [45]. Among these techniques, the Multiband Keying (MBK) modulation is a form of fast frequency hopping, which significantly increases the number of information bits carried in each symbol without sacrificing much of the symbol error rate. Thus for the same information bit rate the symbol rate can be reduced in order to eliminate the inter-symbol interference (ISI) due to multipath fading [44] [45].

The basic idea of MBK modulation is to divide the whole symbol interval into P subintervals of duration T_s. Within each subinterval, the information bits are modulated onto a specific carrier frequency using the conventional MPSK modulation[1]. The carrier frequencies are distinct and are chosen from a set of L different frequencies $\Omega_F = \{F_0, F_1, \ldots, F_{L-1}\}$, which are selected from the UWB band and satisfy the condition

$$|F_{i+1} - F_i| \geq \frac{1}{T_s} \quad i = 0, 1, \cdots, L - 2. \tag{5.1}$$

For each symbol, the sequence of carrier frequencies $\mathbf{f} = \{f_0, f_1, \ldots, f_{P-1} | f_k \in \Omega_F\}$ as well as the phases of symbols within each subinterval are determined by the information bits.

Denote by Ω_S the set of phases that define the MPSK signal set, i.e. $\Omega_S = \left\{ \frac{2\pi l}{M} \mid 0 \leq l \leq M - 1 \right\}$. Then the MBK symbol is given by

$$u(t) = \sqrt{\frac{2E_s}{T_s}} \sum_{k=0}^{P-1} p(t - kT_s) \cos\left(2\pi f_k t + \phi_k\right) \tag{5.2}$$

$$\phi_k \in \Omega_S, \ f_k \in \Omega_F, \ f_k \neq f_j \ \forall k \neq j$$

where $p(t)$ is the pulse shaping function and E_s is the signal energy for each subin-

---

[1]The case of null subinterval is not considered here.

terval. We only consider the rectangular shaping pulse, i.e.,

$$p(t) = \begin{cases} 1, & 0 \leq t < T_s \\ 0, & \text{otherwise} \end{cases} \tag{5.3}$$

The distinction of carrier frequencies implies that $L \geq P$. In this chapter we assume $L = P$. It follows that the total number of MBK symbols is given by [44]

$$N_{total} = (P!)M^P \tag{5.4}$$

Then the number of information bits that an MBK symbol will carry is

$$\log_2 N_{total} = \log_2 P! + P \log_2 M. \tag{5.5}$$

The distinct sequence of carrier frequencies in MBK can be viewed as a form of coding akin to frequency hopping in spread spectrum and provides improved BER [44], multi-access capability for pico-nets and robustness against frequency-selective fading.

5.2 Optimal Receiver of Multiband Keying Signals

Consider an AWGN channel with two-sided power spectral density of $\frac{N_0}{2}$ watts/Hz. Let

$$q_{ij}^k = \int_{kT_s}^{(k+1)T_s} \sqrt{\frac{2}{T_s}} \cos\left(2\pi F_i t + \frac{j 2\pi}{M}\right) r(t) \; dt \tag{5.6}$$
$$k, i = 0, 1, \ldots, P - 1; \; j = 0, 1, \ldots, M - 1,$$

where $r(t)$ is the received signal. Define the set of $P \times M$ matrices $\mathbf{Q^0}, \mathbf{Q^1}, \ldots, \mathbf{Q^{P-1}}$ by $\mathbf{Q^k} = \left[q_{ij}^k\right]$. The maximum likelihood (ML) decision rule can now be stated as follows:

ML Decision Rule 1: *Select one entry from each $P \times M$ matrix $\mathbf{Q^k}$ such that: (a) all entries come from different rows of the matrices (b) the summation of the selected P entries is largest for all possible selections.*

Condition (a) corresponds to the fact that the frequencies $f_0, f_1, \ldots, f_{P-1}$ in every MBK symbol are distinct. Condition (b) maximizes the correlation between the received signal $r(t)$ and the MBK symbol. Note that if the sequence of elements chosen by the ML decision rule is $q_{i_0,j_0}^0, q_{i_1,j_1}^1, \ldots, q_{i_{(P-1)},j_{(P-1)}}^{P-1}$, then the estimation of the transmitted carrier frequencies and MPSK phases are $f_{i_0}, f_{i_1}, \ldots, f_{i_{(P-1)}}$ and $\frac{j_0 2\pi}{M}, \frac{j_1 2\pi}{M}, \ldots, \frac{j_{(P-1)} 2\pi}{M}$, respectively.

The complexity of the exhaustive search for the ML decision rule is clearly prohibitive. The following approach simplifies the decision rule somewhat. Let $v_{ik} =$

$\max_{0 \le j \le M-1}\{q_{ij}^k\}$ for $i, k = 0, 1, \ldots, P-1$ and define the $P \times P$ matrix $\mathbf{V} = [v_{ik}]$. It is straightforward to show that the ML decision rule can then be stated as follows:

ML Decision Rule 2: *Choose P elements $v_{0j_0}, v_{1j_1}, \ldots, v_{(P-1)j_{(P-1)}}$ from $\mathbf{V}$ such that: (a) $\{j_0, j_1, \ldots, j_{(P-1)}\}$ is a permutation of $\{0, 1, \ldots, P-1\}$. (b) The summation $\sum_{i=0}^{P-1} v_{i,j_i}$ is the largest among all permutations.*

We would like to note that the construction of the matrix $\mathbf{V}$ is equivalent to performing MPSK demodulation in each subpulse for every carrier frequency without prior knowledge of the actually transmitted frequencies. The block diagram of the optimal receiver is illustrated in Figure 5.1. For each of the P branches , the MPSK receivers output not only the estimated signal phases but also the corresponding correlation values. The 'ML Detector' module takes all these correlation values to construct the matrix $\mathbf{V}$ and then applies ML rule 2.
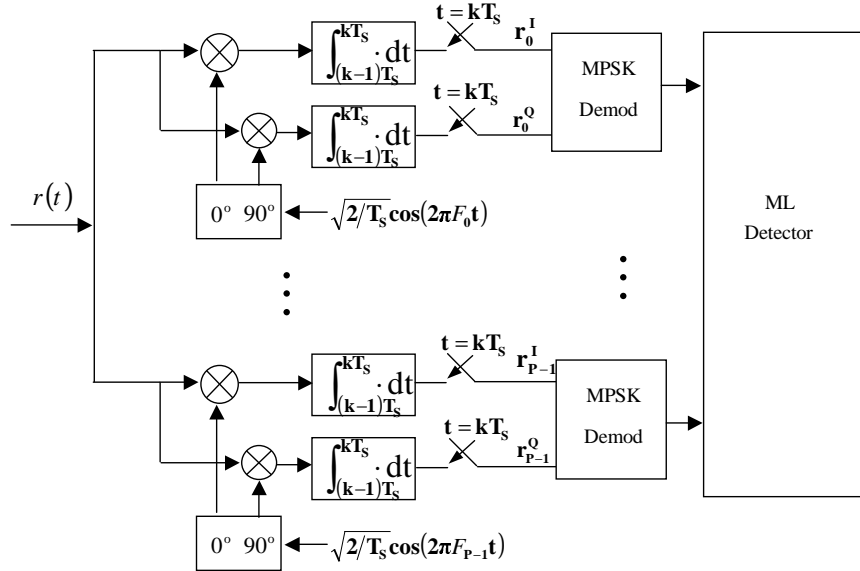

Figure 5.1: Maximum Likelihood receiver block diagram

The minimum Euclidean distance between MBK symbols with MPSK modulation is given by

$$d_{min} = 2\sqrt{E_s}\sin\frac{\pi}{M} \qquad (5.7)$$

The number of neighbors at distance d_{min} is given by

$$N_{d_{min}} = \begin{cases} P(2P-1), & \text{M=2} \\ 2P, & \text{M>2} \end{cases} \qquad (5.8)$$

Thus in the case of large signal to noise ratio (SNR), the symbol error probability

can be approximated by [58]

$$P_e \approx \begin{cases} P(2P-1)\, Q\left(\sqrt{\frac{2E_s}{N_0}}\right), & M = 2 \\ 2P\, Q\left[\sqrt{\frac{2E_s}{N_0}\sin^2\left(\frac{\pi}{M}\right)}\,\right], & M > 2 \end{cases} \tag{5.9}$$

It can be shown that the Euclidean distance between any pair of MBK symbols which have different frequency sequences is no less than $2\sqrt{E_s}$ for any P and M. From this property and (5.7) we conclude that when $M > 2$ the minimum Euclidean distances correspond to MBK symbols having identical frequency sequences but different phases. Thus the symbol error rate is dominated by phase errors when $M > 2$.

The optimal receiver of MBK symbols requires the computation and comparison of different summations of the elements of the matrix $\mathbf{V}$. This requires a total of $(P-1)P!$ additions and $P!-1$ comparisons. When P is large, this complexity is clearly prohibitive. In the following we present a suboptimal search algorithm which reduces the complexity of the ML detector significantly for large P.

5.3   Efficient ML Detection for Multiband Keying Signals

The ML decision rule can be viewed as a tree search algorithm in a P-array tree of depth P. Figure 5.2 represents such a tree graph for $P = 3$. At any depth we label the nodes and the branches from left to right from 0 to $P-1$. The P branches emanating from the root node represent the first row of matrix $\mathbf{V}$ with the jth branch having label $v_{0,j-1}$. Similarly, at depth i, the branches emanating from any node represent the ith row of $\mathbf{V}$ with the branch label for the jth branch equal to $v_{i-1,j-1}$. The ML decision rule now corresponds to finding the path in the

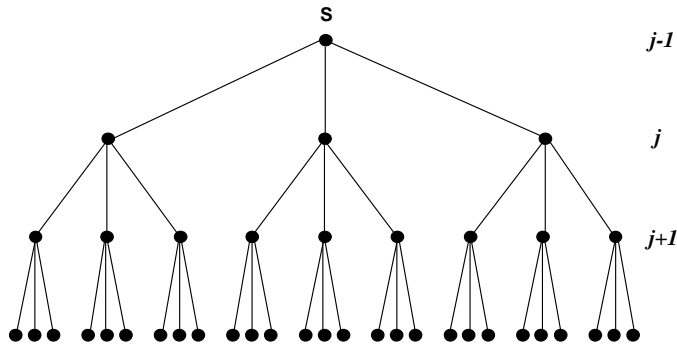Figure 5.2: Tree graph representation of $\mathbf{V}$(P=3)

tree with the maximum weight such that the branch numbers form a permutation of $\{0, 1, \ldots, P-1\}$. While an exhaustive search will result in optimal ML detection of MBK symbols, other suboptimal search procedures with lower complexity, which do not compromise the performance significantly, may also be used. An example is

a depth-first search algorithm which starts at the root node by selecting the branch with the largest label. At every subsequent node, it will choose the branch with the largest label and will back track only when a branch number is repeated. Such an algorithm reduces the complexity of the decision rule especially in the case of large signal to noise ratio where there will be very few, if any, back tracks.

In this chapter, a variant of the depth-first search algorithm is implemented and its performance and complexity are evaluated through simulations. The results are presented in the next section.

5.4   Simulation Results

In this section the receiver having structure of Figure 5.1 is called a 'suboptimal receiver' when the ML detection is performed by the depth-first search algorithm instead of the exhaustive search.

We have simulated the performance of the optimal receiver for two cases, the first one uses QPSK (M=4) and has 4 carrier frequencies ($P = 4$) while the second one uses BPSK (M=2) and has 5 carrier frequencies ($P = 5$). For larger values of P the simulation of the ML decision rule becomes excessively time consuming as a result of exhaustive search. Figure 5.3 shows the symbol error rate (SER) of the optimal ML decision rule vs E_b/N_0 for the two cases described above. In this figure we also plot the symbol error rate obtained from the approximations in Equation (5.9). In both cases the simulation results match the approximation quite well, especially for large E_b/N_0. This result holds for other values of M and P as well.
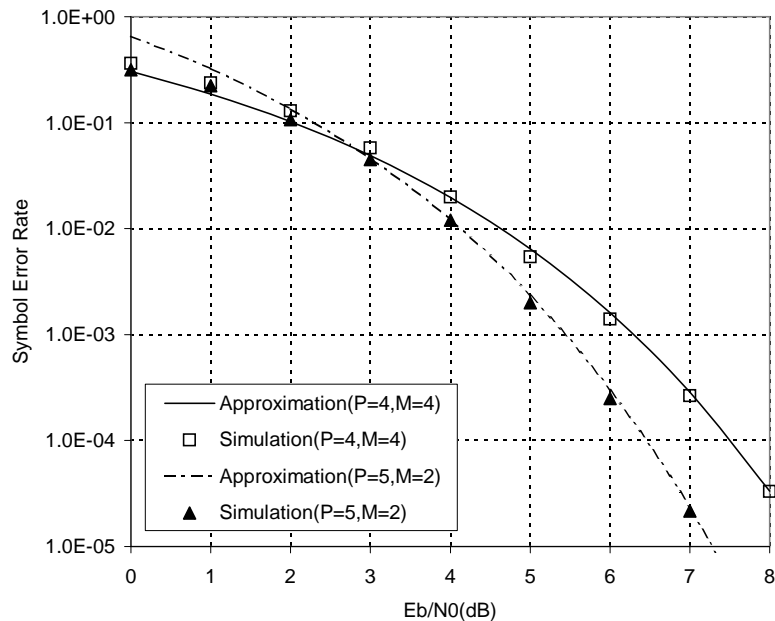

Figure 5.3: Performance of optimal receiver

71

Let P_{e1} be the probability that the estimated carrier frequency sequences not equal to that of the transmitted symbols, and P_{e2} be the symbol error probability given correct carrier frequencies i.e. the probability of phase error, then the symbol error rate can be written as

$$P_e = P_{e1} + P_{e2} - P_{e1}P_{e2} \approx P_{e1} + P_{e2}. \qquad (5.10)$$

We have simulated the probability P_{e1} for the optimal and the suboptimal receivers. Figure 5.4 shows the results for $M = 2$ and $P = 5$, Figure 5.5 shows the results for $M = 4$ and $P = 5$. It can be seen that P_{e1} of the suboptimal receiver is close to that of the optimal receiver. This result holds for other values of M and P also. According to the definition of P_{e2}, it is identical for the optimal and the suboptimal receivers. By (5.10) the overall SER of the suboptimal receiver should be close to that of the optimal receiver. Furthermore, the probability P_{e2} has been plotted in Figure 5.4 and Figure 5.5. It can be seen that P_{e2} is much larger than P_{e1} for the case of $M = 4$ and $P = 5$. This result holds for all M greater than 2, i.e.

$$P_{e2} \gg P_{e1}, \quad \forall M > 2. \qquad (5.11)$$

By (5.10) and (5.11) we draw the same conclusion as Section 5.2 that when $M > 2$ the symbol error rate is dominated by the probability of phase error P_{e2}. Since P_{e2} is identical for the optimal and suboptimal receivers then the performance of them should be almost the same when $M > 2$.
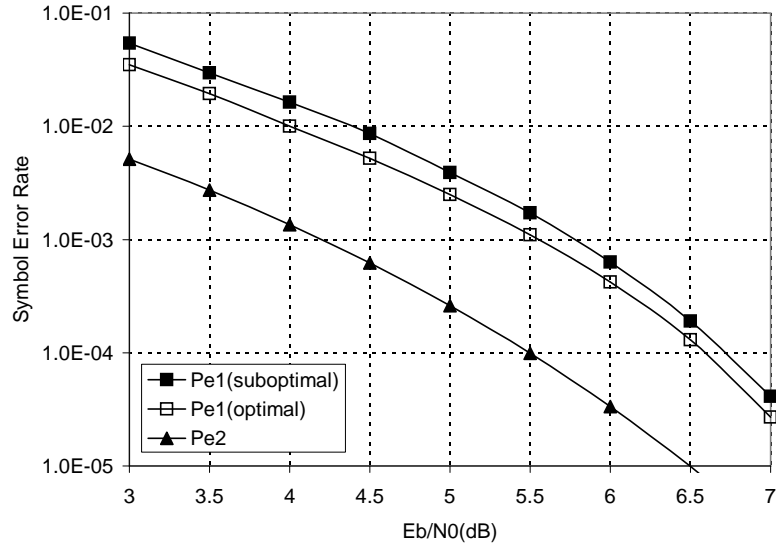

Figure 5.4: Frequency error vs phase error (P=5, M=2)

In Figure 5.6 the performance of the suboptimal receiver is compared with that of the optimal receiver for the case of BPSK MBK signals with $P = 8$, where the SER of
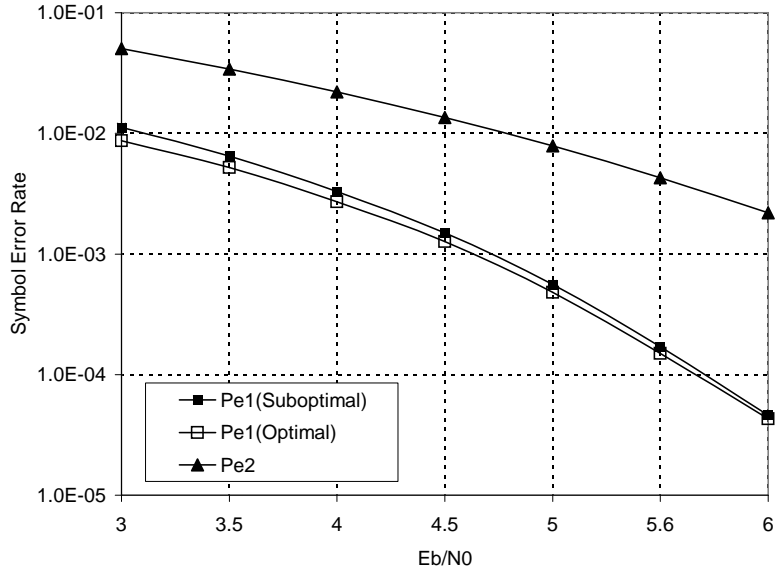
Figure 5.5: Frequency error vs phase error (P=5, M=4)

the optimal receiver was obtained from (5.9). We can see although the performance is slightly worse than the optimal receiver, the difference between them is quite small. For instance, the optimal receiver is merely 0.5dB better than the suboptimal receiver when SER is on the order of 10^{-4}. Figure 5.7 shows similar results for the case of QPSK and $P = 8$. In this case the suboptimal receiver almost has the same performance as that of the optimal receiver.

The computational complexity of the suboptimal receiver is quantified by the number of comparisons and additions per MBK symbol. These are both random variables whose statistical properties vary greatly for different matrix sizes P and different E_b/N_0. As an example, in Figure 5.8 the mean and the standard deviation of the number of comparisons are plotted vs E_b/N_0. It can be seen that, when E_b/N_0 is high the number of comparisons is almost a constant. As E_b/N_0 declines the mean and standard deviation both increase and approach an upper bound. The same property hold for the number of additions.

In Figure 5.9 we present a comparison between the complexity of the optimal receiver, which is constant, and the upper bound on the average complexity of the suboptimal receiver. In both cases the number of additions and comparisons are plotted vs the value of P. The value of E_b/N_0 is fixed at $-10dB$ for the purpose of making the suboptimal receiver's complexity close to its upper bound. It can be seen that while the complexity of the optimal receiver increases as $P!$, that of the suboptimal receiver increases as P^2.
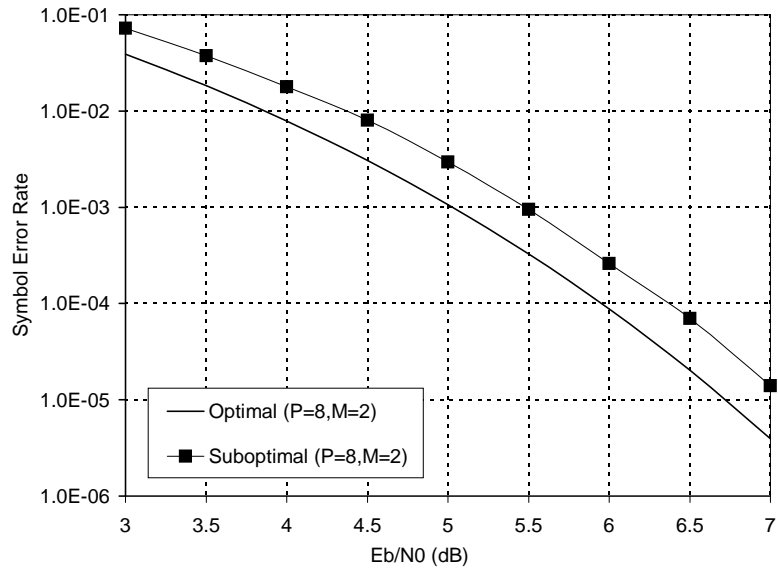
73

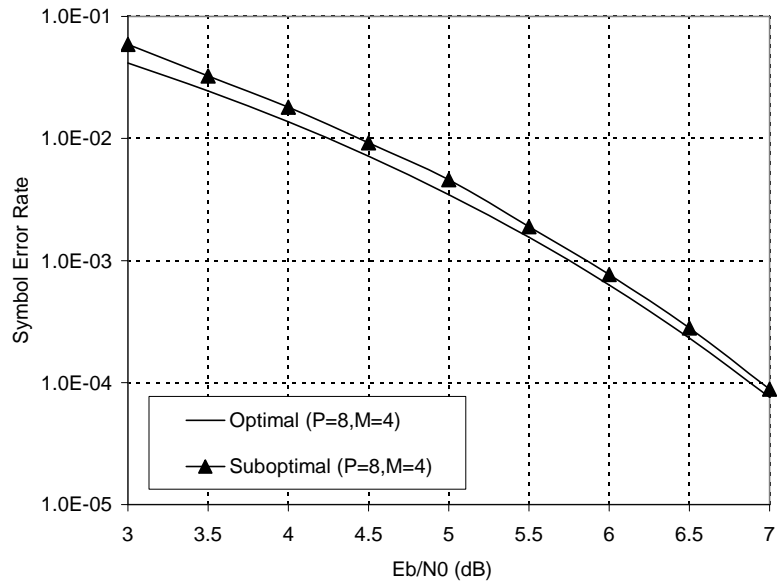Figure 5.6: Performance of suboptimal receiver (BPSK)

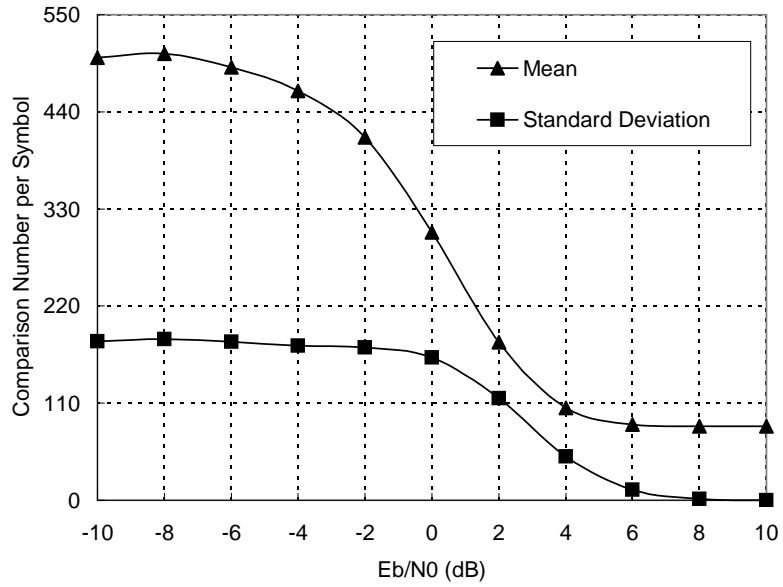Figure 5.7: Performance of suboptimal receiver (QPSK)

74

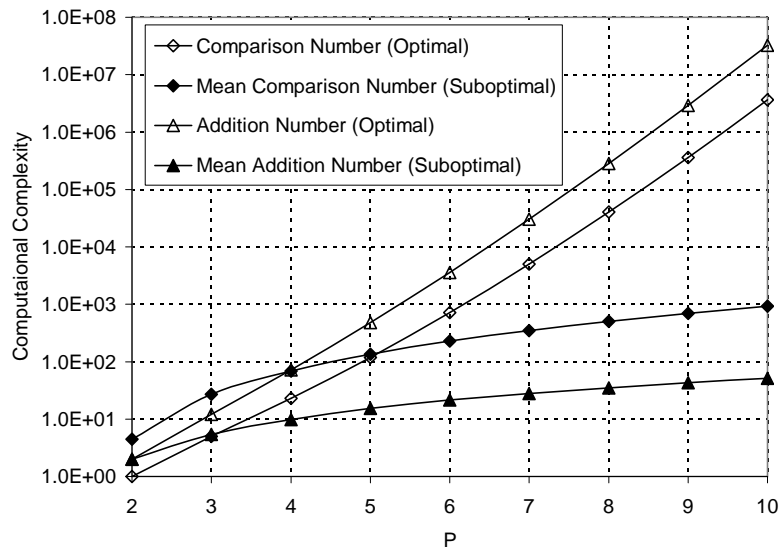Figure 5.8: Complexity of suboptimal receiver vs E_b/N_0 (P=8)

Figure 5.9: Complexity of optimal and suboptimal receivers ($E_b/N_0 = -10dB$)

5.5   Chapter Summary

In this chapter we describe the Maximum Likelihood receiver for Multiband Keying modulation and evaluate the symbol error rate through approximation as well as simulation. The results show that the approximation is very good specially in the case of large signal to noise ratio. We also present a suboptimal ML detector and compare its performance and complexity with that of the optimal ML detector. The results show that while the complexity of the suboptimal detector is significantly lower than that of the optimal detector, its performance in terms of symbol error rate is very close to that of the optimal detector.

CHAPTER 6. CONCLUSIONS

6.1 Channel Modeling in the Frequency Domain

Measurement results in wideband and ultra wideband wireless channels have revealed that a low order AR model is adequate to model the uniformly spaced samples of the CFR. An analytical approach has been presented in this dissertation offering a theoretical explanation to this observation. It is concluded that parametric channel modeling in the frequency domain is possible if and only if the uniformly spaced CFR samples are periodic WSS, which is equivalent to that the discrete CIR is periodic uncorrelated. This condition can be satisfied in wideband and ultra wideband channels as long as the underlying continuous-time channel is WSSUS with independent path gains and arrival times. Moreover, the power delay profile of the discrete CIR is closely related to the PSD of the discrete CFR samples, and this has been used to explain the existence of low order AR model. Theoretical results regarding parametric channel modeling in frequency domain have been verified through extensive simulations.

Although the channel modeling approach in this dissertation is partially motivated by the property of OFDM systems, it requires further investigation before being applied to model the CFR in OFDM systems, since the aforementioned WSS-US condition may not hold in this case. This is highlighted by Equation (1.7), where the elements of CIR are correlated in theory, which violates the US condition. Therefore, in this case, the parametric models discussed in this dissertation becomes less effective. As a suggestion for future work, we propose extending the results in this dissertation to OFDM channels with correlated CIRs (or equivalently non-WSS CFRs).

6.2 Resource Allocation in OFDM Systems

The problem of bit and power allocation in OFDM systems is formulated as a constrained minimization problem, where the overall transmit power is used as a cost function and the data rate and BER are constraints. We have solved this problem for the cases of perfect CSI and imperfect CSI.

In the signal user OFDM system with perfect CSI knowledge, it is concluded that a close-to-optimal bit allocation (and subsequently power allocation) can be obtained by quantizing the square of amplitude of the CFR. Consequently, a computationally efficient bit and power allocation algorithm has been proposed. In addition, the problem of resource allocation has also been considered for multi-user OFDM systems, where a two-step approach involving subcarrier allocation and subsequent bit-power allocation has been adopted. A heuristic algorithm has been proposed to perform subcarrier allocation in the first step, whose effectiveness is verified through

extensive simulation. We would like to notice that, although the proposed subcarrier allocation algorithm is numerically more efficient than other known algorithms, there is a noticeable loss of performance compared to optimal solutions. Further work is needed to find a better tradeoff between performance and complexity for the problem of subcarrier allocation.

In case of time-varying channels, the CSI available for bit and power allocation is generally imperfect. The speed of channel variation is shown to have a connection with the accuracy of the delayed CSI. Channel predictors based on Wiener filter and Adaptive filters are used to reduced the error in CSI, whose effectiveness have been tested in a Rayleigh fading channel. Furthermore, bit and power allocation schemes assuming imperfect CSI have been discussed with different approaches. Simulation results have confirmed that, in slowly time-varying Rayleigh channel, the proposed bit and power allocation scheme is able to achieve a performance close to that of the perfect CSI case with the aid of channel prediction.

6.3   ML Detection of Multiband Keying Signals

In the final part of this dissertation, the structure of optimal receiver and the associated ML decision rules have been derived from analysis for the Multiband Keying systems. It is concluded that, the ML decision is equivalent to find P elements with different rows and columns from a P-by-P square matrix such that the sum of them are the largest, in which P is the number of subpulses in every MBK symbol. An exhaustive searching algorithm guarantees to find the optimal solution but has a prohibitive complexity ($O(P!)$) for large P. Based on a depth-first tree search, we propose a suboptimal approach with much lower complexity $O(P^2)$. Simulation results have shown that the proposed suboptimal approach has an excellent performance, which is very close to that of the exhaustive searching approach.

BIBLIOGRAPHY

[1] H. Kim, "Turbo Coded Orthogonal Frequency Division Multiplexing for Digital Audio Broadcasting", *IEEE Inter. Conf. on Commun.* vol. 1, pp. 420-424, 2000.

[2] A. Batra et al., "Physical Layer Submission to 802.15 Task Group 3a: Time-Frequency Interleaved Orthogonal Frequency Division Multiplexing (TFI-OFDM)," IEEE P802.15-03/142r2.

[3] P.A. Bello, "Characterization of randomly time-variant linear channels", *IEEE Trans. Commun.*, Vol. 11, pp. 360–393, Dec. 1963.

[4] H. Chernoff, "A measure of asymptotic efficiency for test of hypothesis based on the sum of observations," *Annals Math. Statistics*, vol. 23, pp. 493-507, 1952.

[5] R. Cramer, R.A. Scholtz and M.Z. Win, "Evaluation of an Ultra-Wide-Band Propagation Channel", *IEEE Trans. on Antennas and Propagation*, pp. 561-570, Vol. 50, MAY 2002.

[6] M. Failli (ed.), *COST 207: Digital Land Mobile Communications – Final Report*, Commission of the European Communities, 1989.

[7] O. Edfors, M. Sandell, J. van de Beek, S. K. Welson and P. O. Borjesson, "OFDM channel estimation by singular value decomposition", *IEEE Trans. Commun., vol. 47, No. 7. pp.931-939, July 1998*

[8] J. Foerster and Q. Li, "UWB channel modeling contribution from Intel", *IEEE P802.15-02/279r0-SG3a*, March 2003.

[9] R. Ganesh and K. Pahlavan, "On the modeling of fading multipath indoor radio channels," in *Proc. GLOBECOM'89*, pp. 1346-1350, Dallas, TX, Nov. 30, 1989.

[10] S.S. Ghassemzadeh, R. Jana, C.W. Rice, W. Turin, and V. Tarokh, "A statistical path loss model for in-home UWB channels," *Proceedings of IEEE Conf. on Ultra Wideband Systems and Technologies*, May 2002.

[11] S.S. Ghassemzadeh, R. Jana, C.W. Rice, W. Turin, and V. Tarokh, "Measurements and modeling of an ultra-wide bandwidth indoor channel," *IEEE Trans. Commun.*, vol. 52, pp. 1786-1796, Oct. 2004.

[12] S.J. Howard, and K. Pahlavan, "Autoregressive modeling of wide-band indoor radio propagation," *IEEE Trans. Commun.*, Vol. 40, pp. 1540-1552, Sept. 1992.

[13] Intel Corporation, "A Multi-Radio Future? Wi-Fi, WiMAX, 3G, UWB: Complementary?", available at *http://www.techonline.com/community/ related_content/36474*

[14] L. Ljung, *System Identification Toolbox, for Use with MATLAB User's Guide*, The MathWorks, Inc., 1995.

[15] K. Pahlavan, R. Ganesh, and T. Hotaling, "Multipath propagation measurements on manufacturing floors at 910 MHz," *Electron. Lett.*, vol. 3, pp. 225-227, Feb. 1989.

[16] T.S. Rappaport and C.D. McGillem, "UHF fading in factories," *IEEE J. Select. Areas Commun.*, vol. 7, pp. 40-48, Jan. 1989.

[17] L. Rusch, C. Prettie, D. Cheung, Q. Li, M. Ho, "Characterization of UWB propagation from 2 to 8 GHz in a residential environment," www.intel.com/technology/ultrawideband/downloads/Channel_JSAC02_sub_ LR.pdf

[18] A.A. Saleh and R.A. Valenzuela, "A statistical model for indoor multipath propagation", *IEEE J. Select. Area Commun.*, vol. 5, Feb. 1987.

[19] W. Turin, R. Jana, S.S. Ghassemzadeh, C.W. Rice, and V. Tarokh, "Autoregressive modeling of an indoor UWB channel," *Proceedings of IEEE Conf. on Ultra Wideband Systems and Technologies*, May 2002.

[20] G.L. Turn, F.D. Clapp, T.L. Johnson, S.B. Fine, and D. Lavry, "A statistical model of urban multipath propagation," *IEEE Trans. Vehic. Technol.*, vol. 21, pp. 1-9, Feb. 1972.

[21] D. Hughes and Hartogs, "Ensembled Modem Structure for Imperfect Transmission Media." *U.S. Patent Notes 4679226*, July 1987.

[22] P. S. Chow, J. M. Cioffi and J. A. C. Bingham , "A Practical Discrete Multitone Transceiver Loading Algorithm for Data Transmission over Spectrally Shaped Channels." *IEEE Transactions on Communications*, pp. 773-775, Februrary/March/April 1995.

[23] R. F. H. Fischer and J. B. Huber, "A New Loading Algorithm for Discrete Multitone Transmission", *Proc. of GlobalCOM*, February 1996.

[24] S. T. Chung and A. J. Goldsmith, "Degrees of freedom in adaptive modulation: a unified view", *IEEE Trans. on Comm.*, vol. 37, pp.844-855, June 1999.

[25] Ho Seo Kim, Jin Sam Kwak, Jung Min Choi and Jae Hong Lee, "Efficient Subcarrier and Bit Allocation Algorithm for OFDMA System with Adaptive Modulation", *IEEE Vehicular Technology Conference*, V59, n3, pp.1816-1820, 2004.

[26] C. Y. Wong, R. S. Cheng, K. B. Letaief and R. D. Murch, "Multiuser OFDM with Adaptive Subcarrier, Bit, and Power Allocation", *IEEE Jan. Selected Areas Comm.*, Vol. 17, pp.1747-1758, October 1999.

[27] C. Y. Wong, C. Y. Tsui, R. S. Cheng and K. B. Letaief, "A Real-time Sub-carrier Allocation Scheme for Multiple Access Downlink OFDM Transmission", *IEEE VTC'99*.

[28] J. Jang and K. B. Lee, "Transmit Power Adaptation for Multiuser OFDM Systems", *IEEE Jan. Selected Areas Comm.*, Vol. 21, No. 2, February 2003.

[29] Y. F. Chen, J. W. Chen and C. P. Li, "A Real-time Joint Subcarrier, Bit and Power Allocation Scheme for Multiuser OFDM-based Systems", *IEEE VTC'04*.

[30] D. Kivanc, G. Li and H. Liu, "Computationally Efficient Bandwidth Allocation and Power Control for OFDMA", *IEEE Trans. Wireless Commun.*, Vol. 2, No. 6, pp.1150-1158, Nov, 2003.

[31] Y. J. Zhang and K. B. Letaief, "Multiuser Adaptive Subcarrier-and-Bit Allocation With Adaptive Cell Selection for OFDM Systems", *IEEE Trans. Wireless Commun.* Vol. 3, No.5 September 2004.

[32] Y. Pan, K. B. Letaief, Z. Cao, "Dynamic resource allocation with adaptive beamforming for MIMO/OFDM systems under perfect and imperfect CSI", *IEEE Wireless Communications and Networking Conference*, 2004.

[33] X. Gao, M. Naraghi-Pour, "Computationally efficient resource allocation for multiuser OFDM systems", *IEEE Wireless Communications and Networking Conference*, 2006.

[34] B. S. Krongold, K. Ramchandran, and D. L. Jones, "Computationally efficient optimal power allocation algorithms for multicarrier communication systems", *IEEE Trans. Commun*, Vol. 48, No. 1, 2000.

[35] G. Gu, X. Gao, J. He, M. Naraghi-Pour, "Parametric modeling of wideband and ultra wideband channels in frequency domain", To Appear, *IEEE Transactions on Vehicular Technology*.

[36] S. Ye, R. S. Blum, L. J. Cimini, Jr., "Adaptive modulation for variable-rate OFDM systems with imperfect channel information", *IEEE Vehicular Technology Conference*, May 2002.

[37] T. Ekman, M. Esternad and A. Ahlem, "Unbiased power prediction on broadband channel," *Proceedings of IEEE Vehicular Technology Conference,* Vancouver, Canada, Sept. 2002.

[38] M. R. Souryal, R. L. Pickholtz, "Adaptive modulation with imperfect channel information in OFDM", *IEEE International Conference on Communications*, June 2001.

[39] A. Leke and J. M. Cioffi, "Multicarrier systems with imperfect channel knowledge", *The Ninth IEEE International Symposium on Personal, Indoor and Mobile Radio Communications*, 1998.

[40] A. M. Wyglinski, F. Labeau and P. Kabal, "Effects of imperfect subcarrier SNR information on adaptive bit loading algorithms for multicarrier systems", *IEEE Global Telecommunications Conference*, 2004.

[41] S. Falahati, A. Svensson, T. Ekman, M. Sternad, "Adaptive modulation system for predicted wireless channels", *IEEE Transactions on Communications*, Vol. 52, No. 2, Feb. 2004.

[42] T. Eyceoz, A. Duel-Hallen, H. Hallen, "Prediction of fast fading parameters by resolving the interference pattern", *Proc. of the* 31st *ASILOMAR Conf. on Signals, Systems, and Computers*, 1997.

[43] FCC, "Revision of Part 15 of the Commissions Rules Regarding Ultra-Wideband Transmission Systems", First Report and Order, ET Docket 98-153, FCC 02-8, adopted/released Feb. 14/Apr. 22, 2002.

[44] Naiel Askar, "Overview of General Atomics PHY Proposal to IEEE 802.15.3a", *IEEE 802.15-03/105r1*, Sep 2003.

[45] Charles Razzell, *et. al.* "Philips TG3a CFP Presentation", *IEEE 802.15-03/125r2*, March 2003.

[46] Matt Welborn, "XtremeSpectrum CFP Presentation", *IEEE 802.15-03/153r5*, May 2003.

[47] Roberto Aiello, "Discrete Time PHY Proposal for TG3a", *IEEE 802.15-03/099r1*, March 2003.

[48] Jeff Foerster, *et. al.* "Intel CFP Presentation for a UWB PHY", *IEEE 802.15-03/109r1*, March 2003.

[49] Dillenburg, John F. and Nelson, Peter C. "Improving the efficiency of depth-first search by cycle elimination", *Information Processing Letters*, v 45, n 1, Jan 25, 1993, p 5-10.

[50] Aiello, G. Roberto and Rogerson, Gerald D.,"Ultra-Wideband Wireless Systems", *IEEE Microwave Magazine,* v 4, n 2, June, 2003, p 36-47.

[51] Porcino, Domenico and Hirt, Walter, "Ultra-wideband radio technology: Potential and challenges ahead ", *IEEE Communications Magazine,* v 41, n 7, July, 2003, p 66-74.

[52] Ahmad R. S. Bahai, Burton R. Saltzberg, and Mustafa Ergen, *Multi-Carrier Digital Communications: Theory and Applications of OFDM*, Springer Science+Business Media Inc., New York, NY, 2004.

[53] T. Rappaport, *Wireless Communications: Principles and Practices*, 2nd edition, Printice Hall, New Jersey, 2001

[54] G.E.P. Box and G.M. Jenkins, *Time Series Analysis: Forecasting and Control*, Holden-Day, San Francisco, 1976.

[55] G. Grimmett and D. Stirzaker, *Probability and Random Processes*, 3rd edition, Oxford University Press, New York, NY, 2001.

[56] G. H. Golub and C. F. Van Loan, "Matrix Computations", 2nd Edition, Baltimore: The Johns Hopkins University Press, 1989.

[57] H. Meyr, M. Moeneclaey, and S.A. Fechtel, *Digital Communication Receivers*, John Wiley & Sons, Inc., New York, N.Y.,1998.

[58] J. G. Proakis, *Digital Communications, Fourth Edition*, MacGaw-Hill College, 2000.

[59] G. Stüber, *Principles of Mobile Communication*, Kluwer Academic Publishers, 1996.

[60] S. Haykin, *Adaptive Filter Theory, Fourth Edition*, Prentice Hall, 2002.

[61] Stephen Boyd and Lieven Vandenberghe, *Convex Optimization*, Cambridge University Press, 2004.

[62] P.P. Vaidyanathan, *Multirate Systems and Filter Banks*, Prentice-Hall, Englewood Cliffs, New Jersey, 1993.

[63] P. Stoica and R.L. Moses, *Introduction to Spectral Analysis*, Prentice Hall, Feb., 1997.

[64] Robert G. Gallager, *Information Theory and Reliable Communication.* John Wiley & Sons, New Youk, 1968.

APPENDIX: LETTER OF PERMISSION

From: Jacqueline Hansson Date: 03/05/2007

Subject: Re: Request for Permission

Dear Xiang Gao:

This is in response to your letter below, in which you have requested permission to reprint, in your upcoming thesis/dissertation, the described IEEE copyrighted material. We are happy to grant this permission.

Our only requirement is that the following copyright/credit notice appears prominently on the first page of the reprinted paper, with the appropriate details filled in: ©[Year] IEEE. Reprinted, with permission, from (complete publication information).

It is our understanding that University Microfilms, Inc., may supply single copies of the dissertation.

Sincerely yours,

Jacqueline Hansson

IEEE Intellectual Property Rights Office 445 Hoes Lane, Piscataway, NJ 08855

Telephone: +1 732-562-3966 Fax: +1 732-562 1746

w.hagen@ieee.org http://www.ieee.org/copyright

-=--=-=

Dear Sir or Madam,

This is Xiang Gao from Louisiana State University. I want to ask for your permission to reprint the following article accepted by an IEEE journal:

Author(s) : Guoxiang Gu, Xiang Gao, Jianqiang He, Morteza Naraghi-Pour

Paper Title: Parametric Modeling of Wideband and Ultra Wideband Channels in Frequency Domain

Journal Title: IEEE Transactions on Vehicular Technology

As one of the authors of this paper, I want to reprint the entire article as Chapter 2 in my dissertation with the tile "Channel Modeling and Resource Allocation in OFDM Systems". The requested permission extends to any future revisions and editions of my dissertation including non-exclusive world rights in all languages, and to the prospective publication of my dissertation by the UMI Company. These rights will in no way restrict republication of the material in any other form by IEEE or by others authorized by IEEE. Your permission of this request will also confirm that IEEE owns the copyright of the above-described material.

If these arrangements meet with your approval, please response this email no later than Monday March 5th, 2007. Thank you for your cooperation.

Sincerely

Xiang Gao
Feb. 28, 2007

VITA

Xiang Gao was born in Jiangsu Province, China, on May 12, 1975. In July 1998 and July 2001, he received, respectively, the Bachelor of Science degree in Electrical Engineering and the Master of Science degree in Electrical Engineering from Peking University, Beijing, China. In August 2002, he entered the graduate program in the Department of Electrical and Computer Engineering at Louisiana State University, where he is currently a candidate for the degree of Doctor of Philosophy in electrical engineering.